THE CONTRIBUTION OF INNATE IMMUNE CELLS TO REGENERATION OF THE ZEBRAFISH OLFACTORY EPITHELIUM

by

Sinay Mollamustafaoğlu

B.S., Molecular Biology and Genetics, Boğaziçi University, 2020

Submitted to the Institute for Graduate Studies in
Science and Engineering in partial fulfilment of
the requirements for the degree of
Master of Science

Graduate Program in Molecular Biology and Genetics

Boğaziçi University

2023

ACKNOWLEDGEMENTS

"In the early stages of creation of both art and science, everything in the mind is a story", said E. O. Wilson, a famous biologist and writer. So, what you are holding right now, is the story of mine. An action-thriller-comedy tale on excitements and disappointments, successes, and failures… my story in this department ends here, but my journey has just begun. I'm more than grateful to my supervisor Stefan, for being an incredible mentor, also for his tremendous support and patience towards me. I admire the way he sees and practices science. I also appreciate the cozy friendship that he showed when needed. I am and will always be proud to be his student, and the things I've learnt from him will always stay engraved in my mind. I'm grateful to dear Anıl Doğan, for his precious friendly chats to encourage me on following my extracurricular works. I'd like to thank Aslı Kumbasar for accepting without hesitation to become a jury member despite her busy schedule. I'm grateful to my dear friends Davod, Semin and Özlem for their company and endless support throughout my journey. Even from many miles away, my dearest friend Nuşin Naki knew how to give her unconditional love and support. I'd like to thank Yiğit and Mehmet Can for their sincere friendship and scientific guidance.

I'm grateful to my family and to my mother Yeşim, for being my best friend, as her love and support was the only thing that made me get up in some mornings. I admire her patience, will and never-ending joyful energy. She is and will always be my inspiration in my personal and professional life.

I was thirteen when I first stepped in to Boğaziçi University which I had no idea about, to give a small piano recital in ALH. But little did I know that this place would be my second home for many years to come. Now I'm leaving, to chase the dreams that I shaped here once, lying on the grass with the sun in my eyes. This story ends here, another will begin. Because the goal in this journey is not to reach the end, but to always be on the way.

Work on this thesis was supported by Boğaziçi University Research Fund Grant Number 17822 (Project Code: 21BM1), entitled "The contribution of innate immune cells and cytokine expression to zebrafish olfactory system regeneration".

ABSTRACT

THE CONTRIBUTION OF INNATE IMMUNE CELLS TO REGENERATION OF THE ZEBRAFISH OLFACTORY EPITHELIUM

Tissue injury is immediately followed by a strictly coordinated immune response, which is necessary to restore the functional and structural integrity of the tissue. The regulation of the immune response is closely linked to the quality and extent of the regeneration process. Higher vertebrates exhibit a limited ability to accomplish complete regeneration of neuronal tissues. The peripheral olfactory epithelium (OE) on the other hand, undergoes a lifelong continuous turnover of sensory neurons. Regenerating organisms like the zebrafish, have even a higher capacity to achieve a rapid and full recovery of both central and peripheral nervous system tissue. This study aims to understand the relationship between innate immune cells and the regenerative events in the adult zebrafish OE by analyzing neutrophil and macrophage contributions to OSN neurogenesis following experimental injury. Qualitative analysis and quantitative assays established the baseline occupancy of neutrophils and macrophages in the intact tissue as well as their level of recruitment in response to injury. Using a cell type-specific depletion approach, temporal systemic elimination of neutrophils and macrophages was applied via VMO-knockdown and clodronate liposome administration, respectively. The selective contribution of neutrophils and macrophages to zebrafish olfactory sensory neurogenesis and regeneration were examined at the structural level. Systemic depletion of neutrophils resulted in a sharp decrease in the proliferative activity in the degenerated tissue and severely impaired the neurogenic process. Altogether, the results indicate that neutrophils may be regulating injury-induced repair neurogenesis and are necessary to achieve full regeneration of the OE. In contrast, neutrophils had no significant functional influence on the physiological turnover of the OE via maintenance neurogenesis events. Macrophages on the other hand, did not exhibit notable recruitment or showed any functional contribution to OSN neurogenesis.

ÖZET

DOĞAL BAĞIŞIKLIK HÜCRELERİNİN ZEBRA BALIĞI OLFAKTÖR EPİTELİ REJENERASYONUNA OLAN KATKISI

Doku hasarını, hemen ardından sıkı bir şekilde koordine edilen immün cevabı takip eder. Bu cevap dokunun fonksyonel ve yapısal bütünlüğünü geri kazanmak için gereklidir. İmmün cevabının regüle ediliş biçimi, ardından gelen rejenerasyon süreciyle yakından alakalıdır. Gelişmiş omurgalılar nöronal doku rejenerasyonunda kısıtlı bir kapasiteye sahiptir. Ancak, periferal olfaktör epiteli, duyu nöronlarını hayat boyu devam eden bir devir daim ile yeniler. Zebra balığı gibi rejenerasyon kapasitesi yüksek organizmalar, sinir sistemi dokularını daha hızlı ve efektif biçimde yenileyebilirler. Bu çalışma, doğal bağışıklık hücreleri ile yetişkin zebra balığı olfaktör epiteli rejenerasyonu arasındaki ilişkiyi araştırmayı hedefler. Bu amaçla, nötrofil ve makrofajların olfaktör duyu nörojenezine olan katkıları deneysel hasar sonrası olfaktör epitelinde incelenmiştir. Karakterizasyon odaklı kualitatif çalışmalar ve kuantitatif analizler ışığında nötrofil ve makrofajların hasarsız dokudaki bazal yoğunlukları ve hasardan sonra dokuya infiltrasyonları belirlenmiştir. Hücre-tipi spesifik deplesyon yöntemiyle, nötrofiller morfolino oligomerleri kullanılarak ve makrofajlar liposomal klodronat kullanarak sistemik olarak elimine edilmiştir. Nötrofil ve makrofajların olfaktör epiteli nörojenez ve rejenerasyonuna olan fonksyonel etkileri araştırılmıştır. Nötrofillerin sistemik eliminasyonu hasarlı epiteldeki proliferatif aktiviteyi keskin bir düşüşle azaltmıştır ve nörojenik olayları ciddi biçimde zayıflatmıştır. Deneysel sonuçlar, nötrofillerin hasar kaynaklı tamir nörojenezini regüle ediyor olabileceğini ve olfaktör epitelinin tam rejenerasyonu için gerekli olduklarını göstermektedir. Ayrıca nötrofillerin, olfaktör epitelin fizyolojik durumlar altında gerçekleştirdiği bakım nörojenezine fonksyonel bir katkıda bulunmadıkları gözlenmiştir. Makrojajların ise, olfaktör epiteline hasar sonrası istatistiksel olarak kayda değer bir infiltrasyon göstermedikleri, aynı zamanda olfaktör duyu nörojenezine fonksyonel bir katkıda bulunmadıkları gözlemlenmiştir.

TABLE OF CONTENTS

LIST OF FIGURES

LIST OF TABLES

LIST OF SYMBOLS

h	Hour(s)
hpi	Hours post injection
hpl	Hours post lesion
kDa	Kilodalton
l	Liter
mg	Milligram
mM	Millimolar
N	Normal
n	Number of samples
μg	Microgram
μl	Microliter
μm	Micrometer

LIST OF ACRONYMS / ABBREVIATIONS

ANOVA	Analysis of Variance
BrdU	5-bromo-2-deoxyuridine
Csf3r	Colony Stimulating Factor 3 Receptor
Ctr	Control Condition
DNA	Deoxyribonucleic Acid
DPBS	Dulbecco's phosphate-buffered saline
EdU	5-ethyl-2’-deoxyuridine
FIJI	Fiji is Just Image J
GBC	Globose Basal Cell
Gcsfr	Granulocyte Colony Stimulating Factor Receptor
GS	Normal Goat Serum
HBC	Horizontal Basal Cell
HuC/D	Hu Protein C / D
Hz	Hertz
ILC	Inter Lamellar Curve
IP	Intrapertoneal
KD	Knock-down
L-CLOD	Clodronate liposomes
L-PBS	PBS containing liposomes
Lcp1	L – Plastin
Lyz	Lysozyme C
Mfap4	microfibril Associated Protein 4
Mpx	Myeloid Specific Peroxidase
MS222	Tricaine Methanosulfonate
OB	Olfactory Bulb
OCT	Optimum Cutting Temperature
OE	Olfactory Epithelium
OO	Olfactory Organ
OSN	Olfactory Sensory Neuron
PBS	Phosphate Buffered Saline

PBST	Phosphate Buffered Saline with Tween 20
PFA	Paraformaldehyde 4,0%
pH	Power of Hydrogen
RGB	Red Green Blue
RNA	Ribonucleic Acid
RO	Retro Orbital
ROI	Region of Interest
S/NS	Sensory / Non-Sensory Border
SC	Sustentacular Cell
SEM	Standard Error of Means
TrX	1% Triton X-100
VMO	Vivo Morpholino

1. INTRODUCTION

1.1. Inflammation and Its Role in Regeneration

Inflammation has developed throughout evolution as a protective response to various harmful stimuli caused by infectious microorganisms and chemical or physical trauma, aiming to re-establish tissue homeostasis (Gusev et al., 2019). Inflammation is not a far concept to us, and it is definitely not a recent subject of study in the world of biological sciences. Indeed, very first evidence of inflammation study dates back all the way to the 1st century AD when Roman physician, writer and encyclopedist Aulus Cornelius Celsus characterized the common indicators of inflammation as *rubor et tumor cum calore et dolore* (redness and swelling accompanied by heat and pain; Freire and Van Dyke, 2013; Keightley et al., 2014; Tedgui, 2011). In the 19th century, several important revelations have been established in the field. In addition to the four main determinants of inflammation previously defined by Celsus, *fucntio laesa* (loss of function) was added to the identification of inflammation following the works of Rudolph Virchow (Freire and Van Dyke, 2013). Robert Koch and Louis Pasteur also brought massive contributions to the field with their works on the involvement of microorganisms in promoting the inflammatory response (Freire and Van Dyke, 2013). Later on, Metchnikoff showed that certain phagocytic leukocytes help resolve the inflammation by engulfing and eliminating any foreign bodies, as well as dead cells and debris from the inflamed area (Rock et al., 2010; Tauber, 2003).

Inflammatory process is complicated by the fact that it is underlined by a sophisticated interplay between diverse molecular and cellular events, aiming at protecting the host tissue against noxious stimuli with the nature of physical trauma, ischemia, chemical or reperfusion injuries as well as penetration of invasive microorganisms (Freire and Van Dyke, 2013). The inflammatory response is the first line of action following disruption of tissue homeostasis by an irritant stimulus (Medzhitov, 2008).

Following such an incident, smooth muscles around local arterials relax, lead to vasodilation which may appear as redness and heat sensation around the insulted area (Rock et al., 2010), as fundamental indicators of inflammation that have been recognized since ancient times (Freire and Van Dyke, 2013). The increase in vascular permeability is coupled with a rise in hydrostatic pressure at the site, which result in the selective diffusion of certain molecular agents to the inflamed area, causing edema (Chazaud, 2020; Rock et al., 2010). The inflammatory response aims at bringing all types of molecular and cellular factors that help combat infection and tissue damage to the site of damage, quickly, and efficiently (Medzhitov, 2008). The injured tissue also sends molecular signals that form chemoattractant gradients around the inflamed site (Sommer et al., 2020), providing the recruitment of additional immune cells and soluble agents from the circulation (Powell et al., 2017), to mediate the inflammatory process (Chen and Nuñez, 2010). First and foremost task of these recruited, as well as resident inflammatory mediators, is to eliminate any foreign irritants (pathogens, chemicals etc.) as well as dead cells from the inflamed site (Freire and Van Dyke, 2013), and settle the tissue damage caused by the disruptive stimulus (Gray et al., 2011; Sommer et al., 2020). Eliminating irritant agents and unwanted debris from the injured tissue, initiates a series of restorative events that can be summarized as, the resolution of inflammation (Sugimoto et al., 2019), tissue repair, and finally, regeneration and tissue remodeling (Oishi and Manabe, 2018; Wang, 2018).

The inflammatory process that occurs in the absence of any invading microorganisms, has been named as *sterile inflammation* (Chen and Nuñez, 2010; Rubartelli et al., 2013). In such cases, tissue damage that causes an immediate inflammatory response may originate from physical trauma, chemical irritants, ischemia related injuries as well as endogenous events (Peiseler and Kubes, 2019; Rock et al., 2010). Various autoimmune disorders and autoinflammatory diseases are associated with sterile inflammation (Rock et al., 2010). As an example, in Alzheimer's Disease a chronic sterile inflammation is seen as beta-amyloid plaques induce pro-inflammatory mechanisms that attract immune cells (Freire and Van Dyke, 2013; Rock et al., 2010). A diverse range of other autoimmune disorders are related to sterile chronic inflammation, including rheumatoid arthritis (See and Lord, 2004), type 1 diabetes (Atkinson et al., 2014), inflammatory bowel disease (Subasinghe et al., 2011), and atherosclerosis (Chen and Nuñez, 2010; Subasinghe et al., 2011).

In sterile inflammation, the molecular signals that trigger an immune response are not foreign but are released endogenously from the dead cells and extracellular matrix (ECM) within the injured tissue (Chen, 2010; Julier et al., 2017). Then it is again the responsibility of the inflammatory mechanism, to resolve the injury and mediate the healing process towards tissue repair (Freire and Van Dyke, 2013).

In recent decades, the effects of inflammation on tissue repair and regeneration have attracted considerable attention as a subject of study among researchers in biology and medicine (Karin and Clevers, 2016). It has been shown that the cellular and molecular events mediating inflammation are intertwined with the processes that mediate tissue repair and regeneration (Kokaia et al., 2012) and are highly conserved in vertebrates (Yoo and Huttenlocher, 2011), indicating an evolutional significance of these processes in the survival of organisms (Karin and Clevers, 2016). Studies have established that dynamics and outcome of a particular inflammatory process is one of the most important determinants in the extent and quality of the repair and regeneration of the damaged tissue (Goodman et al., 2019; Mescher, 2017). Although historically it has been a common one-sided idea that inflammation is harmful to tissues, advancements on the field have revealed that, quickly resolving transient inflammation is, in fact an important protective response that activates the cascades involved in tissue repair and remodeling (Iribarne, 2021; Kizil et al., 2015). However, if the inflammatory process cannot be resolved for long periods of time, the quality and extent of tissue repair and regeneration will be negatively affected (Karin and Clevers, 2016; Kizil et al., 2015). In addition, leukocytes release peroxidases, proteases, reactive oxygen species (ROS) and other toxic factors to combat pathogens, which can also be noxious to the endogenous cells if the acute phase of inflammation fails to resolve (Karin and Clevers, 2016). Furthermore, leukocytes may not be able to clear all apoptotic cells and necrotic cell debris, as well as in some cases, leukocytes themselves cannot be eliminated from the area (Isles et al., 2019), which in turn causes a delay and increases the risk of permanent endogenous tissue damage (Freire, 2014). In such cases of *chronic inflammation*, the healing process is incapacitated, and the tissue cannot undergo proper restoration which may result in scar formation, fibrosis, loss of function (Chen and Nuñez, 2010), and further tissue degeneration leading to incomplete recovery of tissue morphology, and in extreme cases, potential organ failure (Zhang et al., 2018).

For example, in patients with asthma, unresolved leukocyte accumulation and pro-inflammatory factors leads to acute inflammation of the airways and results in defective tissue healing and restoration (Murdoch, 2010). Such drastic implications of chronic and persistent inflammation may also be observed in neurodegenerative (Martins et al., 2019), cardiovascular (Xu et al., 2018), and autoimmune disorders (Li et al., 2020; Sugimoto et al., 2019). The recognition of the fact that inflammatory processes have a pivotal role in the context of tissue restoration and repair (Karin and Clevers, 2016), paved the way to the rise of more and more studies focusing on the regulation of inflammatory response (Sugimoto et al., 2019), and its relationship between tissue renewal and regeneration in different tissue contexts (Oishi and Manabe, 2018), as well as in different model organisms (Julier et al., 2017; Kizil et al., 2015).

The remarkable ability of certain organisms such as reptile species, fish, frogs, and spiders to regenerate fully functional tissues and organs has always been a matter of curiosity in the scientific world (Sabin and Echeverri, 2020), considering the inability of mammals of undergoing such a high level of efficient tissue recovery (Ghosh and Hui, 2018). It has been shown that the characteristics of the initial immune response to damaged or lost tissue parts, is the major effector in determining the regenerative capacity and efficacy of tissue repair (Karin and Clevers, 2016). However, the mechanisms underlying the regenerative capacity of species are still not fully understood. As mentioned earlier, the molecular and cellular mechanisms involved in inflammation and regeneration are highly complex (Sugimoto et al., 2019), and therefore have multi-faceted consequences in different tissue contexts and across phyla (Tauber, 2003). Studies have uncovered that the regenerative ability is inversely proportional to the level of complexity and sophistication of the immune system (Gusev et al., 2019; Mescher, 2017). This argument may explain why for example the lower vertebrates such as fish and amphibians are remarkably better at regenerating fully functional tissues and organs than higher vertebrates like mammals (Ghosh and Hui, 2018; Uemoto et al., 2020).

In response to traumatic injury, increased proliferative activity leads to new tissue formation (Mescher, 2017; Sabin and Echeverri, 2020). In organisms that undergo complete regeneration of lost tissues or organs, the remodeling of newly produced tissue provides regaining the exact structural assembly and function of the old one (Sugimoto et al., 2019).

However, depending on the regeneration capacity of the organism and the particular tissue, as well as the extent of the injury, healing process may also have different consequences (Freire and Van Dyke, 2013; Julier et al., 2017). In case of an incomplete regeneration, new tissue construction may result in a disruption in molecular and cellular structure, which may ultimately result in full or partial loss of tissue function (Goodman et al., 2019). Thus, it is important to distinguish tissue repair from complete regeneration (Oishi and Manabe, 2018). Although, tissue repair may restore homeostasis and reconstruct part of the loss tissue, unlike regeneration, accumulated collagen in the wound and residues of the granulation tissue usually lead to fibrotic scar formation (Iribarne, 2021; Keightley et al., 2014; Oishi and Manabe, 2018; Shanley et al., 2021).

In recent decades, the interplay between inflammatory response and tissue regeneration have been investigated in cellular and molecular level (Karin and Clevers, 2016). A muscle regeneration study on mice, investigated the functional effects of neutrophilic granulocytes in a snake venom induced inflammatory response in the skeletal muscle (Teixeira et al., 2003). Neutrophil deficient mice were unable to regain tissue homeostasis and accomplish a structural and functional regeneration in response to snake venom induced injury (Teixeira et al., 2003). The necrotic cell debris and unwanted noxious venom substances could not be eliminated in the absence of neutrophils and a notable amount of fibrotic scar deposition was recorded (Teixeira et al., 2003). In a separate study, the crucial role of monocytes/macrophages in regulating tissue regeneration was demonstrated with a cryoinjury model on mice (Summan et al., 2006). Upon monocyte/macrophage depletion with clodronate liposomes, the muscle regeneration was partially impaired with a necrotic debris deposition and a decrease in growth factor and chemoattractant release in the injured tissue (Summan et al., 2006). A more recent study focused on immunomodulatory effects of hyaluronic acid to alter the concentration of the cytokine TNF α, promoting tissue restoration in a burn model (Friedrich et al., 2014).

In a neuronal regeneration study on zebrafish brain, immunogenic particles were injected to the cerebroventricular space of immunosuppressed fish, which resulted in an impaired regenerative response and stem cell activity (Kyritsis et al., 2012).

Further evidence from several *in vitro* studies also indicated that inflammatory cytokines such as TNF α (Widera et al., 2006) and IL-1β (Wang et al., 2007) may trigger or promote neural stem cell (NSC) proliferation and neuronal regeneration (Kizil et al., 2013). Despite a considerable amount of development has been established in the field, the pro-regenerative machinery of the innate immunity has not been fully elucidated.

To understand the relationship between inflammatory response and regenerative mechanisms, one must dive further into the principal molecular and cellular dynamics of inflammation which may be roughly divided into two successive processes as the *acute phase* and the *resolution of inflammation* (Medzhitov, 2008). As mentioned earlier, transient, and temporal chronic inflammation and a quick resolution without fibrotic scar formation are necessary and perquisite for a successful healing process, as well as a complete restoration of tissue function (Hasegawa et al., 2017).

It goes without saying that every inflammatory response is particular and unique by the fact that numerous parameters affect the fate of inflammation including the tissue location, the extent and nature of the injury, circulatory properties, as well as the cellular and molecular construction dynamics of the tissue (Iribarne, 2021; Julier et al., 2017).

A noxious stimulus may lead to cell death, disruption of structure and metabolic balance of the tissue (Rubartelli et al., 2013). The acute phase of inflammation starts immediately after encounter with such an injury. In such circumstances, a diverse range of danger signals are released into the tissue milieu, to report the abnormality and seek help for restoring tissue homeostasis (Sipka et al., 2021).

Cytokines, and *chemokines* are among those signaling molecules, which are small proteins that have chemotactic ability to induce leukocyte motion as well as mediate molecular cascades by the activation of various cellular receptors (Chen and Nuñez, 2010). These factors are released by the structural cells, resident immune cells, as well as degranulating mast cells that reside in the connective tissue around the damage zone (Chen and Nuñez, 2010).

In addition, the inflammatory process is dominated by the release of pathogen associated molecular patterns (PAMPs) if any microorganisms present, and danger associated molecular patterns (DAMPs), in the case of sterile inflammation (Havixbeck and Barreda, 2015). DAMPs span a wide variety of endogenous molecules and molecular patterns that normally reside within cells or ECM (Medzhitov, 2008), such as fibronectin, collagen, hyaluronic acid, and elastin, which become exposed in case of a structural deconstruction (Julier et al., 2017). In addition, cells may undergo necrosis in consequence of an intense disruption which causes membrane integrity to be compromised, thereby resulting in release of cellular components (Chen and Nuñez, 2010; Julier et al., 2017). A diverse range of molecules normally reside within cells may also recognized as DAMPs, and released as a result of necrotic cell death, such as mitochondrial and genomic DNA, heat shock proteins, cytoskeletal particles, ATP, and uric acid (Rock et al., 2010).

Necrotic cell death is an abnormal and uncontrolled process which usually ends up with uncontained release of the contents to the extracellular space (Chen and Nuñez, 2010). In contrast, apoptosis is a monitored and programmed method of cell death in which, the cell follows several strictly regulated processes like DNA and nuclear fragmentation, chromatin condensation, and cell shrinkage, which enable the cell to be phagocytosed by leukocytes without releasing any immunogenic material inside (Chen and Nuñez, 2010). Therefore, necrotic cell death is one of the fundamental events to trigger inflammatory response by the uncontrolled release of DAMPs to the extracellular environment (Chen and Nuñez, 2010).

Cytokines, growth factors, enzymes and other mediatory factors that are released in response to inflammatory process are incredibly diverse (Rubartelli et al., 2013). The complex interplay among this collection of inflammatory mediators and their individual, as well as collective impact on inflammatory events have not been fully explained.

Coagulation factors are induced and platelets form aggregates to act on potential ruptured blood vessels as an immediate response to restore disrupted tissue homeostasis (Chen and Nuñez, 2010), in addition, release certain growth factors and chemokines such as platelet-derived growth factor (PDGF), transforming growth factor (TGF- β) and monocyte chemoattractant protein-1 (MCP-1) to recruit additional leukocytes to the site of injury (Mescher, 2017).

The recruited innate immune cells, mainly neutrophils and monocyte/macrophages, clear necrotic cell debris, combat pathogens (Sugimoto et al., 2019), release regulatory peptides as well as cytokines like tumor necrosis factor (TNF) and several proinflammatory interleukin family members, ROS, also proteases such as matrix metalloproteases, which induce degradation and clarence of disrupted ECM to reserve space and sterilization prior to tissue renewal (Chen and Nuñez, 2010).The molecular mediators released by the innate immune cells also involve fibroblast growth factor, leptin and factors mediating ECM repair, growth factors that promote angiogenesis, and interleukin family proinflammatory cytokines including IL-6, IL-1β, IL-8, IL-12, and IL-18 (Borders et al., 2007; Freire and Van Dyke, 2013).

All molecular and cellular events that occur in the chronic inflammatory phase are in fact actors in a tightly controlled feed-back mechanism that guides the whole process towards resolution of inflammation (Sugimoto et al., 2019), and initiates the regenerative events by activating stem cells which are capable of repopulating the lost tissue, providing cell proliferation and differentiation (Kizil et al., 2015; Kokaia et al., 2012).

Stem cells are multipotent cells that can produce daughter progeny which can differentiate into specialized cell types that regain the structural arrangement of the tissue (Bond et al., 2015). Stem cells stay in constant communication with their microenvironment and susceptible to outer stimuli (Aurora and Olson, 2014). They carry out division upon external triggers when there is need for replacement of dead or lost cells. The fact that inflammation is a major mediator of tissue renewal and regenerative process, indicates that inflammation may also be mediating stem cell activity (Aurora and Olson, 2014; Kizil et al., 2015).

One might find the molecular and cellular processes involved in the inflammatory response somewhat chaotic and out of order because of the immense number of diverse molecules and mediating factors involved within. In fact, the inflammatory response consists of highly organized chain of intertwined cellular and molecular events that mediates the recovery, remodeling, and regeneration of lost and damaged tissues (Rock et al., 2010; Rubartelli et al., 2013).

1.2. The Olfactory System

The olfactory system is uniquely developed to provide sensory information vital for the survival of organisms. The odorants are a large group of diverse chemicals recognized by highly specialized olfactory sensory neurons (OSNs) located in the nasal cavity (Su et al., 2009). The perceived odorant signals mediate fundamental behaviors related to mating, feeding, predators nearby or the condition of the habitat (Su et al., 2009). Due to the large structural variety of the odorant molecules, OSNs are highly specialized to achieve perception (Poncelet and Shimeld, 2020). Indeed, each OSN is characterized to only express a specific type a functional odorant receptor (OR), which is practically similar to the mammalian "one-neuron-one-receptor" principle in the olfactory sensory system (Braubach et al., 2012). Olfactory receptors are transmembrane G protein-coupled receptors (GPCRs) that mediate the Ca^{+2} – gated chloride channels via cAMP concentration to transform the chemosensory stimulus to an electrical signal and eventual travel of the signal through the neural circuits (Calvo-Ochoa and Byrd-Jacobs, 2019; Orecchioni et al., 2022). OSNs are bipolar sensory neurons that protrude their dendritic extensions apically in the olfactory epithelium (OE), to receive chemosensory stimuli efficiently, thus are in direct contact with the external environment that may easily deliver noxious and toxic agents, metabolic stress factors, inflammatory substances, and physical damage (Lakshmanan et al., 2022). Due to their constant exposure to the harsh environmental conditions, their lifespan is limited to approximately 30 – 90 days (Mackay-Sim and Kittel, 1991).

The chemosensory stimuli are signaled through the olfactory nerve formed by the axons of the OSNs, and arrive at the olfactory bulb (OB) of the forebrain, where they deliver the electrical signal via forming synapses with the bulbar mitral cells and the interneurons (Calvo-Ochoa and Byrd-Jacobs, 2019). OSNs that are expressing the same OR, that recognizes the same ligand, are distributed randomly throughout the OE, but they extend their axons to the same region on the OB (Braubach et al., 2012). These regions on the OB have been named as the *glomeruli* (Braubach et al., 2012). Therefore, different odorant stimuli have spatially distinct centers on the surface of the OB that provides further specialization of the olfactory perception (Su et al., 2009).

The number of the glomeruli differs among species. For example, mice were shown to have up to 2000 glomeruli in the OB (Mombaerts, 2006), while zebrafish only has 80 per each OB (Braubach et al., 2012).

The peripheral OE is remarkably unique that it undergoes a lifelong neuronal turnover, providing a continuous OSN population in the OE as well as interneurons in the OB, to maintain odor sensation (Su et al., 2009). The structural and functional organization of the OE exhibits striking similarities across phyla (Poncelet and Shimeld, 2020). Intriguingly, adult neurogenesis is very limited in some organisms, especially in higher vertebrates (Kokaia et al., 2012). However, the olfactory system has been evolutionarily conserved to provide generation of new neurons to sustain a lifelong odor perception (Schwob et al., 2017), which can be appreciated from the fact that one of the very limited sites of adult neurogenesis in the central nervous system of vertebrates is the ventricular-subventricular zone of the lateral ventricles on the forebrain (Kokaia et al., 2012), and it is particularly specialized on the generation of new granule cells of the OB (Calvo-Ochoa et al., 2021).

1.3. The Zebrafish Olfactory Epithelium

Due to its high regenerative abilities, as well as the genetic and functional resemblance in olfactory system and many cell types, the zebrafish serves as an excellent animal model to study neuronal regeneration (Calvo-Ochoa et al., 2021; Pazhakh et al., 2017). The peripheral olfactory system of the zebrafish, consists of a pair of olfactory epithelia (OE), located dorso-anterior on each side of the head within the nasal cavity (Byrd and Brunjes, 1995; Figure 1.1b; dashed box). The OEs are connected to a pair of OBs of the forebrain (telencephalon; Figure 1.1b; Tel) via the olfactory nerve, which are located just posterior to the each nasal cavity (Calvo-Ochoa and Byrd-Jacobs, 2019).

OE of the zebrafish consists of staggered lamella structures that lie along the from the central-most non-sensory region, the median raphe, to the peripheral margin of the organ (Byrd and Brunjes, 1995; Figure 1.1c).

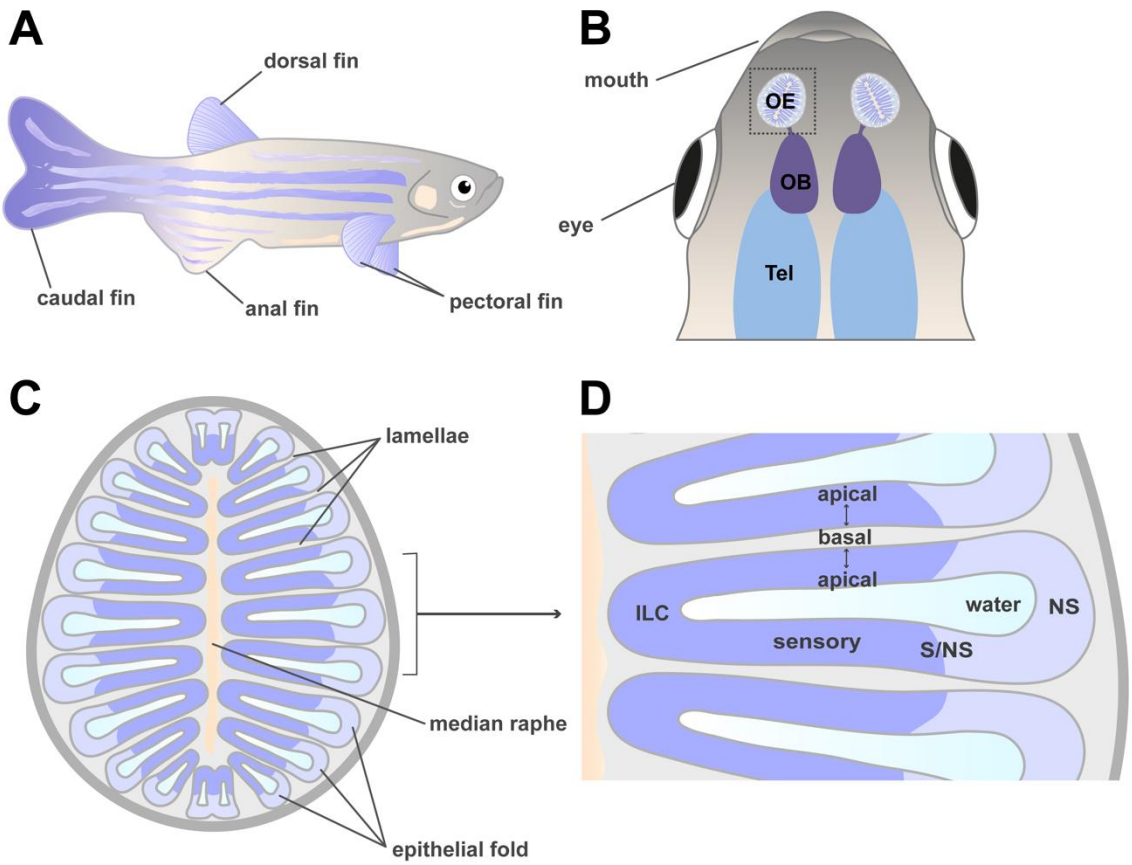

Figure 1.1. Anatomy of the zebrafish olfactory system. (a) Adult zebrafish. (b) Dorsal view of the zebrafish head. OE: Olfactory Epithelium; OB: Olfactory Bulb; Tel: Telencephalon (c) Cross section of the OE. The plane of the cross section is perpendicular to the dorsoventral axis of the olfactory organ. (d) Central portion of the hemi-OE.

The individual lamellae are composed of two epithelial sheets that are connected at their basal sides, attached to the lamina propria which contains the blood vasculature, axon extensions of the OSNs, and several types of non-sensory supportive cells (Byrd and Brunjes, 1995; Calvo-Ochoa et al., 2021). The apical sides of the epithelia are found in direct contact with the aqueous medium, where OSNs extend their dendritic protrusions, form cilia-like protrusions to maximize the surface area for odorant detection (Byrd and Brunjes, 1995).

Near the median raphe, the lamellae are connected via the folding of the single sheets of sensory epithelia, forming the Inter Lamellar Curves (Calvo-Ochoa et al., 2021; ILC; Figure 1.1d).

The epithelial sheets are organized to be populated by OSNs, which occupy the central two thirds of each epithelial fold (Figure 1.1c; sensory region; purple), and various non-sensory cells that form a peripheral ring around the sensory region (Figure 1.1c; non-sensory region; lilac), providing structural and functional support to the OO (Byrd and Brunjes, 1995; Calvo-Ochoa and Byrd-Jacobs, 2019). Figure 1.1d exhibits a more detailed view onto the structural and functional anatomy of the zebrafish OE. There is a sharp boundary between the sensory epithelium that is populated by the OSNs and the non-sensory tissue which is entirely occupied by non-sensory supportive cells such as mucus producing goblet cells and ciliated cells that provide motility of the aqueous environment (Byrd and Brunjes, 1995). This boundary has been referred as the sensory/non-sensory border (Bayramli et al., 2017; S/NS; Figure 1.1d). In addition, the apical regions of the sensory epithelium has been demonstrated to be almost entirely populated by the OSN cell bodies, while basal layers of the epithelia are reserved to the non-sensory cells that provide the continuous turnover of all cell types of the OE (Demirler et al., 2020). Generation of new epithelial folds is a lifelong continuous process in zebrafish, which is mostly centered around the anterior region of the OO (Calvo-Ochoa et al., 2021). Therefore, the number of epithelial folds is generally proportional to the age of the individual fish (Hansen and Zeiske, 1998). Newly generated young epithelial folds are generally found at the anterior end, while more mature ones occupy the medial region of the organ (Calvo-Ochoa et al., 2021).

The sensory neuron subtypes in the zebrafish OE share similarities with mammals, while also showing further diversity (Calvo-Ochoa and Byrd-Jacobs, 2019; Poncelet and Shimeld, 2020). Ciliated and microvillus OSNs are two primary subtypes found in both the zebrafish and in the mammalian OEs (Hansen and Zeiske, 1998; Poncelet and Shimeld, 2020). Ciliated OSNs are typically exclusive for the mammalian main OE, while microvillus OSNs typically occupy the vomeronasal organ (Calvo-Ochoa et al., 2021). In contrast, these two prominent OSN subtypes are distributed more evenly throughout the entire OE in the zebrafish with distinct apicobasal preference of their localization in the epithelial layer, indicative of an evolutional inferiority compared to mammals (Calvo-Ochoa et al., 2021).

Intriguingly, zebrafish has three additional OSN subtypes that have been named as cryped, kappe, and pear cells convenient with their morphological profiles, which have very short dendrites and selectively occupy the apical-most strata of the sensory epithelium near the tips of the ILC (Calvo-Ochoa et al., 2021; Calvo-Ochoa and Byrd-Jacobs, 2019). There is evidence in literature indicating that these three additional OSN subtypes may recognize distinct types of chemosensory stimuli, and in some degree may resemble certain cell types found in the mammalian olfactory system (Calvo-Ochoa et al., 2021; Poncelet and Shimeld, 2020), the exact molecular and cellular mechanisms that determine their distinct functional roles in the olfaction, have not been described in detail.

In addition to the goblet cells, similar to the Bowman's glands in mammals and ciliated columnar epithelial cells located in the peripheral most region of the non-sensory epithelium, the zebrafish OE has several other non-neuronal cell types that help sustain the tissue homeostasis and structural integrity (Poncelet and Shimeld, 2020). Glia like sustentacular cells (SCs) are located mostly in the sensory region, providing structural support, and contributing to the maintenance of the metabolic balance of osmotic pressure and chemicals (Schwob et al., 2017). At the basal most strata of the epithelial sheets, two distinct types of resident stem/progenitor cells, horizontal basal cells (HBCs) and globose basal cells (GBCs) reside (Demirler et al., 2020; Iqbal and Byrd-Jacobs, 2010). GBCs are a group of fast cycling OE-specific stem cells, dedicated progenitor cells, transit amplifying cells and neuronal precursors that mediate the continuous turnover of the sensory neurons as well as the non-neuronal cells of the epithelium (Schwob et al., 2017). In contrast, HBCs are characterized by their dormant state under physiological conditions, which is only switched to mitotically active state upon severe damage situations (Poncelet and Shimeld, 2020). The spatial localization of these cells significantly differs between zebrafish and the mammalian counterparts. HBCs form a monolayer between the basal lamina and the GBCs in the rodent OE, and both cell types are distributed evenly on the radial axis (Calvo-Ochoa et al., 2021; Poncelet and Shimeld, 2020; Schwob et al., 2017). In contrast, GBCs are located exclusively near the tips of the ILC and at the sensory/non-sensory border, while HBCs form an evenly distributed layer on the basal lamina (Calvo-Ochoa et al., 2021; Demirler et al., 2020).

The distinct characteristic in the spatial distribution of zebrafish HBCs and GBCs in the OE, offers a spectacular opportunity to understand the mechanisms deriving the neuronal regeneration and distinguish the cellular progeny that are generated by each cell type under different conditions.

1.3.1. Maintenance and Repair Neurogenesis in the OE

OSNs reside at the apical layer of the neuroepithelium therefore stay in direct contact with the external environment, and vulnerable to environmental toxicants as well as physical damage (Byrd and Brunjes, 1995). Thus, the average lifespan of the OSNs is limited to approximately 30 days, indicating that a constant stream of newly generated sensory neurons is necessary to sustain the olfaction throughout the lifespan of the organism (Calvo-Ochoa et al., 2021). Two different stem/progenitor cells were described in section 1.3., to occupy basal layers of the neuroepithelium and are responsible for the generation of new OSNs (Kocagöz et al., 2022). It was previously demonstrated that zebrafish OE, similar to the mammalian counterparts (Schwob et al., 2017), initiates distinct proliferative mechanisms to carry out physiological everyday maintenance neurogenesis that sustains the basal abundance of OSNs, in contrast to the repair neurogenesis that results upon exposure to a harmful stimulus leading to disruption of tissue integrity and a massive loss of OSNs and also non-neuronal cells (Calvo-Ochoa and Byrd-Jacobs, 2019; Kocagöz et al., 2022).

GBCs, that are responsible for the maintenance neurogenesis, spatially limited to only reside near the tips of the ILC and at the sensory/non-sensory border in the zebrafish OE, unlike rodents, where they are distributed evenly (Calvo-Ochoa et al., 2021). Therefore, under physiological conditions young OSNs are born from the central and peripheral margins of the sensory region, and gradually migrate towards the center of the sensory epithelium in zebrafish OE (Bayramli et al., 2017). However, in the rodents, GBCs are evenly distributed on the radial axis and newly generated OSNs do not undergo any lateral migration (Su et al., 2009). Zebrafish offers a great advantage to understand the origin of newly generated cells in the epithelium because of the spatially restricted localization of GBCs (Bayramli et al., 2017).

After a noxious stimulus has been introduced, the OE initiates a different mechanism of neurogenesis where normally quiescent HBCs are responsible for the injury-induced repair events (Schwob et al., 2017; Su et al., 2009). HBCs are located just superior to the basal lamina and evenly distributed along the radial axis of each neuroepithelia (Calvo-Ochoa et al., 2021; Demirler et al., 2020). Upon loss of a large number of OSNs due to tissue damage, the activation of HBCs leads to an increased proliferative activity all along the sensory region, exhibiting a notably different mitotic pattern from the GBC-mediated maintenance neurogenesis (Kocagöz et al., 2022). HBCs most likely response to non-neuronal cell loss, while GBCs mediate the neuronal turnover (Calvo-Ochoa et al., 2021). In case of a big scale harmful stimulus, every cell population in the OE become compromised, therefore activating both stem/progenitor cell pools to work together (Calvo-Ochoa et al., 2021). Altogether, the unique arrangement of maintenance and injury induced repair neurogenesis in zebrafish OE, provides easy monitoring of newly generated OSN subtypes.

Unlike many other organisms, zebrafish exhibits a unique ability to regain tissue integrity and restore all functional cell types with little to no structural compromise with remarkable speed (Sanders and Kent, 2014). Zebrafish can regenerate its OE in just 5 to 7 days, even after the entire OSN population is lost due to chemical irritant treatment, or after the shrinkage of the entire OO with experimental injury (Calvo-Ochoa et al., 2021; Kocagöz et al., 2022). Therefore, understanding the molecular and cellular mechanisms behind injury induced repair neurogenesis may give important insight on the general principles that govern neuronal regeneration.

1.3.2. An Experimental Injury Model to Study Olfactory Neurogenesis in the Zebrafish

There are numerous methods to introduce experimental injury to the olfactory system of zebrafish. Among those, use of surfactant based chemical lesioning is one of the most prominent and conventional approaches among research groups (Calvo-Ochoa and Byrd-Jacobs, 2019). These substances are usually found in commercially used mainstream cleaning products, such as detergents. Detergent based chemical ablation was found to be pro-inflammatory in such a way that it may cause impermeabilization of the endogenous cell membranes eventually resulting in the release of necrotic cell compartments and DAMPs, triggering immune response (Calvo-Ochoa and Byrd-Jacobs, 2019).

An experimental injury model to monitor neuronal regeneration in the zebrafish OE using detergent based Triton X-100 (TrX) solution, has been demonstrated by Iqbal and Byrd-Jacobs (Iqbal and Byrd-Jacobs, 2010). Nasal irrigation of the chemical irritant resulted in significant reduction in the epithelial thickness and structural compromise of the OE integrity with a severe loss of OSNs and non-neuronal cells residing in the OE one day after injury (Iqbal and Byrd-Jacobs, 2010). Serious structural and cellular disruption of the OE was restored and returned to pre-injury conditions within one week in just five days (Iqbal and Byrd-Jacobs, 2010).

Manipulating the concentration, procedure, and the repetition of the TrX application, offers different experimental conditions to investigate. In addition, previous studies have shown that the spatial pattern of proliferative activity significantly changes after chemical ablation, which is consistent with different activation conditions of two distinct populations of stem/progenitor cells in the OE, HBCs and GBCs (Bayramli et al., 2017). Under homeostatic conditions, physiological turnover of the OSNs is provided by the everyday maintenance neurogenesis that is exclusively restricted to the central and peripheral margin of the sensory region in the intact OE (Kocagöz et al., 2022). However, upon chemical ablation the proliferative activity within the sensory region significantly increases and peaks at the third day post lesion (Demirler et al., 2020), and gradually returns to basal levels at the time of approximately five days post lesion, indicating that injury-induced repair neurogenesis is a limited and temporary response (Calvo-Ochoa et al., 2021; Iqbal and Byrd-Jacobs, 2010).

1.4. The Zebrafish Innate Immune System

Immune system is one of the most primal and fundamental defense mechanisms of all living organisms (Renshaw and Trede, 2012). The components and mechanism of immune defense have become sophisticated throughout evolution. However, it exhibits remarkable conservation in molecular, cellular and functional level among phyla (Iribarne, 2021).

Indeed, the development and functional characterization of immune cells, as well as the molecular mechanisms of the innate and adaptive immune responses display a high level of conservation between higher vertebrates like mammals, and the zebrafish (Bennett et al., 2001; Renshaw and Trede, 2012).

Innate immune system of the zebrafish primarily composed of neutrophils and macrophages (Sullivan and Kim, 2008b). Both cell types are derived from a common myeloid progenitor line which is characterized by the expression of *pu.1* (Bennett et al., 2001). While macrophage differentiation from myeloid lineage is mostly dependent on a continuous moderate expression of the *pu.1* gene and the transcription factor *irf8* (Li et al., 2011; Shiau et al., 2015), neutrophil maturation is mostly regulated by a separate gene, which will be discussed in detail in the next section (Rosowski, 2020).

Zebrafish neutrophils mostly resemble mammalian counterparts both morphologically and functionally, with dense cytoplasmic granules and segmented nuclei (Davidson and Zon, 2004), as well as with a high level of myeloperoxidase and acid phosphatase activity (Bennett et al., 2001). Neutrophils are the most abundant leukocytic population in the circulation, and are the first to infiltrate to the injured area (Harvie and Huttenlocher, 2015). Emigrational activity and enhanced velocity of neutrophils are key contributors to the innate immune defense (Havixbeck and Barreda, 2015; Yoo and Huttenlocher, 2011).

Deficiency in the emigrational ability of neutrophils or disruption to the chemosensory cascade mostly regulated by CXCR4 signaling pathway (Tulotta et al., 2019), often result in disease phenotypes characterized by chronic neutropenia such as WAS (Ochs and Thrasher, 2006) and WHIM syndrome (Gorlin et al., 2000; Harvie and Huttenlocher, 2015). Therefore, infiltration of neutrophils on the onset of inflammatory response is a crucial step to regaining homeostasis and tissue repair (Wang, 2018). Primary aim of the early arriving neutrophils is to stabilize and sterilize the inflamed area by eliminating foreign agents, necrotic compartments (Havixbeck et al., 2016; Tauber, 2003), and promoting tissue repair by the release of signaling molecules to the tissue microenvironment (Tulotta et al., 2019; Davidson and Zon, 2004).

Zebrafish macrophages present in most tissues as resident phagocytic cells and contribute to tissue maintenance and homeostasis by the constant surveillance for any harmful stimulus (Sugimoto et al., 2019). Tissue resident macrophages exhibit high levels of tissue-specific heterogeneity (Var and Byrd-Jacobs, 2020), which arranges their transcriptional and phenotypical characteristics according to the condition and necessities of specific tissue types (Das et al., 2015). For example, macrophages that are specifically developed to reside and function in the CNS has been given a separate name, *microglia* (Li and Barres, 2018). Circulating macrophages also show inflammation dependent phenotypic plasticity when they arrive at the site of injury, by changing their morphologic and functional characteristics according to the chemotactic signals in the inflammatory microenvironment (Wiegertjes et al., 2016). Pro- (M1) and anti-inflammatory (M2) macrophage subtypes have been characterized in mammals as well as in the zebrafish (Wentzel et al., 2020), as two functionally distinct polarization states, that these cells can exhibit according to the changing states of the inflammatory response (Chazaud, 2014; Nguyen-Chi et al., 2015).

1.4.1. Zebrafish Myelopoiesis During Embryogenesis and Adulthood

Development of the hematopoietic cells in vertebrates, is initiated early in embryogenesis and is carried out continuously throughout the life span of the organism (Robertson et al., 2016; Willett et al., 1999). Similar to mammals, zebrafish blood formation takes place via two successive waves during embryonic development: *Primitive* and *definitive* hematopoiesis (Ellett and Lieschke, 2010; Willett et al., 1999), which are defined by the strictly regulated transcriptional and cellular events (Davidson and Zon, 2004). Primitive wave regulates the generation of early macrophages and erythroid cells through monopotent hematopoietic precursors (Bertrand et al., 2007), while the definitive wave is characterized by the occurrence of definite multipotent hematopoietic progenitors, which are termed as the hematopoietic stem cells (HSCs; Iwasaki and Akashi, 2007), that serve to generate all types of blood cells including erythroid, thromboid, myeloid and lymphoid lineages and sustains hematopoiesis throughout life (Stachura and Traver, 2011; Willett et al., 1999).

In mammals and birds, primitive hematopoiesis emerges in cells of mesodermal origin outside the embryo (Willett et al., 1999), that migrate to the yolk sac and generate the blood islands, and it mainly produces cells of the erythroid lineage (Davidson and Zon, 2004; Zizioli et al., 2019). Later, the hematopoiesis events shift to the aorta gonad mesonephros, and the fetal liver respectively (Bennett et al., 2001), whereas the final and ultimate site of production of all the blood lineages becomes fixed in the bone marrow for the rest of the adult lifespan (Zizioli et al., 2019).

Unlike mammalian species, the zebrafish primitive hematopoiesis starts around 11 hours post fertilization (hpf; Zizioli et al., 2019) at an intraembryonic location between the notochord and endoderm of the trunk, which is termed as the intermediate cell mass (ICM; Willett et al., 1999), as well as in the rostral blood island (RBI) under the head, and the posterial blood islands in the tail region (Bennett et al., 2001; Davidson and Zon, 2004). ICM serves as an analogous structure to the mammalian blood islands, as the primal sites where the primitive hematopoiesis is initiated (Willett et al., 1999). ICM is dedicated to produce only cells from erythroid lineage, while the cells of the myeloid lineage including early macrophage precursors are generated anteriorly in the RBI (Davidson and Zon, 2004).

In the primitive wave of blood formation, expression of several genes that are essential for HSC formation such as *gata2*, *scl*, and *lmo2*, as well as early erythroid markers like *gata1* can be detected at early somite stages (Bennett et al., 2001; Stachura and Traver, 2011). One of the earliest and essential regulators of the myeloid lineage, is the transcription factor *pu.1*, which is expressed as early as 16 hpf and gradually decrease at 28 to 30 hpf (Bennett et al., 2001) meanwhile the early myeloid precursors start to express more specific monocyte/macrophage and neutrophil lineage genes such as *c/ebp1*, *fms*, lymphocyte cytosolic protein 1 (*lcp1*), also known as L-plastin, lysozyme-c (*lyz*), *mfap4*, *mpeg1*, *csf1ra* and *mpx* (Xu et al., 2012). Circulation starts approximately at 24 hpf and some of the primitive macrophages enter the circulation via the ducts of Cuvier (Davidson and Zon, 2004), while others disperse to seed the other regions in the head (Stachura and Traver, 2011). Functionally active primitive macrophages can carry out phagocytosis of erythrocytes and combat bacterial infection at this stage (Davidson and Zon, 2004). Functionally mature neutrophils with detectable cytoplasmic granules occur at 33-35 hpf with decent expression of neutrophil specific myeloperoxidase *mpx* (Bertrand et al., 2007).

Final act that terminates the primitive and transient wave of blood formation in zebrafish is defined by the migration of the hematopoietic progenitors in the posterior blood island, to the circulatory system (Bennett et al., 2001). Definitive hematopoiesis is initiated when the first HSCs emerge and lasts until the end of the organism's life span (Ellett and Lieschke, 2010). The HCSs first occur from the aortic endothelium at the ventral wall of the dorsal aorta (Stachura and Traver, 2011). From 48 hpf, they travel to the caudal hematopoietic tissue, and they migrate to the kidney as final destination where adult hematopoiesis occurs throughout the rest of the lifespan (Stachura and Traver, 2011; Xu et al., 2012).

Kidney serves as the primary and definitive hematopoietic center of adult zebrafish and is considered analogous to the mammalian bone marrow in terms of cellular arrangement and structure (Davidson and Zon, 2004; Willett et al., 1999). The kidney also carry out renal duties while the hematopoietic parenchyma is situated in between the renal tubules and blood vasculature (Lieschke et al., 2001; Menke et al., 2011). On the other hand, T-lymphocytes are generated in the thymus similar to mammals (Stachura and Traver, 2011).

In addition, cells of lymphoid lineage do not emerge until around 19 days post fertilization (dpf), which also makes larval zebrafish a great model to study innate immunity in isolation (Bader et al., 2021; Davidson and Zon, 2004). The zebrafish kidney is a thin layer of tissue attached to the ventral side of the spinal cord (Menke et al., 2011). The anterior part is referred as the head kidney and has a denser hematopoietic activity, while the posterior part of the organ termed as "trunk kidney" has a more abundant distribution of the renal tubules (Stachura and Traver, 2011). HSCs and all lineages of mature hematopoietic cells (except for T-lymphocytes) along with their precursors are found in the adult kidney parenchyma (Lieschke et al., 2001).

The spleen is also an important member of the zebrafish immune system, despite is lacks any hematopoietic precursors and thus do not host the generation of new blood lineages (Stachura and Traver, 2011). Like other teleost fish, zebrafish do not possess lymph nodes, which help filtering the pathogenic or noxious factors floating in the body and help combat infection in other organisms (Renshaw and Trede, 2012). Instead, this essential duty is fulfilled by the *elliposids* within the splenic parenchyma (Menke et al., 2011).

Macrophages and reticular cells form peripheral layers around the splenic arterioles, forming the ellipsoids, and filter the incoming blood to eliminate unwanted substances from the circulation and contribute to the immune defense (Lieschke et al., 2001; Menke et al., 2011). Therefore, the splenic tissue contains a predominant population of erythrocytes and macrophages (Davidson and Zon, 2004).

In recent decades a mass regulator of the neutrophil differentiation from common myeloid lineage has been identified (Liongue et al., 2009; Richards et al., 2003). *Granulocyte colony stimulating factor receptor* (GCSFR or CSF3R), is the receptor for the cytokine *granulocyte colony stimulating factor* (GCSF or CSF3; Demetri and Griffin, 1991). Both *gcsf* and *gcsfr* encode members of the class I cytokine receptor signaling cascade (Liongue et al., 2009), exhibiting high level of genomic, transcriptional and proteomic conservation between mammals and the zebrafish (Pazhakh et al., 2017). The zebrafish *csf3r* locus is located on chromosome 16 (ZFIN ID: ZDB-GENE-080104-4), while the two cognate ligands *csf3ra* (ZFIN ID: ZDB-GENE-091229-1) and *csf3rb* (ZFIN ID: ZDB-GENE-141212-221) are located on chromosome 12 and 19 respectively (Pazhakh et al., 2017). CSF3R signaling is an essential perquisite for the granulopoiesis of the neutrophil precursors, while also mediating the normal migration, proliferation, and anti-pathogenic abilities of neutrophils (Havixbeck and Barreda, 2015). In physiological conditions, CSF3R is expressed in low basal levels dedicated myeloid progenitors, neutrophils, and monocytes (Liongue et al., 2009). In response to stress conditions such as a pathogenic invasion, the expression of the receptor is enriched, and it works in collaboration with the downstream pathways such as the JAK/STAT cascade (Coates et al., 2011; Liongue et al., 2009).

1.5. Functional Studies on Innate Immunity in Adult Zebrafish

Identification of the genomic and phenotypic characteristics of the innate immune cells offers a fundamental contribution to the investigation of their involvement in tissue repair and regeneration.

However, a sophisticated and complicated interplay of diverse cellular and molecular mechanisms mediates the inflammation as well as regenerative processes (Keightley et al., 2014) and may only be investigated by the contribution of multi-dimensional approaches. *In vivo* functional experimentation is both necessary and essential for these reasons. Functional and transcriptional regulation of the immune system along with most disease phenotypes in zebrafish exhibit high similarity with mammals (Sullivan and Kim, 2008). Therefore, functional studies on innate immunity in zebrafish may give reliable insight about the mammalian counterparts (Sullivan and Kim, 2008). One of the most effective methods to functionally examine innate immune cell behavior *in vivo* is cell type specific depletion assays (Keightley et al., 2014). In recent decades, neutrophil and macrophage specific depletion methods in adult zebrafish have been established and optimized by numerous research groups (Rosowski, 2020). Clodronate liposome injection is a toxin-based method providing highly specific temporal depletion of macrophage populations in adult zebrafish (van Rooijen and Hendrikx, 2010). On the other hand, morpholino induced knock-down is a genetic method used for temporal gene silencing and it is one of the most effective approaches to achieve a significant reduction in systemic neutrophil numbers in larval and adult zebrafish (Sullivan and Kim, 2008).

1.5.1. Clodronate Liposomes

Clodronate (Dichloromethylene-Bisphosphonate) has been widely utilized since 1960s to prevent resorption in bone related diseases like osteoporosis and Paget's disease, as well as in treatment of cancer to inhibit tumor growth in multiple myeloma (Opperman et al., 2019) and breast cancer (Fleisch, 2001; Pavlakis et al., 2005). Injection of the substance provides a temporal elimination of macrophage populations and offers an advantage over transgenic models in the sense that the husbandry of immune-deficient transgenic zebrafish may be challenging.

Clodronate is a synthetic analogue of inorganic pyrophosphate (Moriyama and Nomura, 2018). When cells use clodronate instead of endogenous pyrophosphate, a non-hydrolysable form of ATP is produced, blocking the respiratory pathway (Moriyama and Nomura, 2018). Encapsulating clodronate into liposomes provides an efficacious *in vivo* delivery approach (Rosowski, 2020).

When introduced into animals via intravenous (IV) or IP injection, clodronate liposomes are effectively and specifically engulfed by macrophages but not by other phagocytes due to their relatively large size (van Rooijen and Hendrikx, 2010). Because of its highly hydrophilic nature, clodronate cannot pass the liposomal membranes as well as the phospholipid bilayer of the cell membrane after release into the cytoplasm (van Rooijen and Hendrikx, 2010). When a certain intracellular concentration of clodronate is reached, macrophages undergo apoptosis (Moreno, 2018). In addition clodronate does not pose a toxicity in the blood-stream when released from dead macrophages since its lifespan in circulation is quite short and is immediately eliminated from the body by the renal system (Moreno, 2018).

1.5.2. Vivo-Morpholino Knockdown of Target Genes

Morpholinos (MOs) are antisense oligonucleotide analogs that interfere with the translational pathway of the target mRNA and block protein production, thereby knocking-down gene expression/protein levels (Summerton, 1999; Timme-Laragy et al., 2012). MOs consist of approximately 25 bases, attached to a synthetic non-ionic backbone including methylenemorpholine rings instead of ribose (Timme-Laragy et al., 2012). MOs mechanism of function is primarily based on complementary binding to target RNA sequences and prevent RNA processing, or block translation via presenting steric hindrance on the endogenous target RNA transcript (Morcos et al., 2008). To enable a more efficient delivery into the cells, an octa-guanidine dendrimer moiety has been added to the 3’ site by covalent interactions, which is then referred to as a Vivo-Morpholino (VMO; Morcos et al., 2008). They are highly stable within intracellular environment as they are not affected by nuclease-mediated degradation (Summerton, 1999). In addition, they show minimal off-target effects due to high specificity of the antisense sequence (Morcos et al., 2008; Summerton, 1999). Injection into the blood circulation or to the body cavity is sufficient to introduce the morpholino solutions since they facilitate their own intracellular delivery and do not require any additional methods (Morcos et al., 2008).

Morpholino knock-down is used widely in the embryonic and larval zebrafish (Bernut et al., 2020; Liongue et al., 2009), however the efficiency and reliability of the application has been also proved in the adult zebrafish by several research groups (Kim et al., 2010).

Cerebroventricular microinjection has been developed as a novel approach to deliver MOs into the CNS of adult zebrafish (Kizil et al., 2013). VMOs was also utilized to piggyback multiple antisense deoxyoligomeres into the cell and down-regulated multiple genes simultaneously in the adult zebrafish (Raman et al., 2020). In a separate study in adult zebrafish, thrombocyte function was effectively down-regulated within 24 h after intravenous application of VMOs (Kim et al., 2010). In recent years, retro-orbital (RO) injection has been described in detail as an effective delivery method of MOs into adult zebrafish circulatory system (Kim et al., 2018).

2. PURPOSE

Mammals exhibit a limited regenerative ability of lost or damaged nervous system tissues due to a restricted number of active stem cell niches. On the other hand, the peripheral olfactory system sustains the OSN population via a life-long continuous turnover. In contrast to higher vertebrates, regenerating organisms like the zebrafish, shows an extensive capacity of achieving full structural and functional recovery of the central and peripheral nervous system. Any type of tissue injury is accompanied by the unfolding of an immune response; therefore, tissue repair and regeneration events are intertwined with mechanisms of the immune system. The dynamics of the inflammatory response characterize and often regulate the extent and outcome of regeneration. This study aims to investigate the selective contribution of primary innate immune cells, neutrophils, and macrophages, to the peripheral OE regeneration and OSN neurogenesis in an experimental injury model in the adult zebrafish.

The works presented in this thesis comprises two sets of experiments. The first part focuses on the characterization of the innate immune cell recruitment to the injured OE, while the second part describes the experimental outcomes of the functional characterization of innate immune cell contribution to OE regeneration and neurogenesis. The procedures described in the first section consist of the establishment of a reproducible histochemical protocol to selectively label the innate immune cells, and the analysis of their basal occupancy in the intact tissue. Selective recruitment of neutrophils and macrophages to the OE after traumatic injury will be further presented via qualitative and quantitative evidence. The second part of the thesis aims to understand the functional contribution of neutrophil and macrophage behavior to OE regeneration, by utilizing genetic or toxin-based manipulation methods to achieve cell-type specific depletion of neutrophils and macrophages. IP injection of clodronate liposomes will be applied to provide temporal systemic elimination of macrophage populations, while RO injection of antisense VMOs will be applied to down-regulate the granulopoiesis and achieve systemic reduction of neutrophil abundance. The proliferative and neurogenic activities in the injured OE will then be comparatively analyzed to elucidate the functional impacts of neutrophils and macrophages to zebrafish OE regeneration.

3. MATERIALS AND METHODS

3.1. Materials

3.1.1. Animals

Adult zebrafish (*Danio rerio*) (>6 months old) from AB/AB strain that were bred to reproduce in the facility or zebrafish acquired from local pet shops were used in this study. Animals were maintained in the experimental animal production and care unit (Vivarium) of Boğaziçi University Centre for Life Sciences and Technologies.

3.1.2. Equipment and Supplies

The collection of the chemicals and reagents, as well as disposable and non-disposable equipment used in this study are listed in Appendix A and B.

3.1.3. Buffers and Solutions

Buffers and solutions used in fish maintenance and molecular biology assays were prepared with reference to "The Zebrafish Book" (Westerfield, 2007). Exclusive buffers and solutions are described in the related methods sections.

3.2. Methods

3.2.1. Animal Maintenance and Husbandry

The zebrafish were maintained in a large system supplied with artificial fish water with water and air circulation systems, porous cylinder, carbon filters, and UV light filtration.

Artificial fish water was prepared by adding 2,0 g sea salt, 7,5 g sodium bicarbonate and 0,84 g calcium sulfate to 100 liters of reverse osmosis water. The fish were kept in 1, 3 or 10 - liter tanks in a maximum density of 5 fish per liter. The room was kept at approximately 28,0 ^{o}C and a proper day-night cycle (14 h/10 h) was provided with the automated lighting system. A general cleaning was made every week in which changing and cleaning of tanks with debris or moss formation as well as changing cylinder and carbon filters would take place.

The fish were fed twice a day with flake food, egg yolk and frozen or live brine shrimp (*Artemia sp.)*. Egg yolk was prepared by separating the yolk of freshly boiled eggs, the yolks then mashed and spread on a tray to be left in 60 ^{o}C oven overnight to dry. The dried yolks were then converted to powder form with the help of a blender, separated to small containers and the covers were sealed with parafilm. The yolks were then stored at – 20 ^{o}C ready to use. In order to prepare live brine shrimps, fish water with additional sea salt and a trace amount of sodium bicarbonate was prepared in a cylinder container with an aeration pump attached. The brine shrimp cysts were then added, and live brine shrimps were collected and fed to the fish after 48 hours.

The permission to use experimental zebrafish as a model organism in this study was acquired from the Institutional Ethics Board for Animal Experiments at Boğaziçi University (BUHADYEK) titled as “The contribution of innate immune cells and cytokine expression to zebrafish olfactory system regeneration.” (Ref. No.: E-44697215-050.01.04-8409). All procedures in this study were performed following the ethical instructions defined by the National Animal Protection Act (law number 5199, enactment date 24.06.2004) as well as the directive 2010/63/EU of the European Parliament and of the Council of 22 September 2010 on “The Protection of Animals Used for Scientific Purposes”.

3.2.2. Chemical Lesion of the OE by Nasal Irrigation with TrX

Chemical lesion of the OE was performed by nasal delivery of 1% TrX with a microinjector (FemtoJet express, Eppendorf). 1% TrX solution was prepared by dissolving 5 µl of TrX in 395 µl 1x PBS (pH 7,4) and 100 µl phenol red. In order to acquire maximum homogeneity, the solution was vortexed for 90 seconds.

Fish were anesthetized in 160 mg/l MS222 dissolved in tank water until the opercular movements decelerated and there is no reflexive response to tactile stimuli. Fish were placed dorsal side up on a wet sponge with a slit. The trunk was covered gently with a wet tissue paper and placed under a dissection microscope (Zeiss). TrX (1%) solution was delivered to the left nasal cavity twice in 45 second intervals, within a total incubation period of 90 seconds. The solution was washed off with a gentle influx of tank water delivered with a Pasteur pipette. The fish was transferred back to tank.

3.2.3. Depletion of Macrophages by IP Injection of Clodronate Liposomes

Temporal systemic elimination of macrophages was established by IP injection of clodronate liposomes (Liposoma BV, SKU: CP-005-005). Liposome suspensions were stored at + 4 ^{o}C refrigerator. The containers were gently stirred to homogenize the suspension and aliquots were let reach room temperature before administration. To prepare the injection solution, 10 µl (5 mg/mL) of clodronate ($CH_4Cl_2O_6P_2$) or PBS containing liposome suspension; 5 µl of 1x PBS; 2 µl of phenol red were mixed with the help of a micropipette on a piece of parafilm. The injection solution was then taken up by an insulin syringe (U-100; 30G) and unwanted air bubbles were eliminated by gentle manipulation of the syringe.

Fish were anesthetized applying the same steps described above in section 3.3.2. The fish were positioned ventral side up on a wet sponge with a slit in the middle in order to fit and immobilize the fish. The sponge was then placed under a dissection microscope (Zeiss). The scales between the two pelvic fins were gently manipulated by the tip of the needle to make direct contact with the skin. The needle with the bevel side looking up was pushed gently at a 45^{o} angle to penetrate the abdominal cavity. After the tip of the needle pierced the peritoneal wall, the syringe was positioned almost at a 180^{o} angle and pushed gently towards the apical side of the fish from beneath the abdominal cavity and the solution was released inside. The syringe was gently pulled out from the same route.

In the experimental procedure each fish was injected clodronate- or PBS-containing liposome suspension 24 h prior to nasal irrigation by TrX. Following injection, the fish were transferred back into tank water.

In the experiments that required the fish to be dissected at 5 days post TrX treatment, clodronate liposome injections were applied every day to maintain low systemic levels of macrophages throughout the experimental period.

3.2.4. Preparation of Vivo-Morpholino Solutions for Injection

VMOs (Gene Tools) arrived in freeze-dried solid form in sealed sterile glass vials. VMOs against *csf3r* transcript were acquired with the sequence of: TTTGTCTTTACAGATCCGCCAGTTC; and Vivo Standard Control were acquired with the sequence of 5' CCTCTTACCTCAGTTACAATTTATA 3'. VMO stock solutions were prepared following the instructions of the manufacturer by dissolving the morpholinos in powder form in sterile pharmacy water to a final concentration of 0,5 mM and the concentrations were checked with a Nanodrop spectrophotometer (Thermo Scientific).

3.2.5. Retro Orbital Injection of Vivo-Morpholinos

Retro orbital injection was used to deliver the VMOs (Gene Tools) to the zebrafish bloodstream (Pugach et al., 2009). In this procedure the injection solutions were delivered to the retro orbital venous sinus behind the eye.

The injection solution was prepared with 2 µl of vivo morpholino against *csf3r* (0,5 mM) or vivo standard control morpholino (0,5 mM) and 2 µl of FITC-Dextrane 70 kDa fluorescent dye (50 mg/ml dissolved in 1x DPBS) mixed on a piece of parafilm. The fish were anesthetized with MS222 as described in section 3.3.5 and placed right lateral side up such that the anterior side on a wet sponge under a dissection microscope. A U-100 insulin syringe (30G) was positioned bevel side up at a 45^{o} angle to the antero-posterior axis of the fish. The needle was gently inserted 1-2 mm between the eye socket and the eyeball, to 7 o'clock position. The solution was delivered, and the needle was gently retracted. The fish were kept on the sponge for 30 – 45 seconds after the injection to provide maximum diffusion of the delivered substance to the circulatory system. The fish were then transferred back to fresh tank water and the fluorescent signal was checked under a stereomicroscope (Leica) 3 - 5 minutes after the injection.

3.2.7. Labelling Mitotic Activity by Thymidine Analogue Incorporation

To visualize dividing cells, the zebrafish were incubated in tank water containing 30 mg/l of the halogenated thymidine analog 5-Bromo-2-Deoxyuridine (BrdU; Sigma) at 28 ºC in dark or injected intraperitoneally (IP) with 25 µl of 10 mM 5-Ethynyl-2'-Deoxyuridine (EdU; Thermo Fisher). Visualization of the incorporated BrdU was established by following the regular steps of the histochemical procedure with an anti-BrdU primary antibody (Abcam). Visualization of the incorporated EdU was established with Edu Click-iT^{TM} (Molecular Probes; REF: C10337; LOT: 1654343) reaction with Alexa Fluor 647 azide following the manufacturer's recommendations. Following the regular application of the immunohistochemistry procedure, the sections were incubated with EdU detection solution for 30 minutes at room temperature in a moist incubation chamber. The detection solution was discarded, and the sections were washed with 1x PBST (0,1%) for 10 minutes and with 1x PBS twice for 10 minutes in Coplin jars on a shaker.

3.2.8. Dissection of the Olfactory Organ

The fish were anesthetized by an overdose of MS222 and were immediately transferred to ice - water mixture which leads to sudden fatal hypothermia followed by euthanasia. After the opercular movements stopped, the fish were decapitated with the use of a surgical blade and the heads were placed in dissection plates filled with ice – cold 1x PBS.

Under a dissection microscope (Zeiss), the lower jaw was cut and removed with a multiple scissors. Both eyes were removed with fine forceps and the olfactory organs (OO) were exposed to lateral view by gently peeling of the outer skin residues. The nasal bones were cracked open to expose the soft OE tissue inside. The OOs were scraped and detached from the nasal bones and transferred immediately to a mold filled with optimal cutting temperature compound (OCT) to protect the tissue integrity and transferred to – 20 ºC freezer. After the OCT compound was firmly frozen, the molds were wrapped tight in aluminum foil and labelled, to be stored within 50 ml falcon tubes until cryosectioning.

3.2.10. Dissection of Kidney and Spleen

The fish were euthanized using the same steps described in section 3.2.7. After decapitation with surgical blade, trunk section of the fish was transferred to a dissection dish filled with ice cold 1x PBS. Under a dissection microscope (Zeiss) the fish was kept in a position that the ventral side was looking up. With the help of a micro dissection scissors, the peritoneal wall was cut open starting from the previous decapitation incision, all the way to the anterior tail section. Abdominal cavity was then exposed with the help of forceps and the fish was pinned to the dissection dish in that position using dissection pins to provide immobilization for further steps of the dissection. The intestine, pancreas, liver, and spleen that were sitting in the abdomen as a bundle were removed together. The spleen was dissected from that bundle of organs by gently manipulating the connecting tissue.

To dissect the kidney which is sitting just ventral to the backbone of the fish, the ribs in the precaudal vertebrae were removed to detach the lateral margins of the head kidney. Then starting from the now detached head kidney, the tissue was very gently scraped from the backbone. The dissected organs were immediately embedded into OCT filled molds and transferred to – 20 ^{o}C freezer. The molds were stored as described in section 3.2.7.

3.2.11. Cryosectioning of Tissue Samples

Dissected tissue samples were immediately placed within elastic molds filled with OCT and were left to freeze at - 20 ^{o}C for 10 – 15 minutes. The frozen blocks of OCT were situated on a Leica cryostat (CM30505) with chamber temperature of – 21 ^{o}C and object temperature of – 19 ^{o}C. Horizontal sections of 12 µm thickness were carefully transferred to positively charged slides (Super-Frost Plus, VWR). The slides were placed in individual petri dishes and air dried for 1,5 – 2 hours at 63,5 ^{o}C in a drying oven. For long term storage the petri dishes were sealed with parafilm and kept in – 80 ^{o}C freezer until use.

3.2.12. Heat Inactivation of Goat Serum

The serum bottle (Normal Goat Serum; P30-1001; Pan Biotech) was taken from – 20 ^{o}C storage and was let to thaw in room temperature for several minutes.

A control bottle of same size was filled with water and was put side by side with the goat serum in 56 ºC water bath. The water level was adjusted to not to pass the serum level and reach the cap, as it may affect the integrity of the serum container. A thermometer was set to sit in the water bottle without touching the bottom or sides to monitor the temperature. The bottles were gently swirled every 3 - 4 minutes to acquire homogeneous heating. After the temperature reached 56 ºC, the serum was incubated for 30 minutes. The serum was then immediately transferred to ice and every step were performed on ice from that point. To use in immunohistochemistry assays, 5 % goat serum in PBS - T (0,1 %, pH 7,4) was prepared and aliquoted to 1,5 ml tubes to be stored at – 20 ºC until use.

3.2.13. Immunohistochemistry

The tissue sections that were cryosectioned on glass slides were kept at – 20 ºC for long term storage. The slides were taken from the storage freezer and let reach room temperature. The edges were covered by a hydrophobic PAP-pen (Liquid Blocker).

Table 3.1. List of primary antibodies.

Antigen	Host	Dilution	Manufacturer	Cat. No.
Mpx	Rabbit	1:600	Genetex	GTX128379
Mfap4	Rabbit	1:600	Abcam	Ab229543
Lyz	Rabbit	1:500	Genetex	GTX132379
Lcp1	Rabbit	1:500	Genetex	GTX124420
HuC/D	Mouse	1:600	Life Technologies	1661237
BrdU	Rat	1:250	Abcam	Ab6236

The sections were then rehydrated with 1x PBS for 10 minutes and fixed with cold PFA (4,0% in 1x PBS) for 15 minutes. The slides were put in a Coplin jar and washed with 1x PBST (0,1%) three times for 10 minutes on a shaker (Heidolph).

To disrupt the nucleus and expose the BrdU (if present) that was incorporated into the DNA, the sections were treated with 4 N HCl for 15 minutes. The slides were rinsed with PBS and washed with PBST three times for 10 minutes on a shaker. The tissues were then blocked with 5% Goat serum in 1x PBST for 1 hour at room temperature. The primary antibody solutions prepared in 5% Normal Goat Serum (Pan Biotech) were applied on the slides and left for incubation overnight (16 - 18 h) at + 4 ^{o}C in a moist incubation chamber.

Table 3.2. List of secondary antibodies and imaging kits.

Antigen	Fluorophore	Dilution	Manufacturer
Mouse/rabbit/rat IgG	Alexa Fluor 488	1:800	Genetex
Mouse/rabbit/rat IgG	Alexa Fluor 555	1:800	Genetex
Mouse/rabbit/rat IgG	Alexa Fluor 633/637	1:800	Genetex
Mouse IgG	Cyanine 5 (Cy5 - 647)	1:250	Genetex
-	Azide - Alexa Fluor 647		

Primary antibody solutions were recovered and stored at - 20 ^{o}C. The sections were rinsed with PBS and washed with PBST three times for 10 – 15 minutes. Secondary antibody solutions were prepared in 5% GS and the sections were incubated in secondary antibody solution for 2 hours at room temperature in a humid incubation chamber. At the end of the incubation period the sections were washed with PBS three times for 15 minutes to be ready for imaging.

3.2.14. Imaging with Confocal and Stereo Microscopy

Stained tissue sections were visualized by confocal microscopy with Leica upright SP5-AOBS with x20 or Leica inverted TCS SP8 with x40 magnification lens.

The images were captured at 1024 x 1024 or 2048 x 2048 - pixel resolution and 400 Hz acquisition frequency. Line average of 4 – 8 was used for each channel in order to improve the image quality. In order to eliminate the potential cross talk between certain channels, sequential visualization was used in these circumstances.

3.2.15. Image Processing and Quantitative Analysis

Images of the immunostained tissue sections were processed in FIJI open-source image processing software version 2.3.0./1.53q (Schindelin et al., 2012) and proper brightness / contrast adjustments were applied. To do a quantitative analysis on marker - positive cells in the OE, a rectangular frame having the short edge / wide edge ratio of 2/3 was drawn automatically with a custom macro. The wider edge of the frame was set parallel to the horizontal axis of the image frame and vertical to the median raphe of the OE, and it extended from the tip of the ILC to the tissue periphery of each hemi-OE while the vertical short edge of the frame was also vertically centered.

Two rectangular frames from each OE image were then cropped and saved as separate files. Using the pointer tool, the desired marker – positive cells were counted in each channel and plotted to the region of interest (ROI) manager which records the number and location of the marks. Using a custom macro these ROI data were processed and converted into an RGB image (mask) in which the markings in each channel were assigned a color (red, blue, green). The radial axis of the hemi-OEs were split into 10 equidistant bins and the markings were counted and corrected using R scripts. The data were plotted on xy graphs to present the positional profiling of the marker positive cells and bar graphs were used to determine the total number of marker positive cells.

In order to define the level of neuronal regeneration in the OE, the area covered by HuC/D-positive cells relative to the whole OE tissue area were calculated and normalized using FIJI software. Single channel (HuC/D) images of the entire OE were thresholded, the area covered by HuC/D-positive cells and the whole OE tissue were recorded to ROI manager. The relative are covered by HuC/D-positive cells in each experimental condition were normalized to the controls group.

Two-tailed unpaired Student's t-test with 95% confidence interval were performed in Prism version 9.1.1. for MacOS (Graph Pad, USA) and SPSS data analysis and graphing software. ANOVA (Analysis of Variance) with Tukey's multiple comparisons test with individual variances computed for each comparison, with 95% confidence interval were performed in Prism and SPSS 27 (Licensed by the Institute) software. The graphs were prepared in Prism version 9.1.1. software or R version 4.0.4. programming software and arranged in Adobe Illustrator version 25.4.1.

4. RESULTS

The inflammatory response is mediated by the innate immune cells, mainly neutrophils and macrophages. Their prominent roles in tissue repair and regeneration have been demonstrated in diverse tissue contexts including but not limited to the liver (Iribarne, 2021; Karin and Clevers, 2016), heart (Kaveh et al., 2020), skeletal muscle (Chazaud, 2020; Yang and Hu, 2018) and CNS (Kokaia et al., 2012; Var and Byrd-Jacobs, 2020). Zebrafish has been considered as a well-suited experimental model to study the innate system due to the high morphological and functional similarity of the hematopoietic cells, as well as molecular factors involved in the inflammatory process. In addition, high capacity of the zebrafish to regenerate diverse tissue types like central and peripheral nervous system, which is very limited in higher vertebrates makes it an even more excellent candidate for the experimental procedures described in this study, since it focuses on the interplay between the innate immune cells and the regeneration and neurogenesis of the olfactory system.

The aim of this study is to investigate the potential contribution of the innate immune cells to olfactory system regeneration and OSN neurogenesis. The works in this thesis were described within two sets of experiments: The characterization of the innate immune cells and their recruitment to the injured OE, and the functional analysis of innate immune cell contribution to OE regeneration and neurogenesis. The first subsection will cover the establishment of a reliable approach to identify innate immune cells and the characterization of the basal abundance of neutrophils and macrophages in the OE under physiological conditions. Innate immune cell behavior will be further investigated in an experimental injury model that has been developed to study repair neurogenesis in the OE of zebrafish. The second half of the thesis will focus on the functional examination of the neutrophil and macrophage behavior by the application of systemic cell depletion assays. Morpholino induced knock-down will be used to impair neutrophil granulopoiesis and reduce the systemic abundance of mature neutrophils, while clodronate liposomes will be used to deplete macrophage populations. The functional analyses will cover the inspection of the efficacy of the proposed depletion approaches, then the potential effects of the temporal elimination of neutrophils and macrophages to the efficiency of OSN neurogenesis in the OE after chemical injury will be established.

4.1. Identification of Resident Innate Immune Cells in the Intact OE

Neutrophils and macrophages are the two major innate immune cells that mediate the acute inflammatory process. To understand their potential contribution to tissue repair and regeneration in the context of the experimental injury model utilized in the zebrafish olfactory system, candidate markers that selectively label neutrophils and/or macrophages in the zebrafish were tested in the primary hematopoietic organs, as well as in the OE. Following the confirmation of the reliable markers for these cell populations, the basal occupancy of these cells in the intact OE was assessed under physiological conditions to serve as a reference point for the further procedures that involve experimental injury.

4.1.1. Mpx and Mfap4 are Reliable Markers to Selectively Label Neutrophils and Macrophages in the Zebrafish OE

To identify the innate immune cells and track their behavior, commercially available zebrafish - reactive antibodies were selected. Myeloid specific peroxidase is encoded by the *mpx* gene in the zebrafish, which is highly expressed in neutrophils and is the most commonly used marker for neutrophilic granulocytes due to its high specificity (Bennett et al., 2001; Renshaw et al., 2006; Rosowski, 2020). Mpx is a toxic enzyme that is stored within neutrophilic granules and released in times of inflammation to combat foreign pathogens. Lysozyme C which is encoded by the *lyz* gene in zebrafish is a glycosyl hydrolases that helps in host defense against pathogen invasion with its ability to disrupt and to break down the bacterial cell wall leading to lysis. Although Lyz is predominantly expressed in cells of the myeloid lineage in the early stages of development, it is specific for neutrophilic granulocytes after 2 dpf and can be considered as an alternative neutrophilic marker (Kitaguchi et al., 2009; Rosowski, 2020). Lcp1 is a crucially important protein in cytoskeleton arrangement, and cell migration with its actin bundling ability (Morley, 2012). Lcp1 is highly expressed in neutrophils, macrophages, and monocytes, and therefore has been defined as a reliable pan-leukocyte marker (Kell et al., 2018).

Microfibril-associated glycoprotein 4 (Mfap4) is an ECM protein that is highly expressed in vascular smooth muscles that encapsulate blood vessels and has been demonstrated as an important regulator of elastic fiber assembly, cell adhesion and migration (Walton et al., 2015). Mfap4 has recently been discovered as a highly specific marker for macrophages and monocytes (Walton et al., 2015). Although the selected markers are well established to specifically label different leukocyte populations in transgenic zebrafish, there is no reported analysis on their visualization via immunostaining in the OE. Therefore, to test the validity of the selected markers and define a reproducible experimental protocol, immunohistochemistry against the selected markers Mpx, Lyz, Mfap4, and Lcp1 were applied on dried, thin cryosections (12 μm) of the zebrafish OO on separate slides (Figure 4.1a). The OEs were also counterstained against the pan-neuronal marker HuC/D for acquisition of a visual reference of the OE morphology. In Figure 4.1a two representative confocal images were displayed for each leukocyte marker: Lyz (green; top left), Mpx (green; bottom left), Lcp1 (green; top right), Mfap4 (green; bottom right). Whole OE images are located on the left while the magnified displays of the OE regions within dashed boxes are shown on the right for each marker.

Lyz-positive neutrophils were mostly located near the tissue margins as well as the SNS and the non-sensory OE, where they mostly possessed ramified morphologies as represented with arrowheads in magnified confocal image on the top left (Figure 4.1a). A Lzy-positive neutrophil associated with a HuC/D positive OSN can be observed near the non-sensory region, and is indicated with an asterisk, demonstrating that Lyz positive neutrophils may phagocytose apoptotic OSNs, which is a consistent with their supposed neutrophilic function. These cells may contribute to turnover of OE cells and facilitate maintenance neurogenesis under homeostatic conditions. In contrast, Mpx-positive neutrophils populated the intact OE in larger numbers than Lyz-positive cells in addition to expressing a more spherical cellular morphology with big, distinguishable nuclei as represented in the Figure 4.1a bottom left. These cells were located along the region covering the SNS border and the non-sensory OE in groups of few cells, as well as individual neutrophils. Consistent with the prior studies on zebrafish larvae (Palominos and Whitlock, 2021), Mpx-positive cells were also observed to be associated with nasal blood vessels that surround individual epithelial folds and pass by the median raphe and are denoted with the asterisk on the bottom left of Figure 4.1a.

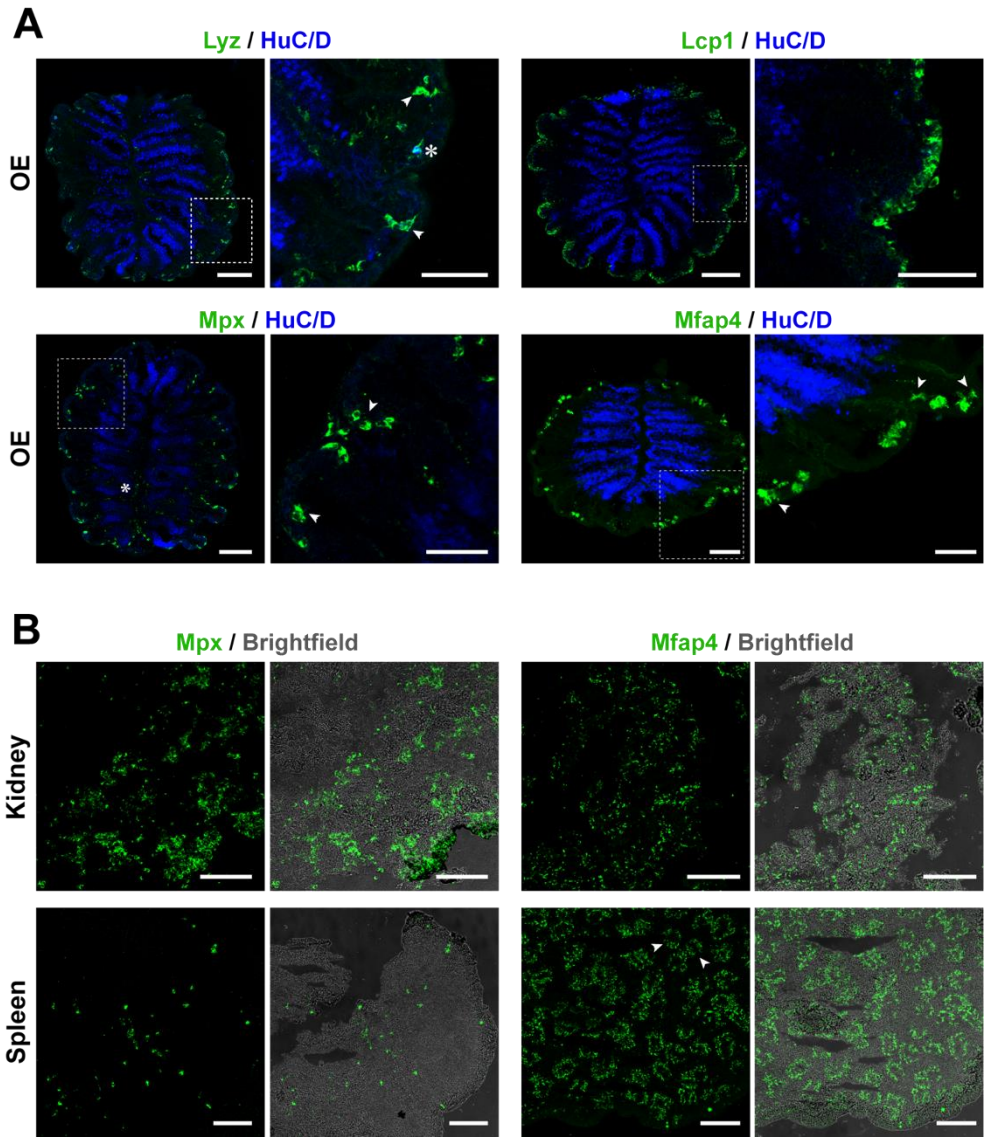

Figure 4.1. IHC is a reliable method to analyze innate immune cell behavior. (a) IHC against selected leukocyte markers (green) and the pan-neuronal marker HuC/D (blue). Whole OEs are shown on the left, magnified display of the respected regions with dashed boxes are shown on the right. Scale bars: 100 μm, 50 μm (for magnified images). (b) IHC against Mpx and Mfap4 on kidney and spleen sections. Scale bars: 100 μm.

The cells that were associated with circulatory blood vessels were thinner and possessed a spindle-shaped cellular morphology. The cellular morphologies and the spatial distribution of Mpx positive neutrophils in the intact OE were consistent with previous studies which established visualization of neutrophils in transgenic adult zebrafish (Palominos et al., 2022).

The pan-leukocyte marker Lcp1 labelled a large number of small cell-like structures in the peripheral margin of the OE, forming a thin ring around the OO (Figure 4.1a; top right). However, the individual structures did not possess a consistent cellular shape, nor the characteristic myeloid cell morphology. Lcp1 immunoreactivity was completely absent from the sensory and son-sensory OE and were limited to the periphery of the OO where a meningeal layer wraps around the tissue periphery.

Mfap4-positive cells could be observed to align with the peripheral margin of the intact OE near the outer meningeal tissue layer (Figure 4.1a; bottom right). These cells had mostly ramified profiles. The cellular branches were clearly observable in the immunoassayed sections, which is consistent with their macrophage identity. Mfap4-positive cells were not observed to be located within the sensory epithelial tissue nor were they physically associated with it in the intact OE, which is consistent with the recent findings from transgenic juvenile fish (Palominos and Whitlock, 2021).

In summary, different potential leukocyte markers were tested for their ability to label specific cellular subpopulations in the intact adult zebrafish OE. The specificity of their staining patterns, the morphological characteristics of stained structures were comparatively evaluated against recent findings using transgenic embryonic and juvenile zebrafish. Based on their strong and selective staining pattern, Mpx and Mfap4 were selected as valid and efficacious markers for neutrophils and macrophages/monocytes, respectively to selectively label innate immune cells in the adult zebrafish OE.

To further confirm the specificity and selectivity of anti-Mpx and anti-Mfap4 antibodies, IHC against Mpx and Mfap4 was also applied on 12 μm cryosections of the primary hematopoietic organs of zebrafish (Figure 4.1b). Just like other teleost fish, hematopoiesis in adult zebrafish takes place in the kidney (Bennett et al., 2001), which is attached to the ventral side of the vertebral column as a thin sheet of tissue. Adult hematopoiesis takes place mostly on the anterior portion of the organ which is named the *head kidney*, while the *trunk kidney* refers to the posterior portion which is less involved in hematopoiesis (Stachura and Traver, 2011). Therefore, a high fraction of the leukocyte population, including neutrophils and macrophages, as well as undifferentiated precursors, reside mainly in the head kidney.

Immunostaining of kidney sections against the selected innate immune cells markers demonstrated that a large number of neutrophils and macrophages reside in the tissue under homeostatic conditions, which is consistent with its hematopoietic function (Figure 4.1b; top panel).

The spleen is another hematopoietic tissue that is located between the liver and bowel, within the internal organ bundle located in the abdominal cavity. The splenic parenchyma consists of two types of tissues with different roles, the *white pulp* and *red pulp*. Red pulp consists of ellipsoid venous structures that are responsible for filtering blood. Ellipsoids also contain a large number of macrophages that phagocytose aging erythrocytes, apoptotic cells, foreign toxicants and unwanted antigens from the blood (Menke et al., 2011; van Rooijen and Hendrikx, 2010; Zhu et al., 2016). Immunostaining of 12 μm cryosections of zebrafish spleen against the selected macrophage marker Mfap4 demonstrated the presence of a large number of macrophages, which are grouped together to form circular structures that were distributed evenly across the splenic parenchyma and resembled ellipsoidal structures (Figure 4.1b; bottom right, arrowheads). In addition, the ramified cellular morphologies of these cells further confirm the specificity of Mfap4 in labelling macrophages. In contrast with the abundance of macrophages, splenic tissue only had a scarce number of neutrophils with rounded morphologies showing no distinguishable pattern of distribution (Figure 4.1b; bottom left).

4.1.2. Neutrophils Reside in the Intact OE

In order to understand whether there is a neutrophil recruitment present in the OE in response tissue damage, it was necessary to first reveal whether neutrophils are present in the intact OE under homeostatic conditions, and if so, determine their basal occupancy in the tissue. In case additional neutrophils are recruited upon damage, quantification of the basal occupancy will be necessary to confirm the degree and the level of significance of this influx. In addition, it also appears to be important to qualitatively describe the localization and behavior of neutrophils in the OE in the absence of an external irritation.

To determine the spatial distribution and basal occupancy of neutrophils in the intact OE, OOs of 12 adult zebrafish were dissected out, cryosectioned, and immunostained against the neutrophil marker Mpx and the neuronal marker HuC/D. Whole OE images (4 or 5 sections per fish) were captured via confocal microscopy at 2048 x 2048 - pixel resolution (Figure 4.2a). Standardized rectangular regions of interest (ROI) were cropped from each hemi-OE for data analysis using FIJI software. The horizontal axis of the rectangular ROIs ranged from the tip of the ILC to the tissue periphery, while the vertical axis was centered and aligned perpendicular to the median raphe and comprised of 2/3rds of the width in length (Figure 4.2a). The OOs of fish often vary in size. Therefore, the rectangular ROI serves to standardize the analyzed region according to a fixed ratio to cover the same range of functional regions and to provide a balanced representation of data from individual fish. For these reasons, standardized ROIs provide a more consistent assessment of the experimental outcomes that do not strongly depend on size differences between OEs. In addition, the OE tissue integrity becomes compromised after chemical lesion with TrX and almost all OSNs are eliminated, limiting the visual cues to recognize the OE structure, which is otherwise defined by anti HuC/D staining. To obtain comparable data sets, all the quantitative analyses of OE in this study were derived from the same hemi-OE cell counting method.

Figure 4.2b exemplifies the distribution pattern of different functional regions across a hemi-OE ROI. The ruler located on the top of Figure 4.2b provides guidance to the locations of ILC, sensory, SNS and non-sensory on the hemi-OE, while the margins of the related sections were emphasized by vertical dashed lines. Staggered lamellae extend perpendicularly from the median raphe to the peripheral non-sensory of the tissue and are nearly parallel to each other. Mature OSNs constitute approximately two-thirds of the OE forming the sensory region on the inside of the section, while a peripheral ring of structural cells surrounds them and constitutes the non-sensory tissue (Calvo-Ochoa et al., 2021; Figure 4.2b; dashed lines). The ILC is located near the median raphe and is composed of connected single sheets of sensory epithelia.

Hemi-OEs from 12 fish (4/5 sections per fish; 2 hemi-OEs per section; 114 hemi-OEs in total) were adjusted for data analysis in the FIJI software. The number of Mpx-positive cells were counted in each hemi-OE and combined to be exhibited in representative diagrams.

Figure 4.2c indicates the average number of neutrophils in different functional zones within the epithelium: ILC, sensory, and non-sensory OE. Error bars were calculated as standard error (SEM) values and are represented with thin black lines on the individual bars. The overall number of neutrophils in a hemi-OE of 12 μm thickness was found to be 6,4 ± 0,5 cells on average across 12 fish (Figure 4.2c; leftmost bar). Despite relatively low numbers of neutrophils in the intact OE, there is a clear pattern of distribution of Mpx-positive cells along the epithelium. The locations of neutrophil populations showed a bias towards the non-sensory region (Figure 4.2c; rightmost bar) with 4,4 ± 0,3 cells. According to this evaluation, the non-sensory OE contained 69,66% of all neutrophils in the hemi-OE, which was consistent with the previous observations on transgenic adult zebrafish (n = 3 OE from 3 fish), which demonstrated that the non-sensory region was significantly more populated by neutrophils than the sensory region (Palominos et al., 2022). Neutrophil occupancy in intact OEs were also investigated for the consistency among individual fish. Combined dataset from 12 fish exhibited a significant fluctuation among the individual fish ($p = 5{,}0 \times 10^{-8}$; F = 6,4; df = 11; one-way ANOVA). After the removal of the datasets of 2 suspected outliers, a reduced but still notable difference among the individual fish was evident ($p = 0{,}001$; F = 3,5; df = 9; one-way ANOVA).

In contrast with the non-sensory region, only 0,97 ± 0,18 cells per hemi-OE were located in the ILC, while another 0,96 ± 0,15 cells could be found inside the sensory region, comprising 15,25% and 15,05% of all neutrophils respectively. One-way ANOVA revealed a significant difference between data sets ($p = 8{,}4 \times 10^{-35}$; $F_{(3, 452)} = 73{,}5$; One-way ANOVA).

Tukey's multiple comparisons test was further applied to investigate the difference between each of the data sets, which confirmed a strong significant difference between non-sensory OE and ILC ($p = 6{,}3 \times 10^{-13}$; One-way ANOVA Tukey's HSD) and between non-sensory and Sensory OE ($p = 6{,}0 \times 10^{-13}$; One-way ANOVA Tukey's HSD; Figure 4.2a; levels of significance are denoted with asterisks).

Furthermore, visual investigation of these cells validated that neutrophils that appeared to be close to the ILC and the sensory epithelium were not associated with the sensory tissue itself but were mostly positioned in the lamina propria between individual lamellae, which is rich in blood vasculature (Figure 4.2a; arrowheads).

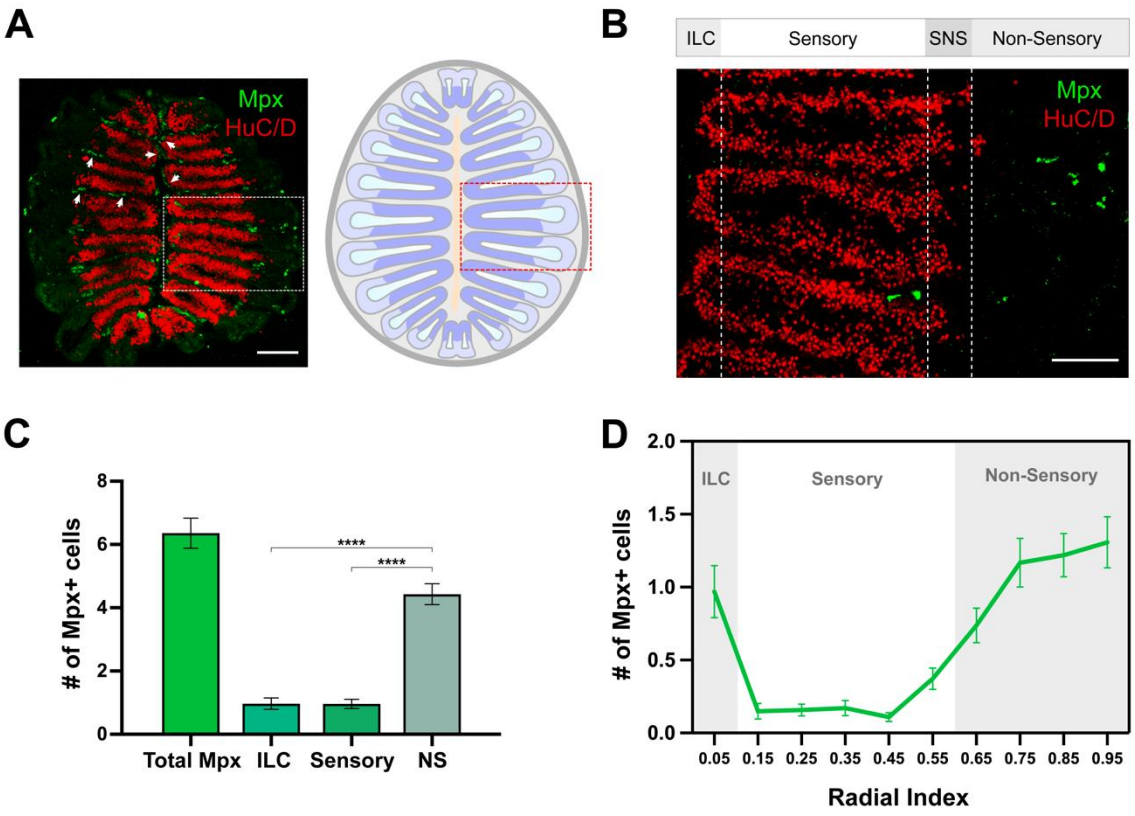

Figure 4.2. Neutrophils are present in the intact OE. (a) Demonstration of selection of the rectangular sections used in data analyses. Scale bar: 100 μm. (b) Demonstration of different functional regions within a hemi-OE section. Scale bar: 50 μm. (c) Bar graph representing the number of Mpx-positive cells in different OE regions. (d) Frequency distribution of Mpx-positive cells across the radial axis of the OE.

In addition, they were associated with nasal blood vessels that wrap around the epithelial folds at the ILC, as mentioned earlier (Figure 4.1a; bottom left; asterisk). These observations were coherent with recent findings on transgenic juvenile and adult zebrafish which, signified that neutrophils are associated with blood and lymphatic vasculature in the OE and utilize this network to migrate to different sites (Palominos et al., 2022).

Figure 4.2d can be considered as a more detailed display of the neutrophil occupancy in the intact OE, which presents the spatial distribution of neutrophils along the radial dimension of the tissue. The radial index refers to the medial-lateral axis of the hemi-OE, which was divided to 10 equidistant bins for analysis, and which are represented by numbers ranging from 0.05 to 0.95 with grid lines in the x-axis.

The number of neutrophils in individual bins are demonstrated by a green line with error bars that indicate SEM values. Functional regions of the OE were indicated with gray and white boxes and are labelled correspondingly. ILC and sensory OE are represented by coordinates 0.05 and 0.15-0.55, respectively, while the non-sensory OE corresponds to radial positions 0.65 to 0.95. The line graph shows a low profile in the sensory OE with an increase towards the non-sensory OE. The gradual increase continued in the non-sensory region until it reached the peak around position 0.95, which indicates this radial position had the highest number of neutrophils on average. Therefore, neutrophils may not be directly associated with mature OSNs in the sensory epithelium.

In summary, resident neutrophils are found in relatively low numbers in the intact OE and mostly occupy the peripheral non-sensory territory. Non-sensory OE is next to peripheral boundary of the tissue where a meningeal membrane surrounds the OO and fuses with an epineurium layer of the olfactory nerve ventral to the OO (Palominos et al., 2022; Palominos and Whitlock, 2021). The observed tendency of neutrophil localization within the peripheral non-sensory tissue in the intact OE, in combination with the recent discoveries in transgenic zebrafish leads to the hypothesis claiming that the peripheral OE may function as a gateway that mediates neutrophil migration in and out of the OE via the rich blood and lymphatic vasculature network in the meningeal membrane.

4.1.3. Macrophages Reside in the Intact OE

Studies in zebrafish that concern innate immune cells and their contribution to tissue renewal and regeneration, have heavily focused on macrophages. There is a significant amount of evidence regarding the positive impact of macrophage activity on tissue repair and remodeling in different organ contexts including but not limited to the heart (Bevan et al., 2020), tail fin (Nguyen-Chi et al., 2017), retina (Bollaerts et al., 2019), spinal cord (Ghosh and Hui, 2018), CNS (Caldwell et al., 2019) and skeletal muscle (Chazaud, 2020). However, the parameters and extent of macrophage behavior in the context of injury induced inflammation and their contribution to regenerative events in the adult zebrafish OE have not been investigated.

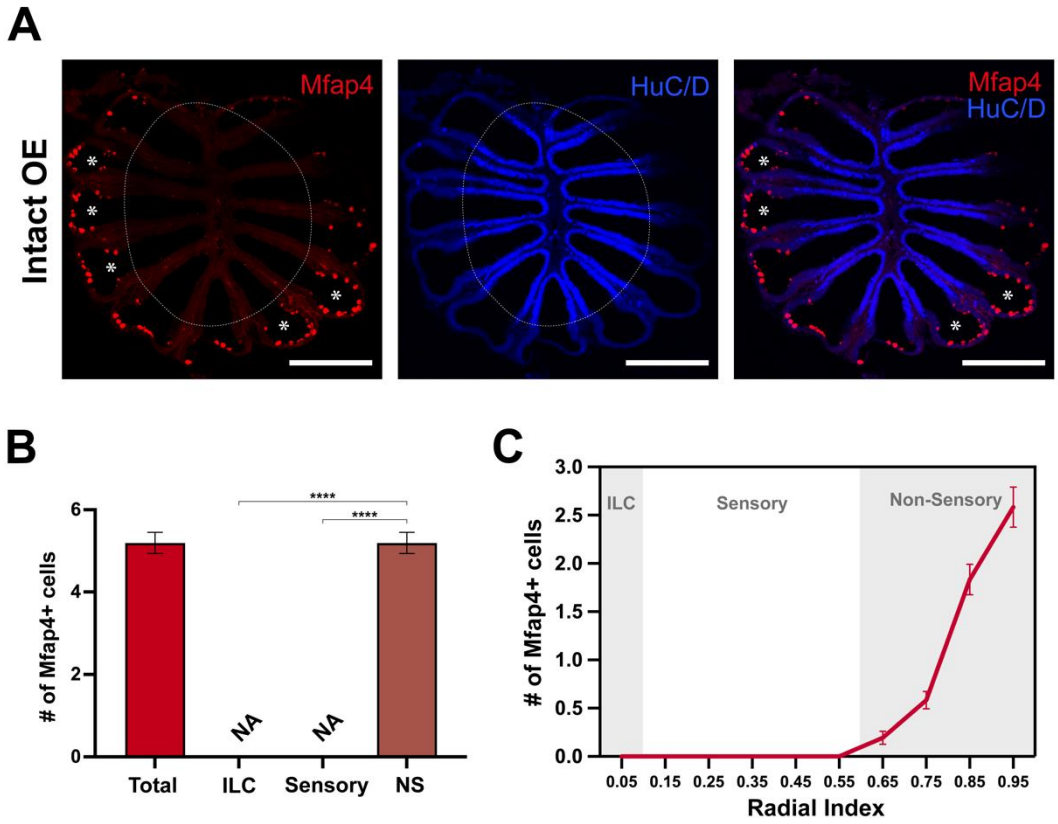

Figure 4.3. Macrophages are present in the intact OE. (a) Confocal images of intact OE that was prefixed (1 h in 4,0% PFA) and stained against Mfap4 and HuC/D. Sensory OE was indicated with dashed circles. Scale bars: 50 μm. (b) Positional profiling of Mfap4-positive cells in the hemi-OE. (c) Frequency distribution of Mfap4-positive cells across the radial axis of the OE.

The spatial distribution of macrophages in the intact OE is exemplified in Figure 4.3a by confocal images of the whole OE, which were subjected to anti-Mfap4 (red) and anti-HuC/D (blue) immunostaining. Prefixation of the OOs in 4,0% PFA (for 1h) resulted in a cytoplasmic HuC/D signal (Figure 4.3a; image in the middle, region within dashed circle). Macrophage localization was limited to the periphery of the OE as could be observed from the leftmost image in Figure 4.3a. The entire population of Mfap4-positive cells could be detected outside of the sensory region, which is encircled with dashed lines. Furthermore, the cells appear to be lined up in an arranged order in the non-sensory OE, where the single sheets of epithelia merge to form individual epithelial folds (Figure 4.3a; leftmost and rightmost image; asterisks).

The labeled cells also did not appear to be associated with the blood vasculature in the median raphe and the lamina propria. In addition, macrophages were not associated with the meningeal membrane. Instead, they could be observed to be localized in the peripheral margin of the non-sensory OE.

To understand the potential contribution of macrophage activity to tissue repair and regeneration, establishing their basal occupancy of Mfap4-positive cells in the intact OE was essential. To do so, the OOs of zebrafish (n = 12) were dissected out and cryosectioned (4/5 sections of 12 μm thickness per fish), and dried on glass slides. IHC against the macrophage marker Mfap4 and the neuronal marker HuC/D was applied, and images of whole OEs were captured by confocal microscopy in 2048 x 2048 - pixel resolution. Rectangular ROIs were cropped from each hemi-OE (108 hemi-OEs in total) and brightness/contrast of the images was adjusted for cell counting in the FIJI software. Mfap4-positive cells in each hemi-OE were counted with the help of a custom macro. Data were organized on Microsoft Excel and GraphPad Prism for graphical display (Figure 4.3b and c).

The graph in Figure 4.3b exhibits the average numbers of Mfap4-positive cells in different functional regions of the hemi-OEs, with SEM value of each data set represented by error bars. Upon a preliminary evaluation, all Mfap4-positive cells appear to be positioned in the non-sensory epithelium. There was no evidence of macrophages to be associated with the sensory tissue, particularly with mature OSNs in the ILC and the sensory OE (Figure 4.3b; NA values for ILC and Sensory). Therefore, non-sensory OE included 100% of all the macrophages residing in the intact tissue with 5,2 ± 0,3 (mean ± SEM) cells per hemi-OE. To establish a rigid scientific claim regarding the apparent absence of macrophages from the sensory tissue, statistical hypothesis testing was performed on the data sets. One-way ANOVA validated a solid significant difference ($p = 3{,}5 \times 10^{-99}$; $F_{(3, 428)} = 273{,}9$; One-way ANOVA). Tukey's multiple comparisons test further confirmed that there is a highly significant difference between the non-sensory OE and the ILC ($p = 4{,}4 \times 10^{-13}$; One-way ANOVA Tukey's HSD), as well as between the non-sensory and the sensory OE ($p = 4{,}4 \times 10^{-13}$; One-way ANOVA Tukey's HSD).

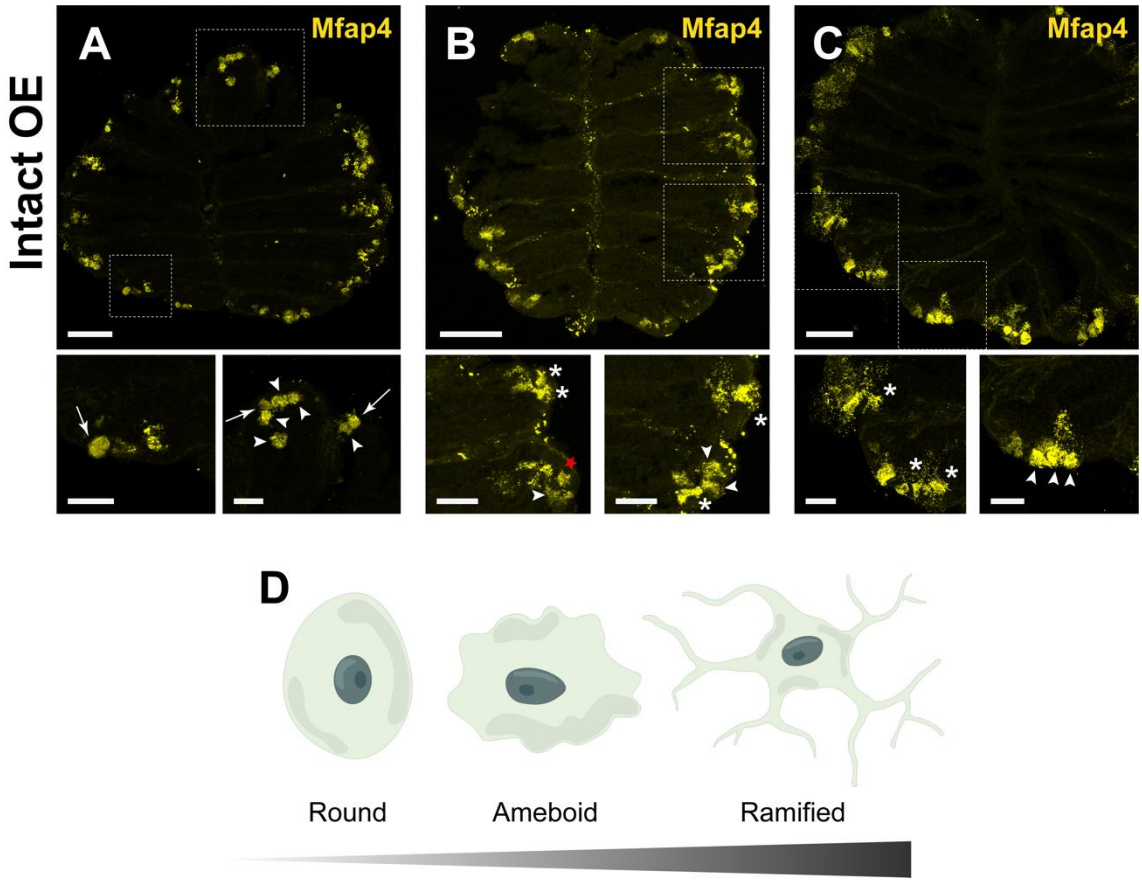

Figure 4.4. Intact OE is inhabited by a phenotypically diverse population of macrophages. (a), (b), (c) IHC against Mfap4 (yellow) applied on intact OEs. Three OEs are exemplified side by side. The regions within dashed boxes (top) are represented in high magnification (bottom). Scale bars: 100 μm (top), 10 μm (bottom). (d) Morphological plasticity of macrophages.

The radial distribution of Mfap4-positive cells is shown in detail in Figure 4.3c and SEM value of each data point are indicated by error bars. ILC, sensory and non-sensory OE are indicated as gray and white boxes with appropriate labels. The mediolateral axis of the OE that ranges from the median raphe to the tissue periphery is indicated by the radial index, which is divided into 10 equidistant bins providing a more detailed positional profiling of macrophages in the OE. The line graph further confirms a strong bias of macrophages towards the non-sensory OE. In addition, macrophages tended to localize further in the peripheral region of the non-sensory epithelium, which can be observed from the strong increase of Mfap4-positive cells between radial positions 0.75 and 0.95 (Figure 4.3c).

Intriguingly, observations of Mfap4-positive cells in the intact OE of 12 fish revealed an evident morphological plasticity among resident macrophages. Figure 4.4a, b, and c demonstrates three examples of intact OE that were immunostained against the macrophage specific marker Mfap4 (yellow). Regions within dashed boxes are displayed in higher magnification below the corresponding images. The macrophages adopted diverse cellular shapes ranging between two opposing poles of a morphological spectrum which were round and elongated/ramified (Figure 4.4d). In between these extremes, cells predominantly exhibited ameboid shapes. Rounded macrophages were distinguished by the lack of protrusions and adopting a firm spherical profile (Figure 4.4a; bottom panel; arrows).

On the other hand, several cells showed a typical ameboid morphology with apparent protrusions along the plasma membrane (Figure 4.4a, b, and c; bottom panel; arrowheads). Intriguingly, some cells were found to be adopting a star-like shape (Figure 4.4b; bottom left; star symbol), consistent with the previous findings in zebrafish embryo (Travnickova et al., 2021) and larvae (Palominos and Whitlock, 2021). This particular morphology was closer to the ameboid profile and was categorized as such, since both shapes can be considered as intermediate phases between two extreme phenotypes.

The third predominant subgroup of cells was observed to have elongated extensions as well as ramified dendritic profiles (Figure 4.4b and c; bottom panel; asterisks). In the bottom right image of Figure 4.4b (asterisks), an elongated Mfap4-positive cell in the bottom can be clearly distinguished near two ameboid cells (arrowheads). Another cell with more ramified properties can be observed on the top right of the same image, adopting dendritic extensions reaching the periphery of the OE. Altogether, these data suggests that the intact OE is inhabited by a phenotypically diverse population of macrophages that exhibit different intermediatory subgroups along a morphological spectrum.

4.3. Characterization of Neutrophil and Macrophage Behavior Following Chemical Lesion

Data obtained from the intact OE provided a preliminary information on the basal occupancy and the spatial distribution pattern of the primary innate immune cells under physiological conditions. To understand their potential contribution to repair neurogenesis and regeneration, this part of the thesis focuses on the investigation of the changes in neutrophil and macrophage numbers and behavior in the OE after chemical lesion. To do so, quantitative analysis was performed to establish the radial distribution and the level of abundance of neutrophils and macrophages at early (6h, 24h), and late (72h, 120h) time points after chemical ablation with irritant TrX (1,0%). Occupancy of the cells within specific functional regions of the OE was comparatively investigated against the internal controls.

4.3.1. Neutrophils are Recruited to the OE Following Nasal Irrigation with TrX

After tissue injury, unfold of an acute inflammatory response serves as the first line of defense to regain homeostasis and restore tissue integrity. The onset of this response is characterized by the recruitment of innate immune cells to the inflamed site (Keightley et al., 2014). As the primary innate immune cells to be recruited from circulation, neutrophils are phagocytic granulocytes that are predominantly responsible for clearing debris and combat pathogens by secreting toxic reagents.

Myeloperoxidase (Mpx) is the most abundant toxicant protein stored within granules, which also serves as a highly specific neutrophilic marker to track these cells *in vivo* (Rosowski, 2020). Elimination of irritant agents as well as clearance of necrotic tissue are imperative for tissue repair and restoration. Neutrophils, as the primary cells in charge on the onset of inflammation, are at utmost importance in setting the inflammatory process forward to resolution, thus paving the way for tissue renewal. This section will describe, upon tissue injury whether, when, and to which sites do neutrophils recruited to potentially contribute to OE regeneration.

To examine whether additional neutrophils are recruited to the injured OE and to define the level of occupancy, as well as the spatial pattern of this recruitment throughout the regenerative period, OOs of the fish were dissected out 6, 24, 72, and 120 h after chemical injury. Detergent based irritant solution TrX (1,0%) was applied to the left OOs of the fish for 90 seconds via nasal irrigation. The untreated right OEs were utilized as internal controls.

Nasal irrigation triggered a quick and temporal rise in the neutrophil numbers in the first 24 hours post lesion (hpl), while the peripheral non-sensory tissue being the predominant region of Mpx-positive signal density (Figure 4.5a). Early after injury at 6 hpl, a clear neutrophil pattern was also seen between the individual lamellae, within the lamina propria. This observation is consistent with the previous studies that suggest neutrophils migrate in association with the nasal veins that are located in the median raphe, lamina propria, as well as those that surround the tissue periphery. One of the first intracellular events that take place in response to tissue damage is the enrichment of cell adhesion molecules in the endothelial cells that construct the vascular tissues, to ease the innate immune cell adhesion and recruitment to the inflamed area (Rock et al., 2010). Therefore, the observations on neutrophil localization on the damaged OE in Figure 4.5a support the hypothesis claiming that the neutrophils migrate through the nasal blood vasculature to travel into and out of the OE. Most of the cells associated with the blood vessels in the basal lamina and the median raphe had travelled and settled to the peripheral non-sensory OE at 24 hpl (Figure 4.5a; bottom panel; 24 hpl).

The untreated intact OEs at 6 hpl and 24 hpl had scarce numbers of Mpx-positive cells that were located mostly in the non-sensory region, with several in association with the vasculature within individual lamellae and the median raphe, which was coherent with the prior observations on the neutrophil occupancy and localization in the intact OE presented in the section 4.1.2. Chemical ablation resulted in a significant shrinkage and overall disruption of the structural integrity of the epithelium in the first 24 h, which has previously been shown as the time point where most of the OSNs are lost due to TrX exposure (Kocagöz et al., 2022). Experimental results utilizing this chemical ablation method on zebrafish OE has also demonstrated that, tissue integrity starts to be restored and the peak of proliferative activity is observed at 72 h after damage. Almost full function of the OE is regained, and tissue integrity is almost fully restored after 120 hpl (Kocagöz et al., 2022).

In consonance with these observations, lesioned OEs appeared significantly similar to the untreated controls at 72 hpl and 120 hpl in terms of tissue integrity (Figure 4.5a; two columns on right). The tissue structure had been rearranged and the neutrophil numbers returned to pre-injury levels. This evidence argue that neutrophils are responsive on the onset of the inflammatory process up to 24 hpl. Therefore, first 24 h after sterile injury might be considered as the early (acute) phase of the inflammation, where the late phase or resolution of inflammation can be observed around 72 to 120 hpl where tissue repair and restoration events predominate in the epithelium.

Quantitative analysis of neutrophil numbers in the injured and intact OEs are represented in Figure 4.5b. For each time point, three fish were utilized. Nasal irrigation applied on the left noses while the untreated noses used as internal controls. The OOs dissected out at the related time points, cryosectioned, and immunostained against the neutrophil specific marker Mpx. Confocal images of tissue sections (4 or 5 sections per fish; 2 hemi-OEs per section) were acquired at 2048 x 2048 - pixel resolution. Quantitative analysis over neutrophil numbers was formulated via the adjusted cell counting technique using FIJI software. Data were organized to display intact and lesioned OEs from each experimental time point in a combined bar graph (Figure 4.5b), in which the horizontal axis indicates the average number of neutrophils per hemi-OE (6 hpl, 72 hpl, 120 hpl: n = 30 hemi-OEs; 24 hpl: n = 24 hemi-OEs) while the vertical axis signifies different time points following chemical lesion. Green and gray bars represent TrX lesioned and untreated intact OEs respectively (Figure 4.5b; top right). The levels of significance that were formulated by the statistical hypothesis testing were indicated by asterisks above the bars (ns: not significant).

Consistent with the visual evidence that was obtained from the confocal images in Figure 4.5a, earliest experimental time points 6 hpl and 24 hpl exhibited the greatest change in the neutrophil numbers upon damage. At 6 hpl, the untreated OEs had 5,43 ± 0,85 (mean ± SEM) neutrophils in a hemi-OE on average, whereas TrX lesioned OEs had 68,80 ± 8,64 cells, corresponding to a near 13-fold increase. Similarly, at 24 hpl the higher number of Mpx-positive cells persist to be present in the damaged OE (Ctr: 5,0 ± 0,7 cells; TrX: 50 ± 7 cells; mean ± SEM) with an approximate 10-fold increase in contrast to the internal controls.

At later time points, neutrophil density reduced back to basal levels in the lesioned OEs with no significant fold change between the untreated controls (72 hpl, Ctr: 7,7 ± 0,9, TrX: 5,2 ± 0,8; 120 hpl, Ctr: 7,1 ± 1,1, TrX: 5,9 ± 0,7), which complies with the previous evidence, which pointed that the period around 72 to 120h after damage roughly corresponds with the resolution phase of the inflammatory response.

As expected, datasets exhibited the highest levels of significance between the TrX lesioned and untreated control OEs at 6 hpl ($p = 9{,}1 \times 10^{-10}$; $F_{(1, 58)} = 53{,}3$; one-way ANOVA) and at 24 hpl ($p = 2{,}5 \times 10^{-8}$; $F_{(1, 58)} = 45{,}0$; one-way ANOVA). A slight significance detected between those at 72 hpl ($p = 4{,}1 \times 10^{-2}$; $F_{(1, 58)} = 4{,}4$; one-way ANOVA), while none detected at 120 hpl ($p = 0{,}34$; $F_{(1, 58)} = 0{,}7$; one-way ANOVA). Two-way ANOVA with post hoc Tukey's multiple comparisons test were further applied to compare datasets between different time points, which pronounced a strong significance (Ctr /TrX; $p = 0{,}22 \times 10^{-19}$; $F_{(1,220)} = 91{,}7$; Time Post Injury: $p = 1{,}1 \times 10^{-17}$; $F_{(3,220)} = 33{,}1$; Two-way ANOVA). In addition, there was no significant change detected in the scored neutrophil numbers between 6 hpl and 24 hpl ($p = 8{,}6 \times 10^{-2}$; two-way ANOVA post hoc Tukey's HSD). However, a notable reduction in neutrophil numbers was evident between 24 hpl and 72 hpl ($p = 1{,}5 \times 10^{-6}$; Two-way ANOVA post hoc Tukey's HSD). Finally, the cell counts did not significantly change between 72 to 120 hpl ($p = 0{,}99$; Two-way ANOVA post hoc Tukey's HSD), which indicates that the neutrophil numbers turn back to basal levels at 72 hpl and remain approximately the same throughout the rest of the inflammatory period.

To obtain a more detailed observation on the neutrophil recruitment, Figure 4.5c, d, and e consists of three graphical displays indicating Mpx-positive cells in different functional regions within the epithelium. How the neutrophil occupancy changes between ILC, core sensory and the non-sensory OE may give an insight into where these cells function at within the tissue. This information can further unveil some insight on the functional characteristics of neutrophils in acute inflammatory response, and unfold their selective contribution, if any, to tissue restoration and neurogenesis in the OE.

The statistical material represented in Figure 4.5c, d, and e are comprised of the same data as in Figure 4.5b. Average numbers of Mpx-positive cells in each hemi-OE are represented in the vertical axes (pay attention to the different maximal values) while

horizontal axes exhibit different time points after TrX exposure (bars in shades of green, TrX lesioned; gray bars, Intact OE). In Figure 4.5c, the number of neutrophils in ILC is shown (6 hpl, Intact OE: 0,4 ± 0,2, TrX: 6,45 ± 1,1; 24 hpl, Intact OE: 0,2 ± 0,2, TrX: 2,1 ± 0,6; 72 hpl, Intact OE: 1,7 ± 0,4, TrX: 0,8 ± 0,2; 120 hpl, Intact OE: 1,4 ± 0,4, TrX: 1,1 ± 0,3 cells/ hemi-OE). In Figure 4.5d, the number of neutrophils in the sensory region is indicated (6 hpl, Intact OE: 0,8 ± 0,3, TrX: 17 ± 3; 24 hpl, Intact OE: 0,06 ± 0,05, TrX: 6,8 ± 1,4; 72 hpl, Intact OE: 1,4 ± 0,3, TrX: 1,07 ± 0,3; 120 hpl, Intact OE: 1,4 ± 0,4, TrX: 1,9 ± 0,4 cells/ hemi-OE). In Figure 4.5e, neutrophil occupancy in the non-sensory region is demonstrated (6 hpl, Intact OE: 4,2 ± 0,7, TrX: 45 ± 5; 24 hpl, Intact OE: 4,7 ± 0,7, TrX: 42 ± 6; 72 hpl, Intact OE: 4,5 ± 0,7, TrX: 3,4 ± 0,7; 120 hpl, Intact OE: 4,4 ± 0,6, TrX: 2,9 ± 0,6 cells/ hemi-OE).

Experimental results were adjusted to statistical testing with two-way ANOVA post hoc Tukey's HSD to confirm the levels of significance (Figure 4.5c, d, and e). There was a notable significance within data sets of ILC (Figure 4.5c; Time post lesion: $p = 1{,}5 \times 10^{-5}$ $F_{(3,220)} = 8{,}8$; Intact OE/TrX: $p = 1{,}8 \times 10^{-5}$ $F_{(1,220)} = 19{,}2$; Two-way ANOVA), the sensory region (Figure 4.5d; Time post lesion: $p = 1{,}2 \times 10^{-11}$, $F_{(3,220)} = 20{,}3$; Intact OE/TrX: $p = 1{,}5 \times 10^{-11}$, $F_{(1,220)} = 50{,}7$; Two-way ANOVA), and the non-sensory OE (Figure 4.5e; Time post lesion: $p = 1{,}9 \times 10^{-18}$, $F_{(3,220)} = 34{,}8$; Intact OE/TrX: $p = 5{,}8 \times 10^{-18}$, $F_{(1,220)} = 89{,}7$; Two-way ANOVA).

The strongest significance was seen in the non-sensory tissue with an approximate 10-fold increase in TrX lesioned OEs as opposed to the untreated controls at 6 hpl ($p = 1{,}1 \times 10^{-10}$; $F_{(1, 58)} = 61{,}5$; one-way ANOVA) and 24 hpl ($p = 1{,}1 \times 10^{-6}$; $F_{(1, 46)} = 31{,}5$; one-way ANOVA), although the basal levels in the untreated controls were higher from the ILC and the sensory region (Figure 4.5c and d). In addition, note the decrease in the number of neutrophils from 6 hpl to 24 hpl in ILC ($p = 0{,}001$; two-way ANOVA post hoc Tukey's HSD) and the sensory region ($p = 2{,}9 \times 10^{-5}$; two-way ANOVA post hoc Tukey's HSD) in contrast to that in the non-sensory OE ($p = 0{,}94$; two-way ANOVA post hoc Tukey's HSD). The level of neutrophil density stays almost the same in the non-sensory tissue from 6 hpl to 24 hpl in the lesioned OEs, although there is an evident reduction in the overall neutrophil numbers in 24 hpl as indicated earlier in Figure 4.5b.

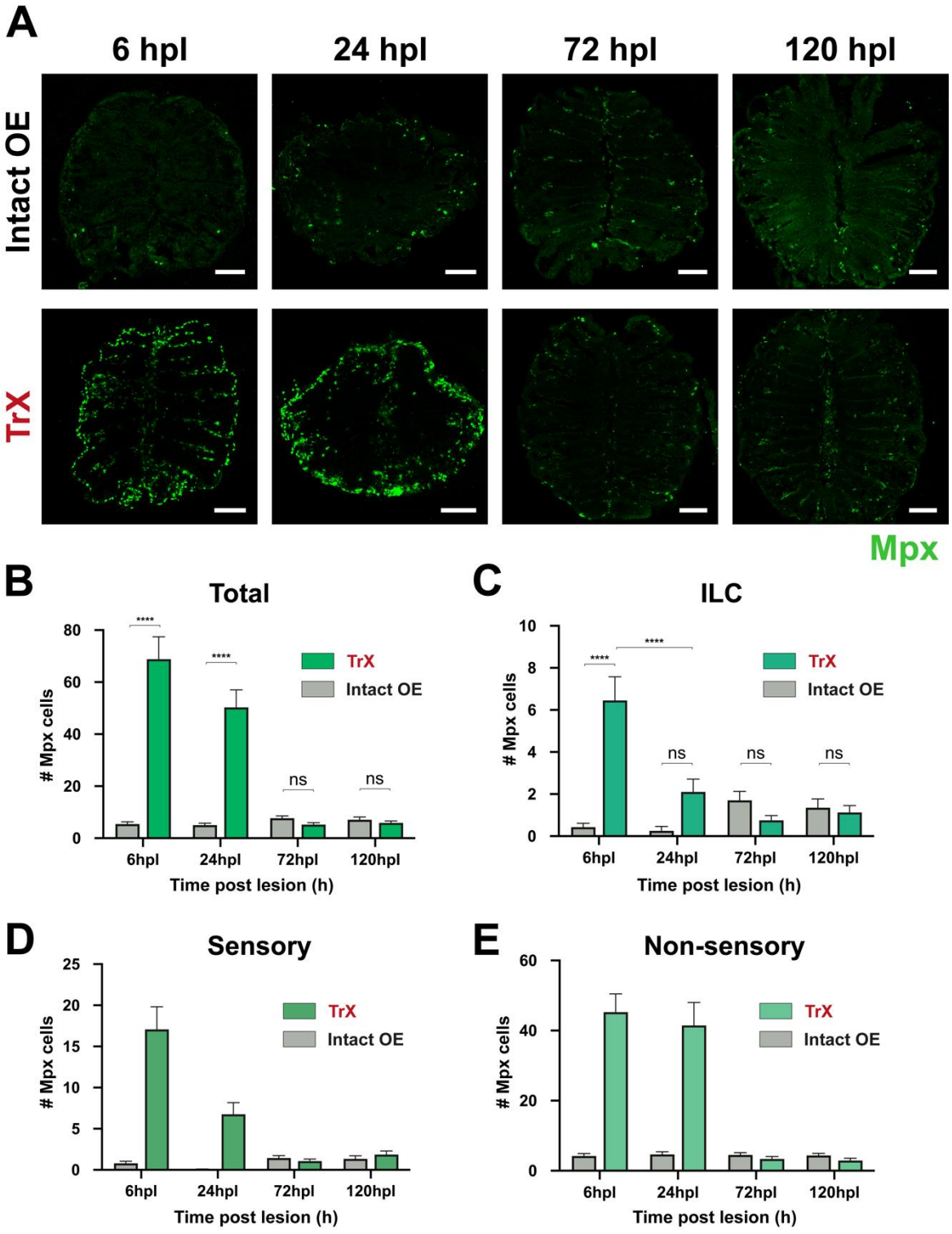

Figure 4.5. Neutrophils are recruited to the OE upon TrX exposure. (a) Images of the whole OEs at 6, 24, 72 and 120 hpl (hours post lesion). Injured OEs (bottom panel) and internal controls (top panel) were imunostained against Mpx (green). Scale bars: 100 μm. (b) Number of Mpx-positive cells at different time points post injury. (c, d, e) Regional distribution of Mpx-positive cells, same data as in (b).

This observation indicates that, even though the overall number of Mpx-positive cells decrease from 6 hpl to 24 hpl, their level of occupancy in the non-sensory OE remains similar, which points to a positional bias of neutrophils towards the non-sensory region. In addition, no pronounced change was recorded between the intact and the lesioned OEs at later time points 72 hpl (ILC: p = 0,056, $F_{(1, 58)}$ = 3,8; Sensory: p = 0,31, $F_{(1, 58)}$ = 1,0; NS: p = 0,093, $F_{(1, 58)}$ = 2,9; one-way ANOVA) and 120 hpl (ILC: p = 0,80, $F_{(1, 58)}$ = 0,063; Sensory: p = 0,28, $F_{(1, 58)}$ = 1,2; NS: p = 0,1, $F_{(1, 58)}$ = 2,8; one-way ANOVA), in any of the functional subregions.

Confocal images exhibited in Figure 4.6a present a closer look into the individual hemi-OEs after TrX exposure. Untreated intact (top) and TrX lesioned OEs (bottom) were immunostained against the neutrophil specific Mpx (green) and the neuronal marker HuC/D (blue). Regional boundaries of ILC, sensory and non-sensory OE were indicated by dashed lines on each image.

Different time points after chemical injury are indicated in separate columns. As expected, a small number of neutrophils were also recognized associated with the peripheral non-sensory region, the median raphe, and the lamina propria in the intact OEs (Figure 4.6a; top panel). Consistent with the prior observations on the intact OE in physiological conditions, several neutrophils were found in association with apoptotic OSNs near the non-sensory region (Figure 4.6a; top panel, right; asterisks), which signifies that neutrophils are responsible for engulfing dead cells and contribute to the tissue turnover and maintenance. As expected, the sensory tissue which was indicated with the anti-HuC/D staining, covered approximately two-thirds of the epithelium under physiological conditions (Figure 4.6a; top panel; blue). Exposure to TrX for 90s results in a near complete loss of the mature OSN population in the sensory tissue up to 24 hpl, as can be observed from the lack of HuC/D signal in the lesioned OEs at 6 hpl and 24 hpl (Figure 4.6a; bottom panel, left). Remarkably, the majority of the OSNs were replaced and the tissue integrity was almost completely restored at 72 hpl to 120 hpl (Figure 4.6a; bottom panel, right). Therefore, nasal irrigation of TrX resulted in a time related pattern of de- and regeneration of the OO, which was consistent with the evidence from the previous studies (Kocagöz et al., 2022).

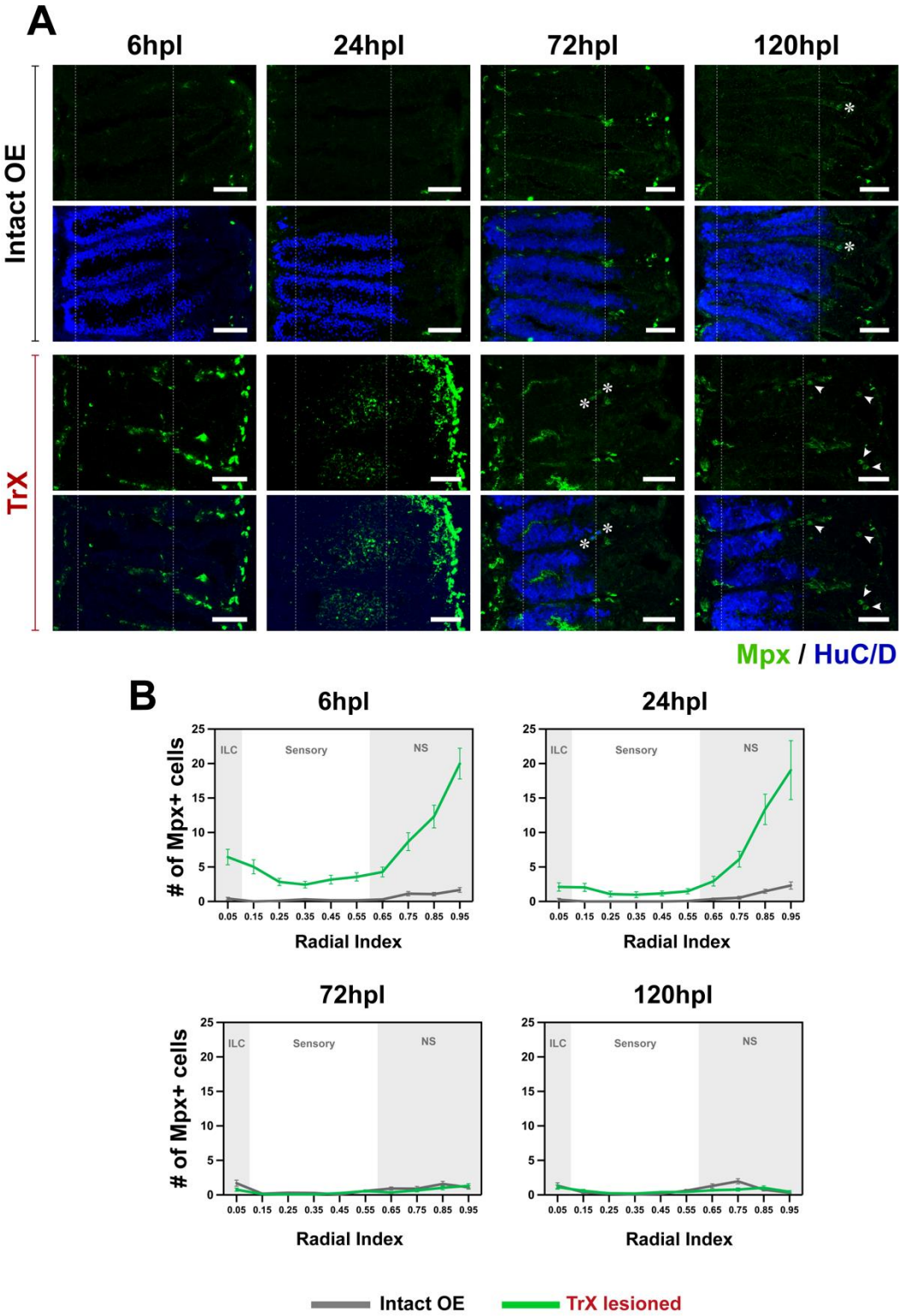

Figure 4.6. Positional profiling of neutrophils at different time points after nasal irrigation. (a) Hemi-OEs of Intact, and lesioned OEs immunostained against Mpx (green) and HuC/D (blue) at 6, 24, 72, and 120 hpl. Scale bars: 50 μm. (b) Line graphs indicate radial distribution of Mpx-positive cells.

Shortly after TrX exposure, at 6 to 24 hpl, neutrophils were present in elevated levels in the tissue and adopted protrusive morphologies, indicating a fast emigrational velocity (Figure 4.6a; bottom panel, left). However, in later time points, neutrophils exhibited a more round and swollen morphology (Figure 4.6a; bottom panel, right; arrow heads), which can be attributed to the increased activity of phagocytosis of apoptotic/necrotic cells and debris. Supporting this argument, two neutrophils (green) engulfing apoptotic OSNs (blue) can be observed in the TrX lesioned OE at 72 hpl (Figure 4.6a; bottom panel, middle-right; asterisks).

Spatial distribution of neutrophils along the hemi-OE provides more detailed evidence, supporting previous observations on the radial positioning of these cells (Figure 4.6b). Positional profiling of Mpx-positive cells was provided for each time point, where green (TrX lesioned) and gray (Intact OE) lines with error bars (SEM) indicate the radial placement of neutrophils along the radial axis.

All together, these data further confirm the strong spatial bias of neutrophils towards the non-sensory epithelium at early time points after chemical ablation, which is evidently detected from the elevated levels of Mpx-positive cells at 6 hpl and 24 hpl (Figure 4.6b). Consistent with a rapidly resolving acute inflammatory phase, the robust neutrophil influx at early stages retuned to pre-injury levels after 72 hpl.

In conclusion, these findings suggest that there is a strong transient elevation in the neutrophil levels shortly after chemical lesion, and the recruited neutrophils settle near the peripheral non-sensory OE in the first 24 h of the inflammatory response.

4.3.2. Mitotic Cell Activity Exhibits a Unique Pattern in the OE After Chemical Lesion

Incorporation of thymidine analogs such as BrdU is a conventional method to visualize dividing cells *in vivo*. BrdU can be incorporated into the newly synthesized DNA during the S-phase of the cell cycle (Salic and Mitchison, 2008). Then, immunostaining of tissue samples with anti-BrdU antibodies can provide efficient and accurate detection of proliferating cells within the tissue. Bayramli et. al. (2017) previously established the pattern of distribution of mitotic cell activity in the zebrafish OE (Bayramli et al., 2017).

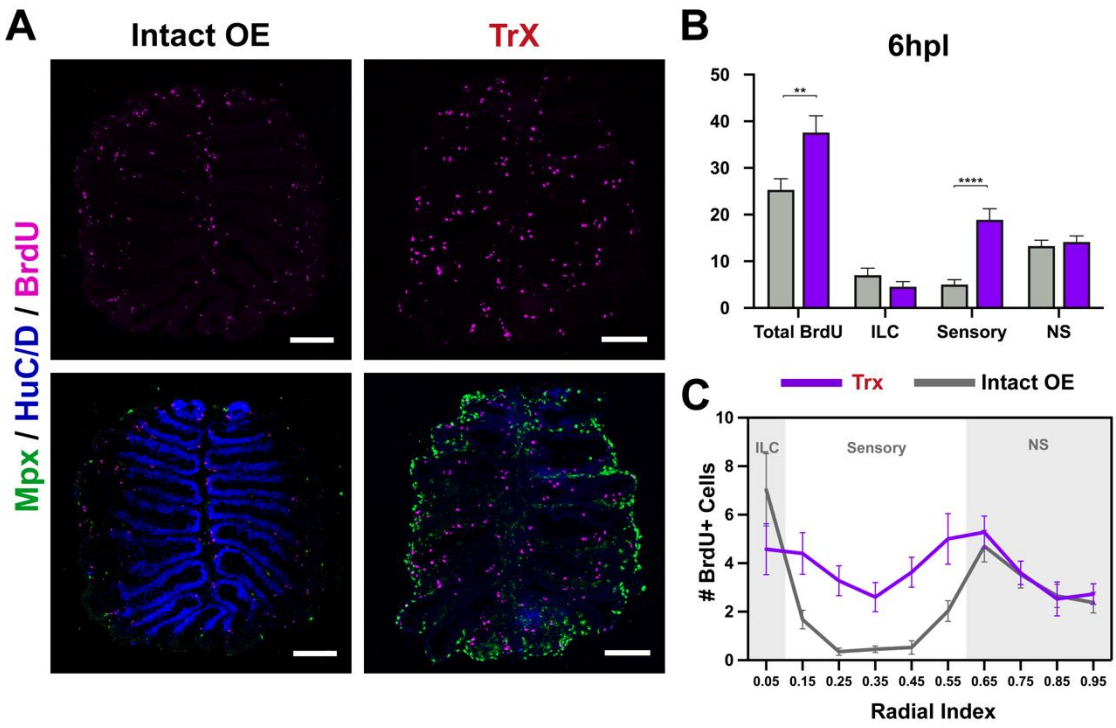

Figure 4.7. A notable change is observed in the pattern of distribution of mitotically active cells in the OE after damage. (a) Intact and TrX lesioned OEs 6 hpl immunostained against Mpx (green), HuC/D (blue), and BrdU (magenta). Scale bars: 100 μm. (b) Number of BrdU-positive cells in different regions of the intact (gray) and TrX lesioned (purple) OE. (c) Radial distribution of BrdU-positive cells along the hemi-OE.

In physiological conditions, cell proliferation in the OE occurs continuously and predominantly at the central and peripheral margins of the sensory region, which corresponds to the tips of the ILC and the sensory/non-sensory border (S/NS). Adult-born cells then gradually migrate towards and inhabit the core sensory region, to replace the dying OSNs, which constitutes the mechanism behind the rapid lifelong turnover rate of OSN populations in the OE (Bayramli et al., 2017; Calvo-Ochoa et al., 2021). Utilizing the same method of chemical injury with TrX, Kocagoz et.al. (2022) defined an altered pattern of mitotic activity after nasal irrigation with TrX in which, proliferating cells were evenly distributed along the radial axis of the OE and elevated levels of BrdU-positive cells were especially apparent within the sensory epithelium (Kocagöz et al., 2022).

To track the potential changes in the pattern of distribution of proliferating cells, and to confirm the efficiency of the TrX exposure, fish were incubated in BrdU containing tanks for 6 h after chemical injury to enable incorporation of the thymidine analogue into newly synthesized DNA of replicating cells.

Immunohistochemistry on the intact and the lesioned OE (6 hpl) samples against BrdU revealed a more even distribution of proliferative cells along the lesioned OEs 6 hpl (Figure 4.7a; top right; magenta) in contrast to the untreated controls (Figure 4.7a; top left; magenta). The bottom panel of Figure 4.7a demonstrates the intact (left) and lesioned (right) OEs 6 hpl with anti-BrdU (magenta), anti-Mpx (green), and anti-HuC/D (blue) immunostaining. The efficacy of the chemical ablation can be recognized from the evident reduction in the number of mature OSNs (HuC/D; blue) in the lesioned OE, as well as from the alteration of the characteristic BrdU pattern, which is normally evident in the untreated controls. Quantitative analysis of mitotic cell activity in the intact and the lesioned OEs (n = 2; 5 sections/fish; 2 hemi-OEs/section) at 6 hpl supported the visual evidence (Figure 4.7b and c). Total number of BrdU-positive cells were increased in the lesioned OE (Figure 4.7b; purple; $p = 0{,}007$; $F_{(1, 38)} = 8{,}1$; one-way ANOVA).

The biggest change between the intact and the lesioned OEs was observed in the sensory region ($p = 4{,}5 \times 10^{-8}$; $F_{(1, 38)} = 28{,}5$; one-way ANOVA), in which mitotic activity is almost absent in the maintenance neurogenesis under physiological conditions (Figure 4.7b). Radial positioning of BrdU-positive cells in the intact (gray) and lesioned (purple) OEs are represented in Figure 4.7c. As expected, proliferative activity was restricted to the ILC and the sensory/non-sensory border, while it was almost absent from the core sensory epithelium in the unlesioned OE (gray). In contrast, BrdU-positive cells in the lesioned OEs (purple) exhibited a more stable and even distribution pattern along the tissue and the sensory region was invaded by proliferating cells as opposed to the intact OEs.

All together, these data exhibit reliable evidence with reference to the prior studies on the level and the spatial pattern of the mitotic cell activity under homeostatic conditions, as well as upon chemical ablation. The monitoring and recording of the proliferative activity in the OE will serve as a fundamental point of reference in the upcoming sections of the thesis.

4.3.4. No Significant Macrophage activity was recorded after TrX Exposure

To investigate whether a dynamic change occurs in the macrophage occupancy and distribution following chemical lesion, OOs of the fish were dissected out 6, 24, 72, and 120 h after TrX exposure, identical to the method used with neutrophils in the section 4.2.1. Left OEs were exposed to nasal irrigation with 1,0% TrX while the untreated intact OEs served as internal controls. Thin cryosections (12 μm) of the organs were dried on glass slides and immunostained against the macrophage specific Mfap4 (red), which were then imaged at 2048 x 2048 - pixel resolution with confocal microscopy. Rectangular ROIs from each image (n=3 fish per time point; 4/5 sections per fish; 2 hemi-OEs per section) were cropped and adjusted for data analysis on the FIJI software.

Representative images of the intact (top panel) and the TrX lesioned OEs (bottom panel) at relative time points after nasal irrigation are displayed in Figure 4.8a. Macrophage specific Mfap4 signals appear in red, while each time point is shown in separate columns. The tissue integrity was disrupted at the early time points (Figure 4.8a; bottom panel; two images on the left), which signifies an accurate and effective application of the nasal irrigation method.

Radial localization of the macrophages shows similarity with that of neutrophils in the intact OE, which exhibited a tendency towards the peripheral non-sensory epithelium. However, an intriguing abundance of macrophages was evident in the intact OEs as opposed to the lesioned OEs at 6 hpl. A notifiable granulated/speckled signaling pattern coupled with lesser discernable cellular shapes were observed in the anti-Mfap4 staining at the early stages after lesion (Figure 4.8a; bottom panel; 6 hpl, 24 hpl). Towards the later periods after lesion (72 hpl, 120 hpl), the granulation pattern decreased, and more distinguishable cellular morphologies could be detected. Note that Mfap4 labels both macrophages and monocytes, which are smaller in diameter and have been shown to be recruited to the inflamed tissues before differentiating into different macrophage subsets (Farache Trajano and Smart, 2021; Italiani and Boraschi, 2014) therefore, the granular pattern of the anti-Mfap4 staining after injury and smaller structures that are harder to define as cells may be attributed to monocytes.

There was no tissue injury related change detected in the morphological plasticity of macrophages (Figure 4.8a). Diverse morphological subgroups remained present throughout the experimental period which were denoted with different symbols in Figure 4.8a (arrows, rounded cells; arrow heads, ameboid cells; asterisks, ramified/elongated cells). In addition, the radial localization of the macrophages appeared to be at the peripheral non-sensory OE, proximal to the circumference of the epithelium, similar to that of the neutrophils. This observation further supports the previous hypothesis that suggests innate immune cells may be mediated in and out of the OE via the extensive blood and lymphatic network in the meningeal membrane that ventrally encapsulates the OO.

The bar graph in the Figure 4.8b exhibits the number of macrophages in the intact and lesioned OEs at different time points after chemical injury. The horizontal axis indicates the average number of macrophages in a hemi-OE (6 hpl, 72 hpl: n = 30 hemi-OEs; 24 hpl, 120 hpl: n = 24 hemi-OEs), while the vertical axis signifies the relative time points following lesion. Red and gray bars represent TrX lesioned and untreated intact OEs respectively. Significance levels were indicated by asterisks. Only a limited rise in the number of Mfap4-positive cells at later time points were observed following lesion, which does not denote a notifiable recruitment of macrophages until 120 hpl. A gradual increase was recorded in the lesioned OEs from early to later periods after injury (6 hpl, 2,0 ± 0,2; 24 hpl, 2,3 ± 0,5; 72 hpl, 4,7 ± 0,6; 120 hpl, 7,6 ± 0,6; average number of cells per hemi-OE ± SEM).

According to this evidence, an approximate 4-fold increase in cell numbers was present between the lesioned OEs at 6 hpl and 120 hpl. One-way ANOVA revealed a highly significant change among the TrX lesioned data sets ($p = 2{,}5 \times 10^{-12}$; $F_{(3, 104)} = 25{,}2$), while post hoc Tukey's HSD further confirmed that the period between 72 and 120 hpl was the major contributor to this increase ($p = 6{,}7 \times 10^{-4}$), while a low significance was recorded between 24 and 72 hpl ($p = 0{,}6 \times 10^{-2}$; one-way ANOVA post hoc Tukey's HSD). Therefore, the macrophages might be recruited to the OE only after 72 hpl. The recruitment of macrophages is ambiguous relative to that observed in the case with neutrophils, in which a firm pattern of time-related recruitment was recorded.

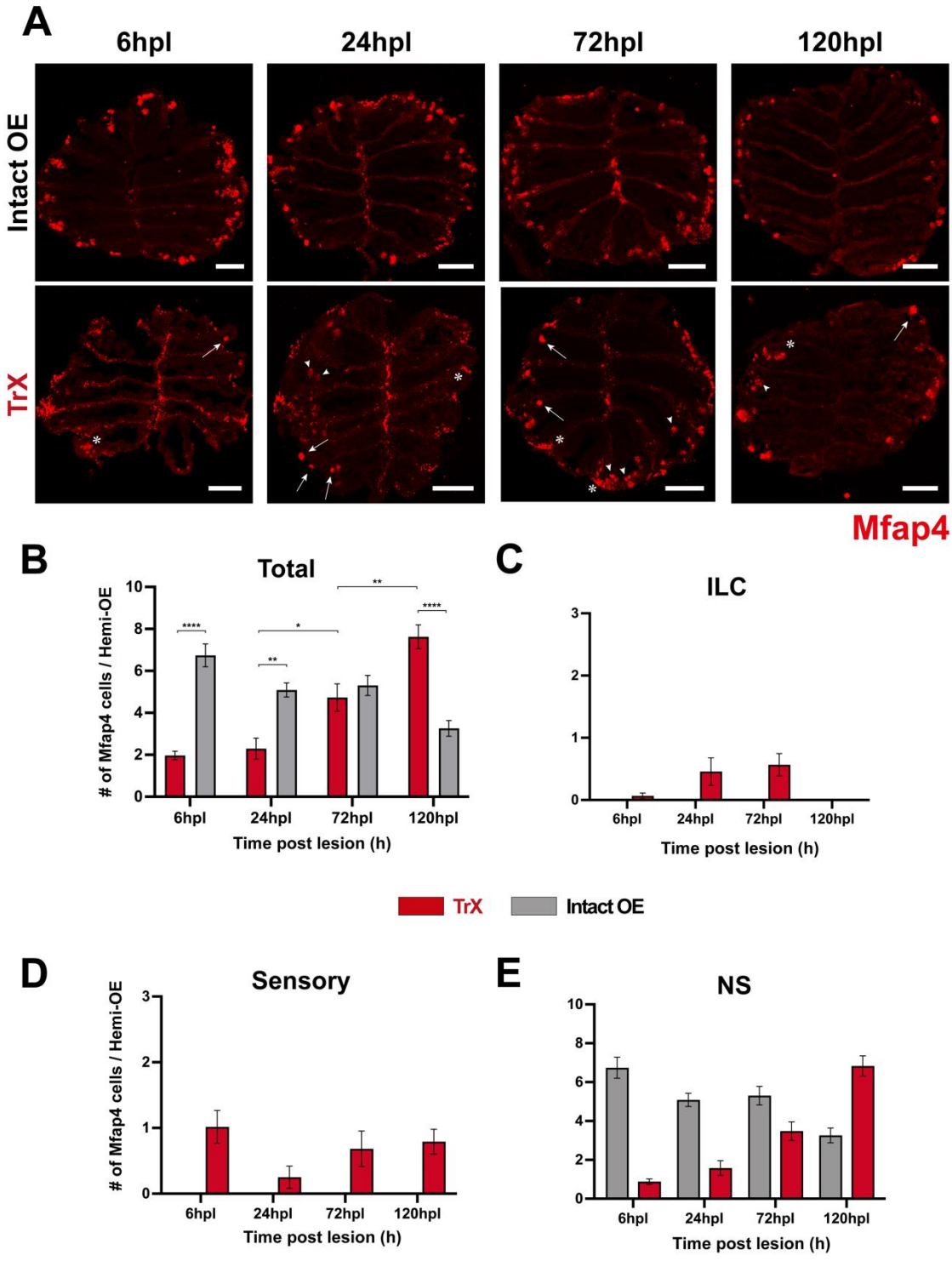

Figure 4.8. Macrophage recruitment is ambiguous upon TrX exposure. (a) Images of the whole OEs at 6, 24, 72 and 120 hpl. Lesioned OEs (bottom panel) and internal controls (top panel) were immunostained against Mfap4 (red). Scale bars: 100 μm. (b) Number of Mfap4-positive cells at different time points post injury. (c, d, e) Regional distribution of Mfap4-positive cells, same data as in (b).

Nevertheless, according to this evidence the most significant increase in the macrophage occupancy following lesion was observed after 72 hpl, which indicates that additional macrophages/monocytes may be recruited to the OE at the later time points in the inflammatory response, mainly around 120 hpl.

In contrast to the lesioned OEs, a gradual decrease in the macrophage numbers was detected in the untreated intact OEs throughout the experimental period of 120 hours (6 hpl, 6,7 ± 0,5; 24 hpl, 5,1 ± 0,3; 72 hpl, 5,3 ± 0,5; 120 hpl, 3,2 ± 0,4; average number of cells per hemi-OE ± SEM), with an approximate 2-fold decrease between 6 and 120 hpl. One-way ANOVA indicated a notifiable change among the intact OE datasets ($p = 1{,}4 \times 10^{-5}$; $F_{(3, 104)} = 9{,}4$), while post hoc Tukey's HSD further revealed that there was a significant decline in the macrophage abundance between 72 to 120 hpl ($p = 0{,}012$), and throughout the whole experimental period between 6 to 120 hpl ($p = 3{,}7 \times 10^{-6}$), but not between other time points (6-24 hpl, $p = 0{,}63$; 24 – 72 hpl, $p = 0{,}99$). This evidence suggests that a marked reduction in the macrophage numbers in the intact OE after 72 hpl should also be considered whilst interpreting the overall observations of the macrophage behavior after TrX exposure.

Building further on these observations, intact and lesioned OE datasets from each time point after chemical lesion were also comparatively analyzed. Intriguingly, an astonishing loss of macrophage abundance was observed in the lesioned OEs compared to the intact controls at the early experimental time points. A near 3,5-fold decrease was detected in the lesioned OEs of 6 hpl compared to the intact OEs ($p = 3{,}0 \times 10^{-11}$; two-tailed unpaired Student's t-test; Figure 4.8b), and approximate 2-fold decrease in the lesioned OEs was evaluated at 24 hpl ($p = 3{,}0 \times 10^{-5}$).

At 72 hpl macrophage occupancy was similar between intact and lesioned OEs ($p = 0{,}48$; two-tailed unpaired Student's t-test), whereas only at the last experimental time point 120 hpl, a marked 2,4 - fold increase in the macrophage numbers were detected in the lesioned OEs ($p = 7{,}3 \times 10^{-8}$). Occupancy in the intact OEs exhibited a gradual reduction towards the later time points after lesion, as opposed to the late/slow occurring rise in the lesioned OEs.

This evidence is supported by the previous observations suggesting that macrophages are recruited later than neutrophils in the inflammatory response and differentiate into M2 subtype, which contributes to the tissue restoration and regeneration after the acute inflammatory phase is over (Chazaud, 2014; Nguyen-Chi et al., 2015).

Macrophage abundance was also assessed in subregion level in Figure 4.8c, d, and e, which are composed of graphical displays exhibiting the number of Mfap4-positive cells in different functional regions of the OE after chemical lesion. The results are comprised of the same data as in Figure 4.8b. It is important to evaluate the pattern of distribution of macrophages in regeneration-related time points after chemical lesion since it may give valuable insight into the functional characteristics of these cells. Under physiological conditions, 100,0% of the macrophages present within the OE were found to be in the non-sensory region, which was consistent throughout all four time points after lesion (Figure 4.8c and d; NA values for intact OEs). In other words, there was a complete absence of Mfap4-positive cells located in the ILC (Figure 4.8c) and the sensory region (Figure 4.8d) in the untreated OEs in any of the experimental time points. In contrast, macrophage distribution expanded proximal to the median raphe in the lesioned OEs and were localized more centrally within the epithelium.

Elevated levels of Mfap4-positive cells in the ILC of the lesioned OEs (Figure 4.8c; 6 hpl: 0,1 ± 0,05; 24 hpl: 0,5 ± 0,2; 72 hpl: 0,6 ± 0,2; 120 hpl: 0,00; average number of cells per hemi-OE ± SEM), as well as in the sensory tissue (Figure 4.8d; 6 hpl: 1,0 ± 0,2; 24 hpl: 0,2 ± 0,2; 72 hpl: 0,7 ± 0,3; 120 hpl: 0,8 ± 0,2) presented a noteworthy contrast with the complete absence of macrophages in the intact OEs. One-way ANOVA revealed a significant change among the number of macrophages located in the ILC in the lesioned OE ($p = 1{,}1 \times 10^{-2}$; $F_{(3, 104)} = 3{,}9$), while post hoc Tukey test further validated a pronounced drop in the cell numbers between 72 and 120 hpl ($p = 0{,}031$).

Contrarily, there wasn't any prominent variation among the number of macrophages located in the sensory region upon TrX exposure ($p = 0{,}15$; $F_{(3, 104)} = 1{,}8$; one-way ANOVA). These evaluations indicate that the resident macrophages in the OE have a strong bias towards the non-sensory epithelium under homeostatic conditions, while they are found more centrally within the epithelium upon chemical injury.

The non-sensory OE was the primary region of macrophage localization in the intact tissue, as well as upon TrX exposure, which is exhibited Figure 4.8c (6 hpl, Intact OE: 6,7 ± 0,5, TrX: 0,9 ± 0,1; 24 hpl, Intact OE: 5,1 ± 0,3, TrX: 1,6 ± 0,4; 72 hpl, Intact OE: 5,3 ± 0,5, TrX: 3,5 ± 0,5; 120 hpl, Intact OE: 3,2 ± 0,4, TrX: 6,8 ± 0,5; mean ± SEM). The gradual increase in the number of Mfap4-positive cells among the lesioned OEs was found to be exhibiting a marked significance ($p = 5{,}4 \times 10^{-18}$; $F_{(3, 104)} = 42{,}4$; one-way ANOVA Tukey's HSD) with a notable change between 72 and 120 hpl datasets ($p = 2{,}4 \times 10^{-7}$).

In summary, macrophages are specifically located in the peripheral non-sensory OE in the intact tissue, while they distribute to a wider area along the radial axis of the OE upon injury. Macrophages are completely absent from the sensory tissue (ILC and the sensory OE) in the intact OE under homeostatic conditions. In addition, no association was detected with the dying OSNs near the non-sensory epithelium, that previously discussed about neutrophils in section 4.2.1.

Detailed presentation of the individual hemi-OEs after TrX exposure is displayed by the hemi-OE ROIs in the Figure 4.9a. Untreated intact (top panel) and TrX lesioned (bottom panel) cross sections of the OE were immunostained against the macrophage specific marker Mfap4 (red) and the neuronal marker HuC/D (blue). Functional territories ILC, sensory, and the non-sensory OE were emphasized by dashed lines on each image. De/regeneration related time points after chemical injury are indicated in separate columns. Almost complete loss of mature OSN population can be observed 6 and 24 hours upon TrX exposure, which is a good indicator of the efficacy of the nasal irrigation process (Figure 4.9a; bottom panel; blue). As expected, most of the lost OSNs were regained from after 72 to 120 hpl, as could be recognized from the anti - HuC/D staining in blue.

Graphical displays of the radial distribution of macrophages along the OE after each time point following chemical injury are provided in detail in Figure 4.9b. Radial axis of the hemi-OE is divided into 10 equidistant bins, similar to those mentioned in the previous sections. The red (TrX lesioned) and gray (intact OE) lines with error bars (SEM) exhibits the number of Mfap4-positive cells versus the radial location.

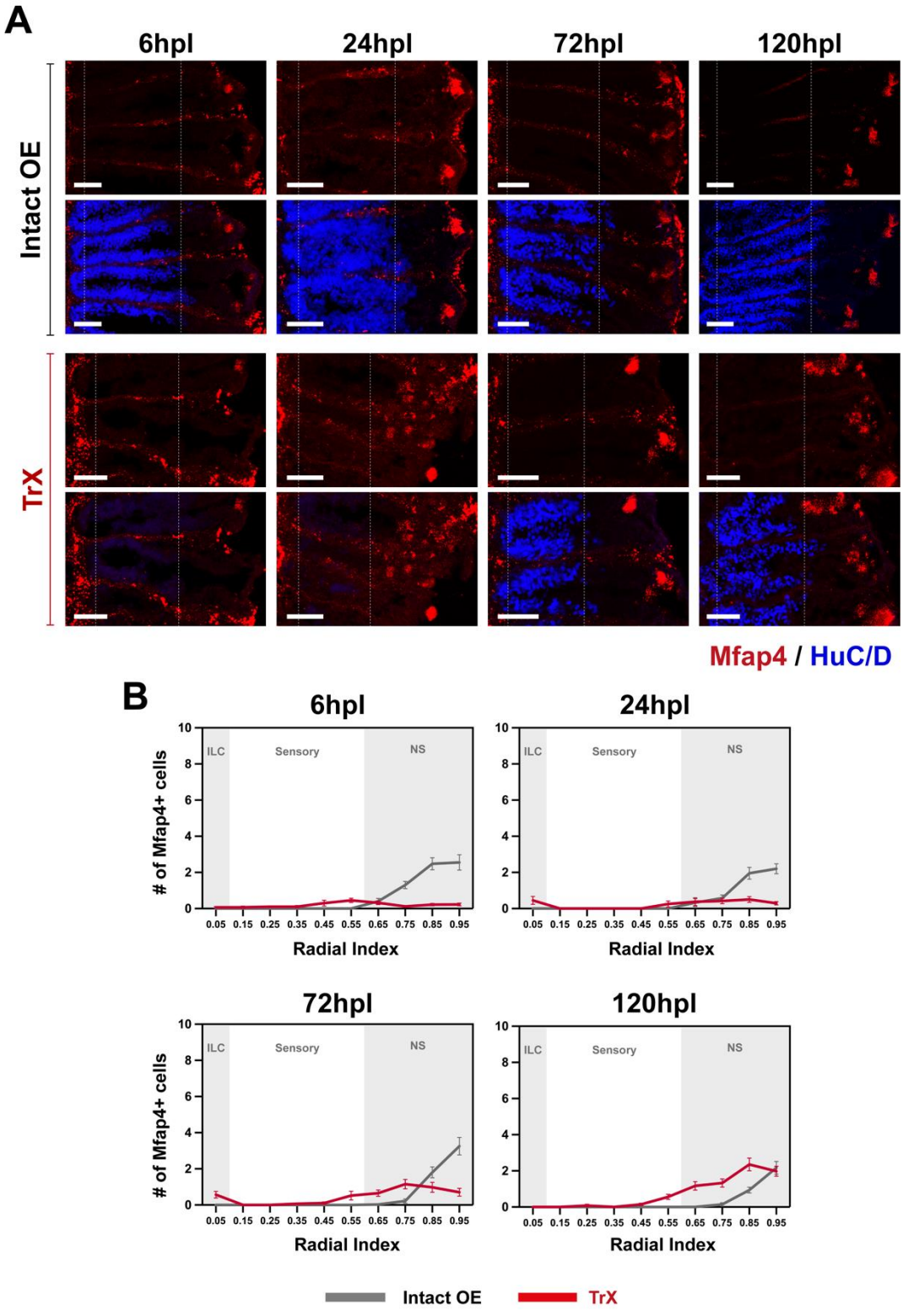

Figure 4.9. Positional profiling of macrophages at different time points after chemical injury. (a) Hemi-OEs of Intact (top panel), and TrX lesioned OEs (bottom panel) at 6, 24, 72, and 120 hpl. Scale bars: 50 μm. (b) Line graphs demonstrating radial distribution of Mfap4-positive cells in the TrX lesioned (red) versus Intact OEs (gray).

Almost all the Mfap-positive cells are located at the non-sensory region, which is indicated by gray shadings on the graphs. At 6, 24 and 72 hpl after lesion the number of macrophages drops below pre-injury levels (Figure 4.9b; see the gray (intact OE) and the red (TrX lesioned) lines). Altogether, the macrophage distribution is expanded towards the central non-sensory region in the lesioned OEs in contrast to the intact OEs, in which the cells particularly tend to occupy the peripheral non-sensory region.

In summary, no notifiable macrophage recruitment was recorded to the OE after chemical injury. In addition, a significant drop in macrophage levels upon damage was observed at 6 to 24 hpl, which reached similar levels with the intact OE at 72 hpl and showed an elevation only at the latest experimental time point of 120 hpl. Therefore, there was a significant reduction in macrophage numbers in the early/acute phase of the inflammatory response which exhibited an elevation at resolution phase after 72 hpl to 120 hpl.

These observations of the late occurring increase in the number of macrophages are consistent with the previous studies on the behavior of the anti-inflammatory (M2) macrophage subtype in zebrafish, which has been shown to have positive contributions on restoration and regeneration in various tissue contexts including heart (Bevan et al., 2020), spinal cord (Ghosh and Hui, 2018), tail fin (Nguyen-Chi et al., 2017; Petrie et al., 2015), and CNS (Kizil et al., 2012).

4.4. Functional Analysis of Neutrophil Behavior upon Sterile Injury

Zebrafish has been a remarkable model organism that offers successful application of *in vivo* genetic depletion methods, which have been appreciated especially in the recent decades. Delivery of morpholino oligomers has been developed as a conventional method to efficient knockdown target gene transcripts in larval and adult zebrafish (Rosowski, 2020). Thrombocyte function was successfully inhibited systematically by injection of morpholinos to the circulation in adult zebrafish (Kim et al., 2010). In addition, recent applications of this method established further confidence on the practicality of morpholino knockdown in larval and adult zebrafish.

Effectiveness of the MO knockdown of target gene transcripts in adult zebrafish was confirmed with significant evidence (Raman et al., 2020). Successful knockdown of serine proteases in adult zebrafish were conducted by morpholino administration to the circulation (Khandekar et al., 2020).

The aim of this part of the thesis is to investigate whether neutrophil depletion influences the regeneration and neurogenesis of the injured OE. To do so, a reproducible protocol was developed to deliver VMOs in the circulatory system of the adult zebrafish by RO injection of a fluorescent dye. Then, the primary hematopoietic organs were analyzed after morpholino knockdown, and after inactive control morpholino administration, to examine the potential effects of vivo morpholinos on the systemic neutrophil levels. Neutrophil depletion was also confirmed in the intact and lesioned OE by analyzing the change in the neutrophil numbers 24 h after morpholino administration.

Finally, the potential effects of the systemic neutrophil depletion on regenerative events were assessed by analyzing the area covered by mature OSNs in the OE five days after TrX exposure.

4.4.1. Retro-Orbital Injection is an Effective Method to Deliver VMOs to Blood Circulation of Adult Zebrafish

RO injection has been developed as a plausible approach to deliver drugs and experimental substances to the bloodstream of adult zebrafish (Pugach et al., 2009). RO injection offers a more efficient delivery of experimental substances to the circulation than the conventionally used intra-venous (IV) injection to the common cardinal vein of zebrafish. Although IV approach may offer a sufficient and effective delivery method for other model organisms, several fundamental characteristics of zebrafish make it more challenging for this method to be practical.

First, zebrafish is a relatively small organism that makes the injection procedure harder because of the narrow diameter of the dorsal aorta, or the common cardinal vein.

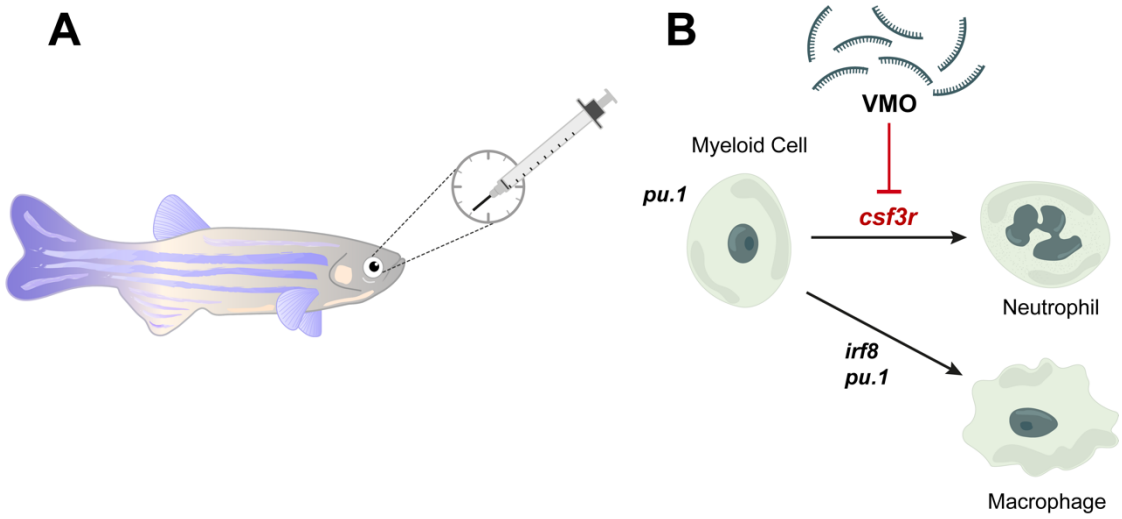

Figure 4.10. Delivery of VMOs into the circulatory system via RO injection. (a) Application of RO injection with an insulin syringe. (b) VMOs against csf3r transcript enables effective temporal elimination of neutrophils by blocking their differentiation from myeloid lineage.

In contrast, the injection is applied into a sinusoidal venous chamber, which enables all the substance to be incorporated into the circulatory system and provides a more efficient distribution of the substance all the way to the tail (Pugach et al., 2009). Since the retro orbital venous sinus can be reached easily from the natural opening behind the eye, the RO method does not cause excessive scarring or additional wound healing process (Pugach et al., 2009). This is also an imperative point considering the subject of study of this thesis, since additional scarring of damage would mean an immune response that may be interpreted as a false positive result. IV to common cardinal vein causes additional tissue injury, scarring, and an elevated mortality rate in comparison with RO method, in which a much quicker recovery is seen.

The injection solution was prepared to include the fluorescent reporter dye FITC-Dextran (70 kDa) to record the success of the procedure under a fluorescence stereomicroscope. The solution was injected to 7 o'clock direction on the eye which corresponds to the correct spot to penetrate into the retro orbital venous sinus located right behind (Figure 4.10a; Pugach et al., 2009). Figure 4.11 demonstrates the images captured with a stereomicroscope (GFP; 488 nm excitation wavelength laser) 5 minutes after RO injection of FITC-Dextran.

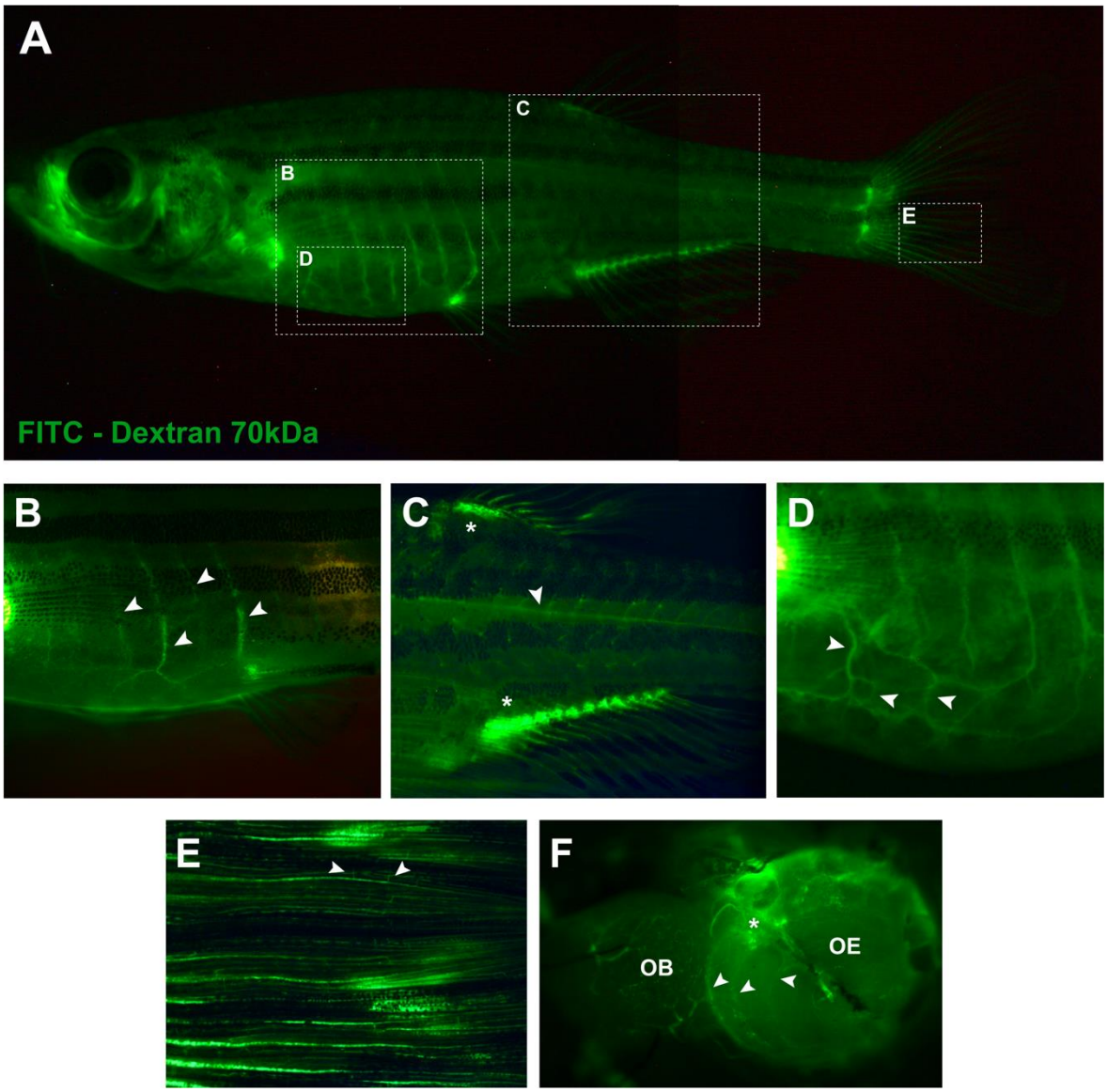

Figure 4.11. Dextran conjugated dye confirms effective delivery of the morpholinos to the circulation. (a) Stereomicroscope image of the whole fish after RO injection of FITC-Dextran. High power images of the abdomen (b), trunk (c), capillaries (d), and tail fin (e) are demonstrated. (f) OE attached to the olfactory bulb.

A composite image of the entire zebrafish is exhibited in Figure 4.11a. Dashed boxes indicate the regions that are illustrated in high magnification below. Successful systematic dispersion of the fluorescent dye unveiled the arrangement of the circulatory system of zebrafish, as well as confirmed the RO injection protocol as an effective and monitorable approach to deliver VMOs in the bloodstream.

Blood vessels in the dorsoventral direction are located parallel to each other and form a segmented pattern in the trunk (Figure 4.11b; arrowheads). Proximal roots of the dorsal and the anal fin displays high signal accumulation (Figure 4.11c; asterisks).

Common cardinal vein can be clearly distinguished traveling through the anteroposterior axis, between the second and third body stripes (Figure 4.11c; arrowhead). The efficacy of RO injection can also be observed from the rigid signaling pattern in the capillaries located in the abdomen (Figure 4.11d; arrowheads). High-power magnification of the tail fin revealed a dense pattern of blood vessels located proximodistal in Figure 4.11e.

The capillary connections between these vessels confirmed that these are elements of circulation but not the individual fin rays, that are the structural elements of the bone construction in the tail fin (Uemoto et al., 2020). The OE was also dissected out in connection with the olfactory bulb and visualized under the stereomicroscope. Figure 4.11f displays the OE from a ventral viewpoint. OB can be seen in the left, while OE can be observed on the right. Blood vessels within the OB are clearly distinguished, indicating that the injection is also successful to penetrate the vasculature within CNS. The olfactory nerve (ON) can be observed connecting OE and OB (Figure 4.11f; asterisk). Strong fluorescence signal reveals the arrangement of the vasculature surrounding the OE. Consistent with the previous evidence in literature, the blood vessels were located between the epithelial sheets, within the lamina propria (arrowheads), and a dense vascular accumulation was detected in the ventral midline of the OO, corresponding to the median raphe (Figure 4.11f).

4.4.2. The Primary Hematopoietic Organs were Assessed to Confirm Systemic Depletion of Neutrophils by Morpholino-Knockdown

Neutrophil differentiation from myeloid lineage, and granulopoiesis is dependent on the signaling cascade mediated by the granulocyte colony stimulating factor receptor (GCSFR), which is also named as the colony stimulating factor 3 receptor (CSF3R; Liongue et al., 2009; Figure 4.11b). Genetic methods that target this receptor has been shown to achieve a successful temporal elimination of neutrophils in zebrafish (Pazhakh et al., 2017). Antisense VMO against *csf3r* pre-mRNA blocks the splice site within exon 4 of the *csf3r* gene on chromosome 16 by complementary base-pairing.

This results in the interference of the translational process, leading to a systematic reduction of the neutrophilic granulocytes (Liongue et al., 2009).

The kidney is the primary hematopoietic organ of the zebrafish where all blood cells (except for T cells) are produced from precursors. The hematopoietic parenchyma is located in between the renal tubules, which carry out the excretory events (Xu et al., 2012). Precursors are born and differentiate into mature hematopoietic cells in the kidney parenchyma. On the other hand, spleen has a crucial role in filtering the blood and eliminating foreign pathogens, toxicants, and irritant agents, as well as aging RBCs and dead cells (Menke et al., 2011). Alongside an extensive population of resident macrophages, there is also a humbler neutrophil population residing in the splenic parenchyma to contribute to the immunological duties of the organ (Bennett et al., 2001).

To understand whether splice blocking antisense VMOs against the *csf3r* transcript is successful to significantly reduce mature neutrophils systematically, the primary hematopoietic organs of the zebrafish were analyzed, and the level of neutrophil depletion were recorded to serve as an independent reference point for the upcoming experiments that are focused on the OE.

Inactive control VMO (n = 3 fish) or VMO against *csf3r* (n = 3 fish) were administered to each fish by RO injection two times at 24 h intervals. The kidney and spleen of the fish were than dissected out, cryosectioned to glass slides to 12 μm thickness, and immunostained against the neutrophil specific Mpx. Three separate sections of the kidney and the spleen from each fish were captured by confocal microscopy. To analyze the area occupied by Mpx-positive cells relative to the overall area of the tissue, a fixed square ROI (679,78 x 679,78 μm^2) was generated. Three separate regions within each section were selected by this ROI and cropped. Overall, 6 fish (3 sections of each organ / fish; 3 separate ROIs / section) were used. The same ROI was used for both spleen and kidney sections.

Therefore, the calculations of the relative area covered by the Mpx-positive cells will be compatible with each other as well as between the spleen and the kidney. The area analysis was normalized to the internal controls to establish the level of decrease in the neutrophil levels upon antisense morpholino knockdown.

Figure 4.12a exhibits the kidney (bottom row) and spleen (top row) sections of the KD (right panel) and the control animals (left panel). Anti-Mpx staining (green) was coupled with the brightfield imaging to understand the boundaries of the tissue sections. The animals injected with the inactive control VMO (VMO-ctr) provides the basal levels of neutrophiles in the kidney and spleen under physiological conditions. Consistent with the insight obtained from the literature, kidney hosted a dense neutrophil population distributed evenly throughout the parenchyma in the control animals (Figure 4.12a; bottom left; green). The cells were mostly situated in the tissue as clusters and there were gaps between these dense cluster of cells which may attributed to the renal tubules. On the other hand, splenic neutrophils in the control animals were distributed along the tissue as individually distinguishable cells, and they were fewer in number relative to those in located in the kidney (Figure 4.12a; top left; green). The brightfield imagery of the spleen reveals that the neutrophils were distributed evenly along within the tissue boundaries.

Upon administration of the VMO against *csf3r* (VMO-csf3r), the number of resident neutrophils located in the spleen and the kidney of the KD animals were severely decreased, and this remarkable reduction was evident to the eye upon analyzing the confocal images (Figure 4.12a; right panel; green). The resident neutrophils of the kidney presented themselves in remarkably low numbers in the KD animals and could be distinguished as individual cells, in contrast to the dense neutrophil clusters that were occupying most of the parenchyma in the controls (Figure 4.12a; bottom right; green). The neutrophils in the spleen of KD animals were also fewer in number than the control animals, distributed along the tissue with large gaps in between (Figure 4.12a; top right; green).

The quantitative analysis of the neutrophil occupancy in the spleen and kidney of KD and control animals revealed that the VMO-csf3r administration resulted in a successful systemic depletion of neutrophils. The results of the analysis were presented in Figure 4.12b, in which kidney (green) and spleen (purple) datasets were represented in different colors, while the administered VMOs were displayed in different shades. The graph plots the normalized values of the area covered by the Mpx-positive cells in the KD and the control animals. The neutrophil abundance was significantly dropped upon VMO-csf3r treatment in the kidney ($p = 4{,}7 \times 10^{-14}$; t = 10,2; df = 52; unpaired Student's t-test) and in the spleen ($p = 1{,}4 \times 10^{-13}$; t = 9,9; df = 52; unpaired Student's t-test).

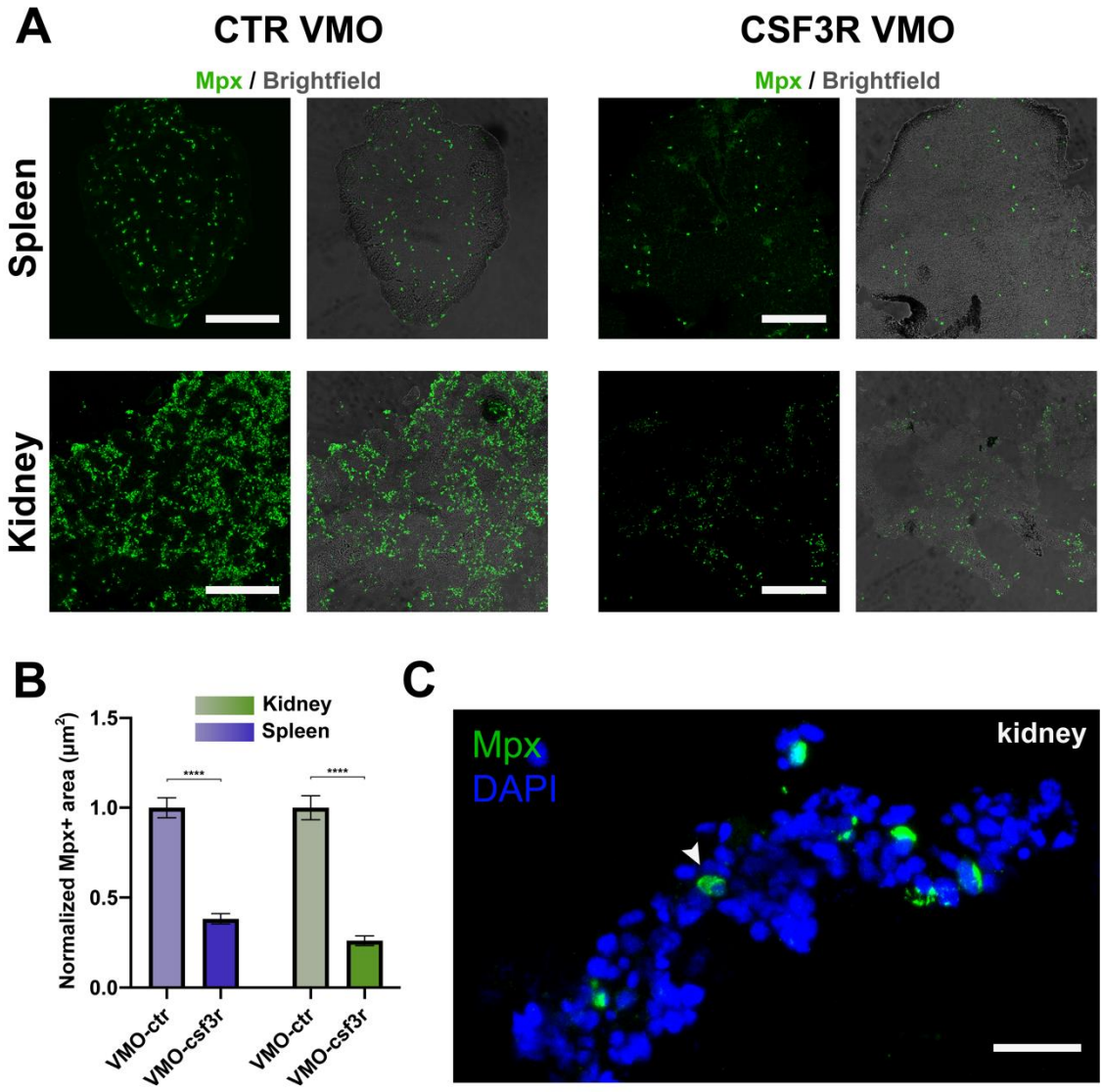

Figure 4.12. Administration of morpholinos against csf3r results in a systemic neutrophil depletion. (a) Kidney and spleen sections of control (left panel), and KD animals (right panel) that were immunostained against Mpx (green), with brightfield imagery (grays). (b) Neutrophil occupancy in the kidney and spleen. (c) Kidney section after morpholino KD; Mpx (green); DAPI (blue). Scale bars: (a) 100 μm, (b) 25 μm.

To confirm the cellular identity of the Mpx-positive signals on the kidney and spleen, DAPI was applied on the organ sections. A high-power magnification of a kidney section of a KD fish with anti-Mpx (green) and DAPI (blue) staining is displayed in Figure 4.12c. The nuclei of the kidney cells are clearly visible with blue DAPI signals. A neutrophilic cell can be observed with cytoplasmic Mpx (green) signal and nuclear DAPI (blue) signal (Figure 4.12c; arrowhead).

4.4.3. Vivo-Morpholinos against *csf3r* Successfully Depleted Neutrophilic Granulocytes in the OE

Following the confirmation of the successful systemic depletion of neutrophils by MO induced knockdown, the resulting effects in the intact and regenerating OE were assessed. RO injection solutions were prepared to include VMO solutions and the fluorescent reporter dye FITC-Dextran (70 kDa) to enable confirmation of the success of the injection. 3 fish were injected with the antisense VMOs against *csf3r* (VMO-csf3r), while 3 fish were injected with the inactive VMO-ctr.

The injections were repeated after 24 hours. The success of the injections was confirmed by monitoring fluorescent signal under a stereomicroscope 5 minutes after each injection. Nasal irrigation with TrX to the left OOs of each of the 6 fish (VMO-csf3r, n = 3; VMO-ctr, n = 3), together with the IP injections of EdU containing solutions to visualize proliferating cells were applied 48 hours after the first morpholino injections (24 hours after the second injection). The OOs were dissected out at 24 hpl, cryosectioned, and adjusted to immunohistochemistry against the neutrophil marker Mpx, neuronal marker HuC/D. A Click-iT reaction procedure was additionally applied to visualize EdU-positive cells on the cross sections. Images of 5 sections from each OE were acquired via confocal microscopy at 2048 x 2048 - pixel resolution, which were than adjusted to cell counting in the FIJI software.

Figure 4.13a displays the intact and lesioned OEs of the knockdown (KD) and the control animals. Images that belong to VMO-ctr and VMO-csf3r injected animals are represented in different panels (Figure 4.13a; VMO-ctr, left panel; VMO-csf3r, right panel). Intact and TrX lesioned conditions are also exhibited in separate columns (Figure 4.13a; Intact OEs, top row; TrX lesioned, bottom row). Consistent with the previous results that were presented in section 4.2.1., a rapid and intense neutrophil influx were observed at 24 hpl upon TrX exposure in the VMO-ctr injected animals. The success and proper application of the nasal irrigation can be detected by the loss of mature OSNs (Figure 4.13a; HuC/D signal; blue) in the lesioned OEs in control and KD animals. Remarkably, the dense neutrophil recruitment, which is normally observed at 24 hpl upon TrX administration, did not appear after MO knockdown has been applied (Figure 4.13a; bottom right; green).

The level of neutrophil occupancy was observed almost at basal levels which is detected in the intact OE (Figure 4.13a; top row; green), which suggests that RO injection of VMOs against *csf3r* were successful in eliminating most of the neutrophils that are recruited to the OE upon chemical injury. Number of neutrophils showed a rapid and robust 20-fold decrease in the lesioned OEs (VMO-ctr: 159 ± 10; VMO-csf3r: 8 ± 1; average number of cells per hemi-OE ± SEM), and a near 3-fold decrease in the intact OEs (VMO-ctr: 10 ± 1,6; VMO-csf3r: 3,2 ± 0,3; Mean ± SEM) 24 h after VMO-csf3r injection compared to the VMO-ctr injected animals (Figure 4.13b).

Note that VMO-csf3r was able to deplete neutrophils below the physiological levels. This evidence suggests that VMO-csf3r achieved a remarkable efficacy in depleting neutrophils in the OE. The cell counts were adjusted to statistical hypothesis testing, which revealed a highly significant change among the datasets (Intact/lesioned OE: $p = 4{,}5 \times 10^{-29}$, $F_{(1,116)} = 226{,}9$; VMO-csf3r/VMO-ctr: $p = 5{,}4 \times 10^{-28}$, $F_{(1,116)} = 212{,}6$; two-way ANOVA). As expected, adjusted p values from the Tukey's HSD indicated no significant difference between the intact OEs of the Ctr and KD animals ($p = 0{,}77$; two-way ANOVA post hoc Tukey's HSD), while a notable change was confirmed between the lesioned OEs of the control and KD animals ($p = 2{,}0 \times 10^{-15}$; two-way ANOVA post hoc Tukey's HSD), which exhibits the level of significance of the neutrophil depletion resulting from VMO-csf3r administration (Figure 4.13b).

Knockdown of *csf3r* further resulted in the neutrophil abundance in the lesioned OEs to drop to similar levels with that in the intact OE of the control animals ($p = 0{,}93$; two-way ANOVA post hoc Tukey's HSD). Building further on these observations, potential change in the neutrophil abundance was also considered in the subregion level (Figure 4.13b). Number of Mpx-positive cells that were located within the ILC (VMO-csf3r: Intact OE, 0,00, TrX, 0,2 ± 0,1; VMO-ctr: Intact OE, 2,2 ± 0,6, TrX, 24,8 ± 2,3), sensory (VMO-csf3r: Intact OE, 0,2 ± 0,14, TrX, 2,3 ± 0,6; VMO-ctr: Intact OE, 2,5 ± 0,7, TrX, 60 ± 4,8), and the non-sensory region (VMO-csf3r: Intact OE, 3 ± 0,3, TrX, 5,3 ± 0,8; VMO-ctr: Intact OE, 5,6 ± 0,9, TrX, 74 ± 5) were recorded and comparatively analyzed.

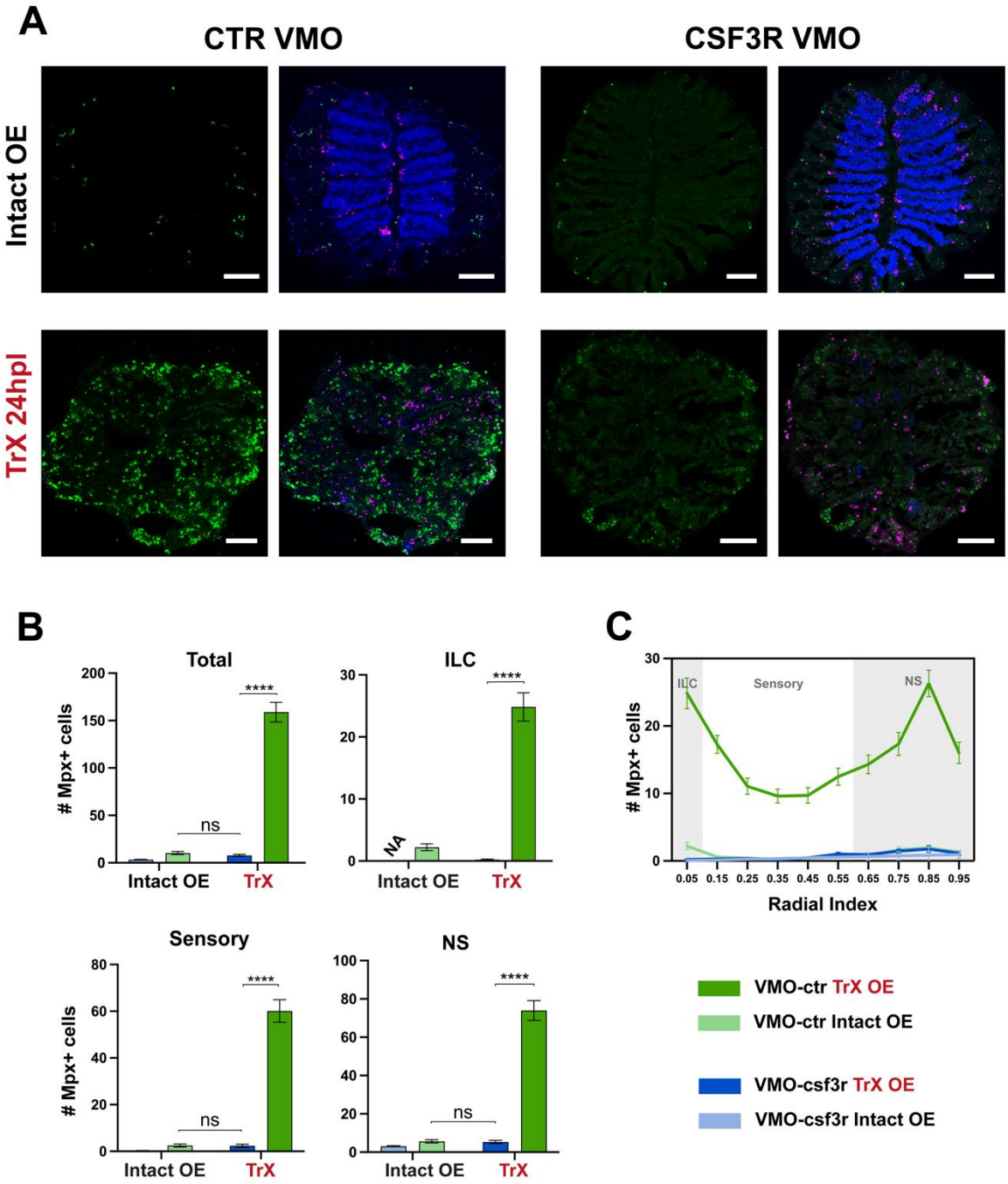

Figure 4.13. Morpholino administration results in a successful neutrophil depletion in the OE. (a) Confocal images of the intact (top panel), and TrX-lesioned OEs at 24 hpl (bottom panel) after VMO-ctr (left panel) or VMO-csf3r (right panel) injection. Scale bars: 100μm. (b) Neutrophil abundance in the intact and the lesioned OEs of the control and the KD animals. (c) Regional distribution of neutrophils. Same data as in (b).

Two-way ANOVA revealed a significance among the datasets that belong to ILC (Intact OE/TrX: $p = 9{,}3 \times 10^{-17}$, $F_{(1,116)} = 95{,}0$; VMO-csf3r/VMO-ctr: $p = 8{,}1 \times 10^{-21}$, $F_{(1,116)} = 131{,}5$). Multiple comparisons elaborated this evidence and indicated a firm significance between the lesioned OEs of the control and the KD animals (Figure 4.13b; top right; $p = 2{,}0 \times 10^{-15}$; two-way ANOVA post hoc Tukey's HSD). Morpholino knockdown resulted in a notable change in neutrophil occupancy also in the sensory epithelium (Figure 4.13b; bottom left; Intact OE/TrX: $p = 1{,}8 \times 10^{-22}$, $F_{(1,116)} = 148{,}2$; VMO-csf3r/VMO-ctr: $p = 1{,}2 \times 10^{-22}$, $F_{(1,116)} = 150{,}0$; two-way ANOVA), with a significant decrease in the lesioned OEs of the KD animals, compared to that of the control animals ($p = 2{,}0 \times 10^{-15}$; two-way ANOVA post hoc Tukey's HSD).

In addition, morpholino knockdown resulted in a drop in the neutrophil abundance in the lesioned OEs to the basal levels, that was recorded in the untreated intact OEs of the VMO-ctr injected animals ($p = 0{,}99$; two-way ANOVA post hoc Tukey's HSD). Finally, similar outcomes were present within the non-sensory region (Figure 4.12b; bottom right; Intact/Lesioned: $p = 5{,}6 \times 10^{-25}$, $F_{(1,116)} = 175{,}7$; VMO-csf3r/VMO-ctr: $p = 2{,}9 \times 10^{-25}$, $F_{(1,116)} = 179{,}0$; two-way ANOVA), which revealed a considerable reduction in the lesioned OEs of the KD animals, compared to that of the control animals ($p = 2{,}0 \times 10^{-15}$; two-way ANOVA post hoc Tukey's HSD), and detected neutrophil numbers dropped to basal levels in the lesioned OEs of the KD animals ($p = 0{,}99$; two-way ANOVA post hoc Tukey's HSD).

4.4.4. Proliferative Activity is Affected by Neutrophil Depletion in the Lesioned OEs

Investigating the potential effects of neutrophil depletion on the proliferative activity in the intact and the lesioned OE, may give an insight into whether neutrophils have a functional influence on the maintenance and/or the regenerative neurogenesis in the OE. Confocal images of the intact and lesioned OEs of KD and control animals are presented in Figure 4.14a. Proliferating cells were marked via Click-iT EdU reaction application on the cross sections. The EdU-positive cells exhibited a regular pattern in the intact OEs of KD and control animals (Figure 4.14a; top panel; magenta), which is consistent with the pattern of maintenance neurogenesis that is observed under physiological conditions.

As expected, the basal pattern of mitotic activity is disrupted, and the level of EdU-positive cells increased 24 hours TrX exposure in the VMO-ctr injected animals (Figure 4.14a; bottom left; magenta). However, morpholino knockdown resulted in a reduced level of mitotic activity at 24 hpl in the KD animals (Figure 4.14a; top right; magenta), which suggests that neutrophil depletion leads to a severe decrease in the proliferative activity after chemical injury.

To record any potential changes in mitotic activity upon neutrophil depletion in the intact and the TrX lesioned OEs, number of EdU-positive cells were also analyzed in the VMO-csf3r injected, and in the VMO-ctr injected animals (Figure 4.14b). Total number of the EdU-positive cells in the VMO-ctr injected zebrafish were recorded as 87 ± 5 (mean ± SEM) cells in the intact OE, and 80 ± 7 cells in the TrX lesioned OE 24 after lesion.

On the other hand, 80 ± 5 cells in the intact OE versus 42 ± 2,6 cells in the TrX lesioned OE were present in the KD animals. Further analysis on these data reveled that there was a near 2-fold decrease in the lesioned OE of the KD fish compared to the control fish, while there was no significant fold change in the intact OEs between two conditions (Figure 4.14b). Therefore, the mitotic activity showed a more robust change in the lesioned OEs at 24 hpl, in which neutrophil abundance also exhibited a much more severe change upon VMO-csf3r application. As expected, two-way ANOVA revealed a considerable change in the mitotic activity upon morpholino knockdown (Intact/Lesioned: $p = 2{,}9 \times 10^{-5}$, $F_{(1,116)} = 19{,}0$; VMO-csf3r/VMO-ctr: $p = 3{,}5 \times 10^{-5}$, $F_{(1,116)} = 18{,}5$; two-way ANOVA).

Building further on this calculation, the highest level of change was recorded between the lesioned OEs of the control the KD animals ($p = 8{,}1 \times 10^{-6}$; two-way ANOVA post hoc Tukey's HSD), which indicated a significant decrease in the proliferative activity after lesion upon neutrophil depletion. In contrast, the intact OEs of control and KD animals did not show a notable difference in the number of dividing cells ($p = 0{,}75$; two-way ANOVA post hoc Tukey's HSD), and morpholino knockdown resulted in a marked reduction in the number of dividing cells upon lesion that dropped significantly below the basal levels that were recorded in the intact tissues of the VMO-ctr injected animals (Figure 4.14b; $p = 7{,}7 \times 10^{-8}$; two-way ANOVA post hoc Tukey's HSD).

This evidence may indicate that the neutrophils have an influence on the mitotic activity only after a lesion is introduced, but do not have a significant effect under homeostatic conditions.

Mitotic activity was also assessed in subregion level (Figure 4.14c) in which EdU-positive cells located in the ILC (VMO-ctr: Intact OE, 9,4 ± 1,4, TrX, 16,6 ± 1,4; VMO-csf3r: Intact OE, 15,3 ± 0,96; TrX, 4,6 ± 0,7), the sensory (VMO-ctr: Intact OE, 49 ± 4, TrX, 35 ± 5; VMO-ctr: Intact OE, 25 ± 2, TrX, 21 ± 1,4), and the non-sensory region (VMO-ctr: Intact OE, 29 ± 2,2, TrX, 28 ± 1,9; VMO-csf3r: Intact OE, 39 ± 3,6, TrX, 16 ± 1,8) were established. Further investigation was imperative to reveal the level of significance between the individual data sets that were belong to ILC (Intact OE/TrX: p = 0,12, $F_{(1,116)}$ = 2,4; VMO-csf3r/VMO-ctr: p = 8,5 x 10^{-3}, $F_{(1,116)}$ = 7,2; two-way ANOVA), sensory (Intact OE/TrX: p = 1,2 x 10^{-2}, $F_{(1,116)}$ = 6,5; VMO-csf3r/VMO-ctr: p = 2,3 x 10^{-7}, $F_{(1,116)}$ = 30,2; two-way ANOVA), and the non-sensory (Intact OE/TrX: p = 2,2 x 10^{-6}, $F_{(1,116)}$ = 24,9; VMO-csf3r/VMO-ctr: p = 0,8, $F_{(1,116)}$ = 0,06; two-way ANOVA), since the outcomes of the two-way ANOVA were peculiar at some parameters.

Upon TrX exposure, the number of dividing cells located within the ILC showed a quick and robust decrease in the KD animals in comparison with the control fish (p = 1,4 x 10^{-10}; two-way ANOVA post hoc Tukey's HSD), while a lower significance was detected between the lesioned OE of the KD animals and the intact OE of the control animals (Figure 4.14c; left; p = 1,7 x 10^{-2}; two-way ANOVA post hoc Tukey's HSD). Cell proliferation in the sensory region also exhibited a notable change upon TrX exposure, between the KD animals and the controls (Figure 4.14c; center; p = 1,6 x 10^{-2}; two-way ANOVA post hoc Tukey's HSD).

In addition, the level of change in the proliferative activity in the non-sensory region was higher between the lesioned OEs of KD and control animals (Figure 4.14c; right; p = 9,2 x 10^{-3}; two-way ANOVA post hoc Tukey's HSD), than the intact OEs of both conditions (p = 2,6 x 10^{-2}; two-way ANOVA post hoc Tukey's HSD). The highest level of significance was recorded between the intact and lesioned OEs of the KD animals (p = 9,6 x 10^{-9}; two-way ANOVA post hoc Tukey's HSD).

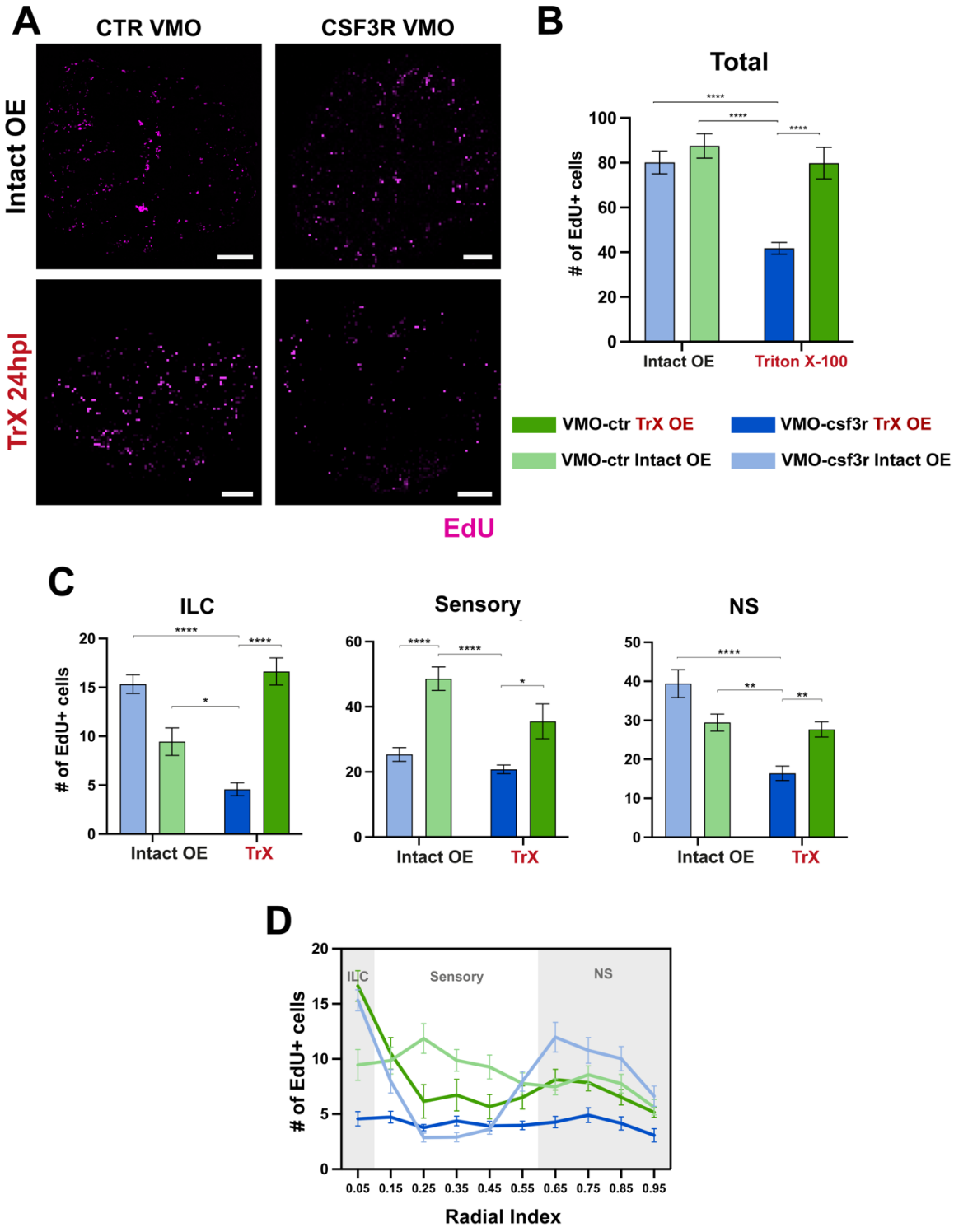

Figure 4.14. Proliferative activity in the OE is influenced by the neutrophil depletion. (a) Confocal Images of the intact and TrX lesioned OEs of the KD and the control animals. Scale bars: 100µm. (b, c) Qualitative representation of the proliferative activity after morpholino knockdown. (d) Positional profiling of EdU-positive cells.

The positional profiling of EdU-positive cells was displayed in Figure 4.14d, which exhibits the changes in the pattern distribution of proliferative activity in the OE upon neutrophil depletion. Data sets of the VMO-csf3r injected animals were indicated by blue shaded lines, whereas datasets of the VMO-ctr injected control animals were demonstrated in green shaded lines. The number of EdU-positive cells were represented in the y-axis, while the radial positions along the hemi-OE were represented in the x-axis, and the subregions were indicated with gray shading. The intact OE of the VMO-ctr injected animals exhibited a profile (Figure 4.14d; light blue line) consistent with the maintenance neurogenesis pattern which is observed under physiological conditions (Figure 4.7c; gray line). As expected, the mitotic activity exhibited a more balanced distribution along the hemi-OE upon TrX exposure in both control and the KD animals (Figure 4.14d; dark blue and dark green lines).

However, the number of EdU-positive cells were severely low throughout the radial axis in the KD animals (dark blue line), in contrast to the internal controls (light blue line), which indicates that neutrophil depletion negatively effects the mitotic activity after chemical injury.

4.4.5. Systemic Neutrophil Depletion Impairs the Efficiency of Regenerative Neurogenesis in the OE

The fish were injected with morpholino solutions two times at 24h intervals (VMO-ctr, n = 3 fish; VMO-csf3r, n = 3 fish). Left OOs of each fish were exposed to nasal irrigation with TrX 24h after the morpholino injections. To monitor the mitotic activity in the 3rd day of the regeneration period, the fish were intraperitoneally injected with EdU containing solutions.

The OOs were dissected out at 120 hpl, cryosectioned, and immunostained against the neutrophil marker Mpx, neuronal marker HuC/D, and adjusted to EdU Click-it reaction to visualize the EdU-positive cells. 5 sections from each OE were captured via confocal microscopy at 2048 x 2048 - pixel resolution.

2 hemi-OEs from each section were cropped using the same rectangular ROI for cell counting, which is discussed in the previous sections, while single-channel HuC/D images of the whole OEs were adjusted for HuC/D area analysis in the FIJI software.

The EdU solution was previously shown to label dividing cells for approximately 24 hours. Therefore, the EdU pulse given at the 48th hour after lesion, would provide monitoring the mitotic activity at the 3rd day of the regeneration period, which was demonstrated to be the time point where the peak in OSN neurogenesis is observed (Kocagöz et al., 2022).

Representative images of the OE sections of the KD (right panel) and the control (left panel) animals at 120 hpl were displayed in the Figure 4.15a. Intact OEs were shown in the top row, while the lesioned OEs were placed into the bottom row. For the sake of a clear visualization of the OSN neurogenesis, anti HuC/D staining (red) were provided in isolation next to the merged images with the addition of the EdU signal (green). Double positive signals (yellow) denote the mitotic activity that generated new OSNs and repopulated the sensory region.

The images of the intact OEs provide a rigid internal control to monitor whether the proliferative activity in the unlesioned tissues exhibited an expected pattern of distribution, which was previously shown (Bayramli et al., 2017; Kocagöz et al., 2022), and discussed in section 4.2.2. Visual assessment of the intact OEs reveals that the radial positioning of the EdU-positive cells was indeed reliable and consistent with the pattern of maintenance neurogenesis which takes place continuously at the tips of the ILC and at the sensory/non-sensory border under physiological conditions. Note that in the intact OEs of both KD (Figure 4.15a; top right) and control animals (Figure 4.15a; top left), the EdU- positive cells (green) are localized to the tips of the ILC, where HuC/D-EdU double-positive signals can be observed in yellow, indicating newly emerging OSNs. The EdU-positive cells were also positioned at the peripheral margin of the sensory region, defining the sensory/non-sensory border.

The quantitative analysis of the mitotic cells indicated a highly significant change among the datasets (Figure 4.15b; left most graph; Intact OE/TrX: p = 1,3 x 10^{-20}; VMO-csf3r/VMO-ctr: p = 2,4 x 10^{-21}; Two-way ANOVA).

A consistent profile was detected between the intact OEs of the KD and the control animals (VMO-ctr: 80,8 ± 5,5; VMO-csf3r: 65 ± 5,6 cells per hemi-OE; mean ± SEM), with a non-significant decrease in the EdU-positive cell number in KD samples (p = 0,81; Two-way ANOVA post hoc Tukey's HSD). In contrast, a notable difference in the proliferative activity was recorded between the lesioned OEs of the KD (77 ± 6 cells per hemi-OE; mean ± SEM), and the control animals (352 ± 23 cells per hemi-OE; mean ± SEM) with a near 80% decrease in the number of EdU-positive cells ($p = 0,2 \times 10^{-14}$; Two-way ANOVA post hoc Tukey's HSD; Figure 4.15b; left most graph). In addition, cell division in the intact OE of the control animals was found to be at similar levels with that in the lesioned OEs of the KD animals (p = 0,99; Two-way ANOVA post hoc Tukey's HSD), which indicates that the morpholino knockdown reduced the mitotic activity to basal levels seen in the intact tissue under homeostatic circumstances (Figure 4.15b; left most graph).

To understand the spatial pattern of the proliferative behavior in the regenerating OE under neutrophil scarcity, the quantitative analysis of EdU-positive cells was also assessed in subregion level (Figure 4.15b). In the intact OE, the neurogenesis is restricted to the tips of the ILC and the sensory/non-sensory border. As discovered in previous studies, upon chemical injury the proliferative activity acquires a distinct profile to regain the lost OSNs, and the overall number of mitotically active cells increase in the injured OE (Kocagöz et al., 2022). Consistent with this evidence, in the VMO-ctr injected animals, 20 ± 2 (mean ± SEM) mitotically active cells were found to be located in the ILC of the intact OEs, while 44,28 ± 4,54 cells were detected in the ILC of the lesioned OEs (Figure 4.15b). In contrast with the control animals, VMO-csf3r injected neutrophil scarce animals showed a robust 90,9% decrease in the number of EdU-positive cells located in the ILC upon TrX exposure (4,0 ± 0,6 cells per hemi-OE; mean ± SEM) in comparison to that of the control animals. Intriguingly, the number of mitotically active cells was found to be 75% lower than that of the intact OEs (16 ± 1,9 cells per hemi-OE; mean ± SEM; $p = 8,6 \times 10^{-3}$; Two-way ANOVA post hoc Tukey's HSD), which may indicate that neutrophils have an exclusive function on the proliferative activity in the OE that is only activated under injury induced degeneration.

Therefore, in the scarcity of neutrophils this exclusive activity may not be fulfilled, which may be impairing the repair neurogenesis and lead to the severe reduction in the mitotically active cells even lower than that recorded in the intact OE.

However, this hypothesis would not be rigidly defendable without further investigation is made on the remaining subregions within the OE. The observations on ILC were supported by statistical hypothesis testing, which confirmed a rigid significance in the cell proliferation at ILC (Intact/Lesioned: $p = 2{,}6 \times 10^{-2}$; VMO-csf3r/VMO-ctr: $p = 3{,}3 \times 10^{-13}$; Two-way ANOVA).

Two-way ANOVA revealed a strong significance in the proliferative activity in the sensory region upon neutrophil depletion (Intact/Lesioned: $p = 2{,}8 \times 10^{-29}$; VMO-csf3r/VMO-ctr: $p = 1{,}9 \times 10^{-21}$; Two-way ANOVA). A lower proliferation rate was detected within the sensory region of the intact OEs of both KD and control animals (VMO-ctr: 20,6 ± 2; VMO-csf3r: 23 ± 4 cells per hemi-OE; mean ± SEM; $p = 0{,}99$; Two-way ANOVA post hoc Tukey's HSD), exhibiting an expected pattern of maintenance neurogenesis (Figure 4.15; bottom center). Upon TrX exposure EdU-positive cells in the sensory region increased to 237 ± 14 cells in the control animals, while only 48 ± 5 cells were recorded in the KD animals, corresponding to a near 80% decrease upon neutrophil depletion (Figure 4.15; bottom center; $0{,}2 \times 10^{-14}$; Two-way ANOVA post hoc Tukey's HSD).

In addition, the proliferative activity in the lesioned OEs of KD animals was again reduced to similar levels of maintenance neurogenesis in the intact OEs ($p = 0{,}12$; Two-way ANOVA post hoc Tukey's HSD). Similar to the observations on the ILC and the sensory OE, mitotic activity in the non-sensory region showed a notable change after systemic neutrophil depletion (Figure 4.15; bottom right; Intact/Lesioned: $p = 4{,}0 \times 10^{-4}$; VMO-csf3r/VMO-ctr: $p = 1{,}8 \times 10^{-11}$; Two-way ANOVA). Number of EdU-positive cells in the control animals increased approximately 40% after lesion compared to internal controls (Intact OE: 40 ± 4; TrX: 70 ± 6 cells per hemi-OE; mean ± SEM; $p = 2{,}6 \times 10^{-6}$; Two-way ANOVA post hoc Tukey's HSD), while there was no significant change recorded between the lesioned and intact OEs in the KD animals (Intact OE: 26 ± 2; TrX: 25 ± 1,6 cells per hemi-OE; mean ± SEM; $p = 0{,}99$; Two-way ANOVA post hoc Tukey's HSD). A negative effect of morpholino induced systemic neutrophil depletion on the proliferative activity after injury was also detected in the non-sensory region, similar to the findings in the other subregions.

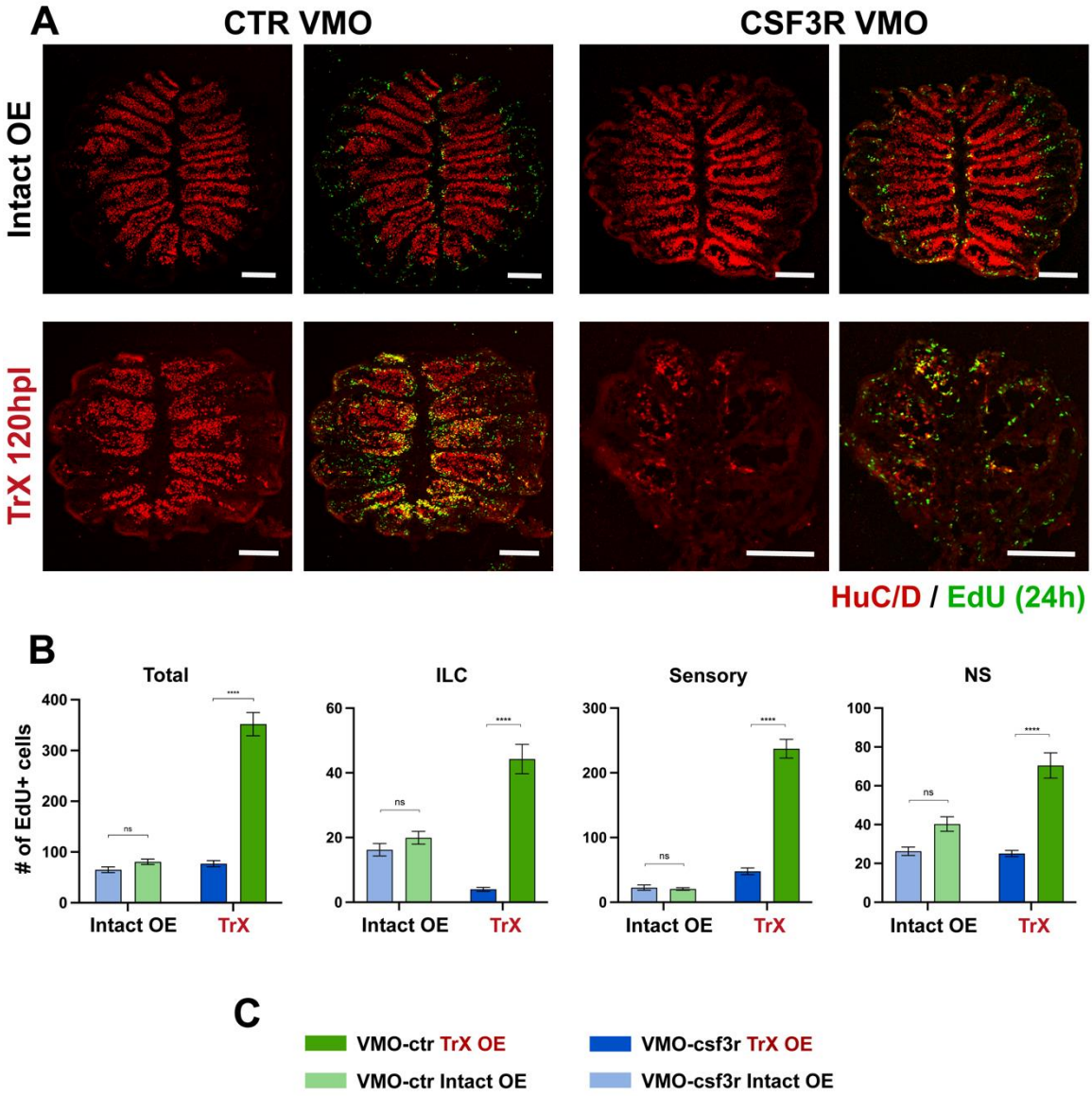

Figure 4.15. Systemic neutrophil depletion impairs the efficiency of regenerative neurogenesis in the OE. (a) Scale bars: 100 µm. (b) Proliferative activity in the 3rd day post lesion. (c) Figure legend.

The major evidence of this indication was a near 64% reduction in the EdU-positive cell number in the non-sensory region of the KD animals after lesion, compared to that of the control animals (p = 4,9 x 10^{-13}; Two-way ANOVA post hoc Tukey's HSD).

Figure 4.16a displays the same data in Figure 4.15b, with a more detailed presentation of the spatial distribution of EdU-positive cells along the radial axis of the hemi-OE.

To avoid confusion, the intact and lesioned OEs of VMO-ctr and VMO-csf3r injected animals were shown separately in smaller graphs on the bottom right (VMO-ctr; Intact OE: light green line; Lesioned OE: dark green line), and the bottom left (VMO-csf3r; Intact OE: light blue line; Lesioned OE: dark blue line). Relative data representing the lesioned OEs of the control and KD animals were summarized in a graph that was situated in the middle of the figure (Figure 4.16a; top; lesioned OE of VMO-csf3r: dark blue; lesioned OE of VMO-ctr: dark green) to put an emphasis on the significant change in the level and pattern of proliferative activity in the lesioned OEs between the control and KD animals. As can be observed from the bottom right graph that displays the datasets of the intact and lesioned OEs of the control animals, there is a considerable gap on the y-axis between the light green (intact OE) and the dark green (lesioned OE) lines.

The intact OE on the control animals exhibited a normal pattern of maintenance neurogenesis that peaked at the 0,05 and 0,65 radial positions which correspond to the tips of the ILC and the peripheral margin of the sensory region (Figure 4.16a; bottom right; light green line). In contrast, upon TrX exposure the tissue was activated to exhibit a pattern of repair neurogenesis, which can be observed in the highly elevated level of EdU-positive cells that was more evenly distributed along the radial axis (Figure 4.16a; bottom right; dark green line).

This evidence confirms that the control MO injected animals exhibited a normal pattern of maintenance and repair neurogenesis, thus no side effects of the inactive morpholino was found regarding the proliferative activity in the OE. Considering these observations, the investigation went further to the KD animals. The intact OEs of the VMO-csf3r injected animals showed a similarly normal pattern of maintenance neurogenesis, which indicates that systemic neutrophil depletion does not have a significant effect on the pattern of mitotic activity in the intact OE under homeostatic conditions (Figure 4.16a; bottom left; light blue line). In contrast, the level and density of the EdU-positive cells were severely decreased upon TrX exposure in the KD animals, but the mitotic cells were more evenly dispersed on the radial axis, therefore maintained a normal repair neurogenesis pattern (Figure 4.16a; bottom left; dark blue line; note the difference in maximal values between separate graphs).

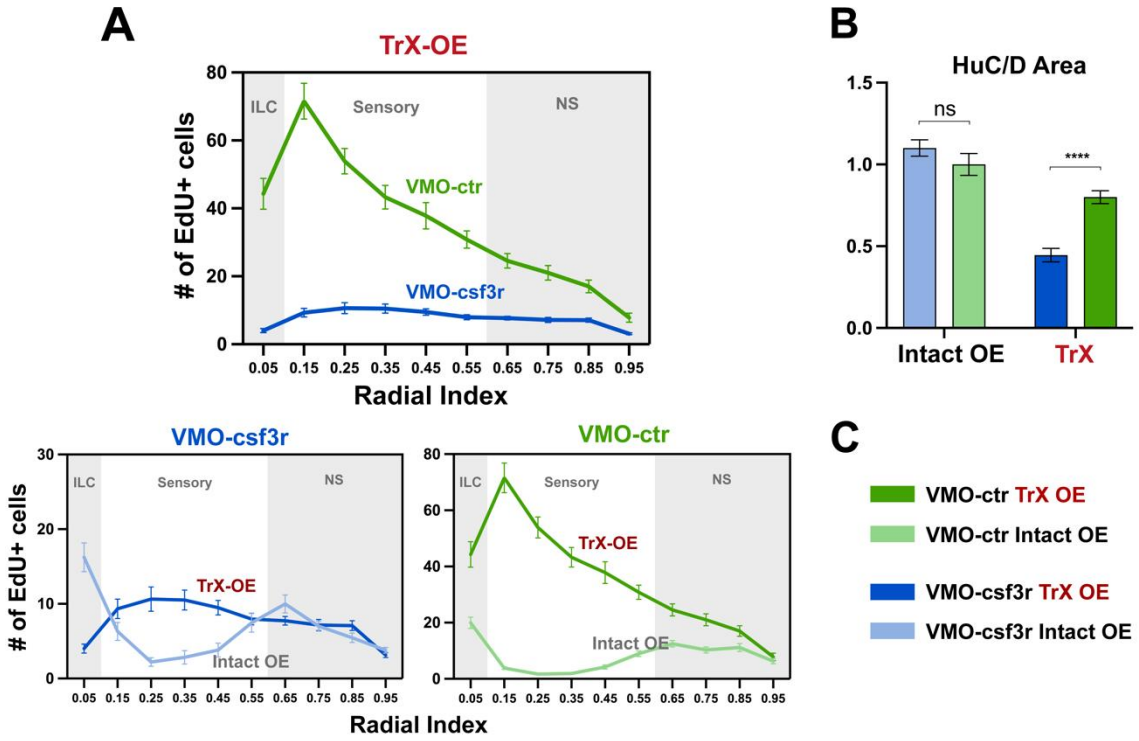

Figure 4.16. Systemic neutrophil depletion results in a notable reduction in the mitotic activity and the level of neurogenesis in the OE after chemical injury. (a) Radial distribution of the proliferative activity in the 3rd day post lesion. (b) Efficiency of OSN neurogenesis at 120 hpl. (c) Figure legend.

The high difference in the mitotic activity between the KD and control animals after lesion can be evidently observed in a bigger graph on Figure 4.16a (top; VMO-csf3r: dark blue; lesioned OE of VMO-ctr: dark green). The level of significance of these datasets were further investigated by statistical hypothesis testing to confirm that morpholino induced temporal elimination of neutrophils results in a severe decrease in the proliferative activity in the regenerating OE after chemical injury (Radial Position: p = 1,9 x 10^{-49}; VMO-csf3r/VMO-ctr: p = 1,6 x 10^{-94}; Two-way ANOVA Šídák's multiple comparisons test).

To investigate relationship between the impaired proliferative activity under neutrophil scarcity with the OSN neurogenesis in the injured OE, the area covered by the regained OSNs after 120 hpl was compared between the VMO-ctr and VMO-csf3r injected animals (Figure 4.16b).

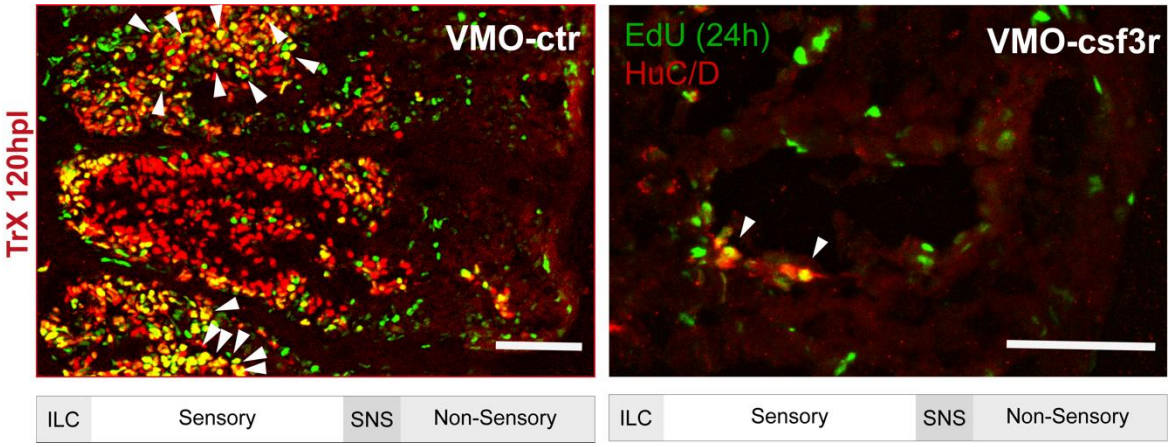

Figure 4.17. Lesioned OE at 120 hpl with mitotic cells labelled in the 3rd day. VMO-ctr (left), VMO-csf3r (right). HuC/D (red), EdU (green), double positive cells (yellow; arrowheads) Scale bars: 50 μm.

Without any neutrophil deficiency, the zebrafish can restore and regain the lost OSNs up to 75-80% after 120 hours post experimental injury with TrX, and almost complete restoration of the entire OSN population can be achieved after approximately one week (Bayramli et al., 2017).

To examine whether a significant change occurs in the OSN neurogenesis after a systemic neutrophil depletion, the area covered by mature OSNs that are labelled by the neuronal marker HuC/D, was measured in the intact and lesioned OEs (120 hpl) of the control and the KD animals and normalized to the average value which was acquired from the intact OE of the VMO-ctr injected animals (Figure 4.16b).

Statistical hypothesis testing concluded that a major significance was present among the datasets (Intact OE/TrX: $p = 1{,}6 \times 10^{-11}$; VMO-csf3r/VMO-ctr: $p = 1{,}6 \times 10^{-2}$; Two-way ANOVA). According to the results of the analysis, 80% of the lost OSNs were regained in the VMO-ctr OEs after 120 hpl, while only 40,5% of the sensory tissue was restored in the KD animals, therefore a near 50% decline in the repair neurogenesis occurred after systemic neutrophil depletion by morpholino knockdown.

Figure 4.17 exhibits high power magnification images of the lesioned OEs (120 hpl) of the VMO-ctr (left) and VMO-csf3r (right) injected animals.

Mature OSNs were labelled with the neuronal marker HuC/D (red), while cell proliferation was marked with EdU incorporation (green). EdU-HuC/D double-positive cells which are regained OSNs that had gone cell division on the 3rd day after the lesion, appear in yellow consequently.

An evident difference between the length of the scale bars (50 μm), indicate that the OEs of the VMO-csf3r injected animals may had failed to restore the tissue integrity and maintained a shrinked and smaller shape than usual (Figure 4.17; right). A denser pattern of EdU-positive cells (green) can be observed in the control fish while a fewer number of mitotic cells were labelled in the KD animals. In addition, almost the entire morphology of the sensory tissue (ILC and the sensory region) and the overall tissue integrity was restored in the controls in contrast to the KD animals. The level of change in the OSN neurogenesis can be recognized by comparing the double positive signals (yellow) in both images. While there is a dense pattern of double-positive cells (arrowheads) in the control animals, there is severely fewer OSN neurogenesis in the OE after systemic neutrophil depletion (Figure 4.17).

4.5. Functional Analysis of Macrophage Behavior upon Sterile Injury

To study the functional contribution of macrophages in the context of tissue regeneration, clodronate liposome mediated specific depletion has been developed as a highly effective and conventional technique in zebrafish and mammalian models (Kameka et al., 2014; Rosowski, 2020).

Clodronate (Dichloroethylene - Bisphosphonate) has been a conventionally prescribed drug in the treatment of several disease conditions. In recent decades it has been widely used in by the immunology focused research groups with the aim of performing functional studies on macrophage behavior *in vivo*. To enable specific engulfment of clodronate by macrophages and provide easy delivery *in vivo*, it has been encapsulated into small liposomic vesicles.

In adult zebrafish, a temporal systemic macrophage depletion with IP injection of clodronate liposomes has been previously demonstrated to be an effective and rather economic application (Moreno, 2018; Rosowski, 2020). The experiments that are described below includes the investigation of the efficacy of the macrophage depletion by clodronate liposome administration by analyzing the primary hematopoietic organs. The effectiveness of the drug in elimination of macrophages were further examined in the OE. Finally, potential effects of clodronate liposome administration on the proliferative activity and OSN neurogenesis in the OE after injury were assessed.

4.5.1. Clodronate Liposome Administration Effectively Reduces Macrophage Numbers in the Primary Hematopoietic Organs

Clodronate liposomes were demonstrated to be affective in depleting macrophages within the first 24 hours after IP injection (Nguyen-Chi et al., 2017). IP injections of 10 µl of either L-CLOD (n = 3 fish) or L-PBS (n = 3 fish) were applied to zebrafish, and the fish were immediately transferred to normal fish-water containing tanks and incubated for 1 day under physiological conditions. To establish the level of decrease in the systemic macrophage numbers upon clodronate liposome administration, the primary hematopoietic organs (kidney and spleen) were dissected out 24 h after the injections. The organs were cryosectioned, and immunostained against the macrophage specific Mfap4.

The cross sections were captured by confocal microscopy at 2048 x 2048 - pixel resolution (Figure 4.18a). For each condition (L-CLOD or L-PBS), 3 fish were used in total. 3 sections from each organ (9 sections in total for each condition) were gathered and adjusted to data analysis utilizing the same method described in section 4.3.2. The area covered by Mfap4-positive cells were assessed and normalized to the internal controls to establish a relative normalized measure of the level of macrophage depletion in the spleen and kidney (Figure 4.18b).

Figure 4.18a exhibits the representative confocal images of the primary spleen (top row) and kidney (bottom row) sections of L-CLOD (right panel) or L-PBS (left panel) injected zebrafish at 24 hpi, immunostained against the macrophage specific Mfap4 (red) with brightfield imagery (grays).

As discussed in section 4.1.1., there is a major splenic macrophage population under physiological conditions to serve for the hemophagocytic duties of the tissue (Menke et al., 2011). Consistent with this information, rigid Mfap4-positive signals can be observed in the control animals (L-PBS injected fish; Figure 4.18a; top left panel; red). Here, splenic macrophages formed circular aggregates that were distributed evenly throughout the parenchyma, which were also consistent with the ellipsoidal structures that has been identified as the hemophagocytic sites (Menke et al., 2011). The ellipsoids were also demonstrated with higher power magnification in the Figure 4.18b with dashed lines. These observations serve as further evidence that Mfap4 is an effective and successful marker in labeling macrophage populations, and the inactive L-PBS administration did not result in any physiological abnormality in terms of macrophage localization and behavior in the hemopoietic organs. Therefore, it was safe and reliable to continue to the assessment of the potential influences of clodronate.

The spleen sections of the L-CLOD fish exhibited a humbler (in terms of signal power and intensity) but similar pattern of distribution in the splenic macrophage populations (Figure 4.18a; top right; red). The ellipsoidal structures were visible and clearly identifiable; however, the signal intensity was decreased in contrast to the control animals, which may indicate the number of macrophages reduced upon exposure to clodronate.

In contrast, the kidney sections the control animals and the L-CLOD fish exhibited similar and dense Mfap4-positive signal patterns evenly distributed throughout the parenchyma (Figure 4.18a; bottom panel; red), which did not evidently suggest any reduction in the number of macrophages.

To understand whether any significant decrease in macrophage populations took place in the primary hematopoietic organs 24 h after clodronate liposome application, quantitative analysis with statistical hypothesis testing were applied on the data sets. Figure 4.18c displays the results of these analyses which investigated the macrophage occupancy in the kidney and spleen of L-CLOD and L-PBS injected animals at 24hpi. The datasets that are belong to kidney were shown at the right side of the graph in dark and light orange colors, while those belong to the spleen were situated at the left side with dark and light red color.

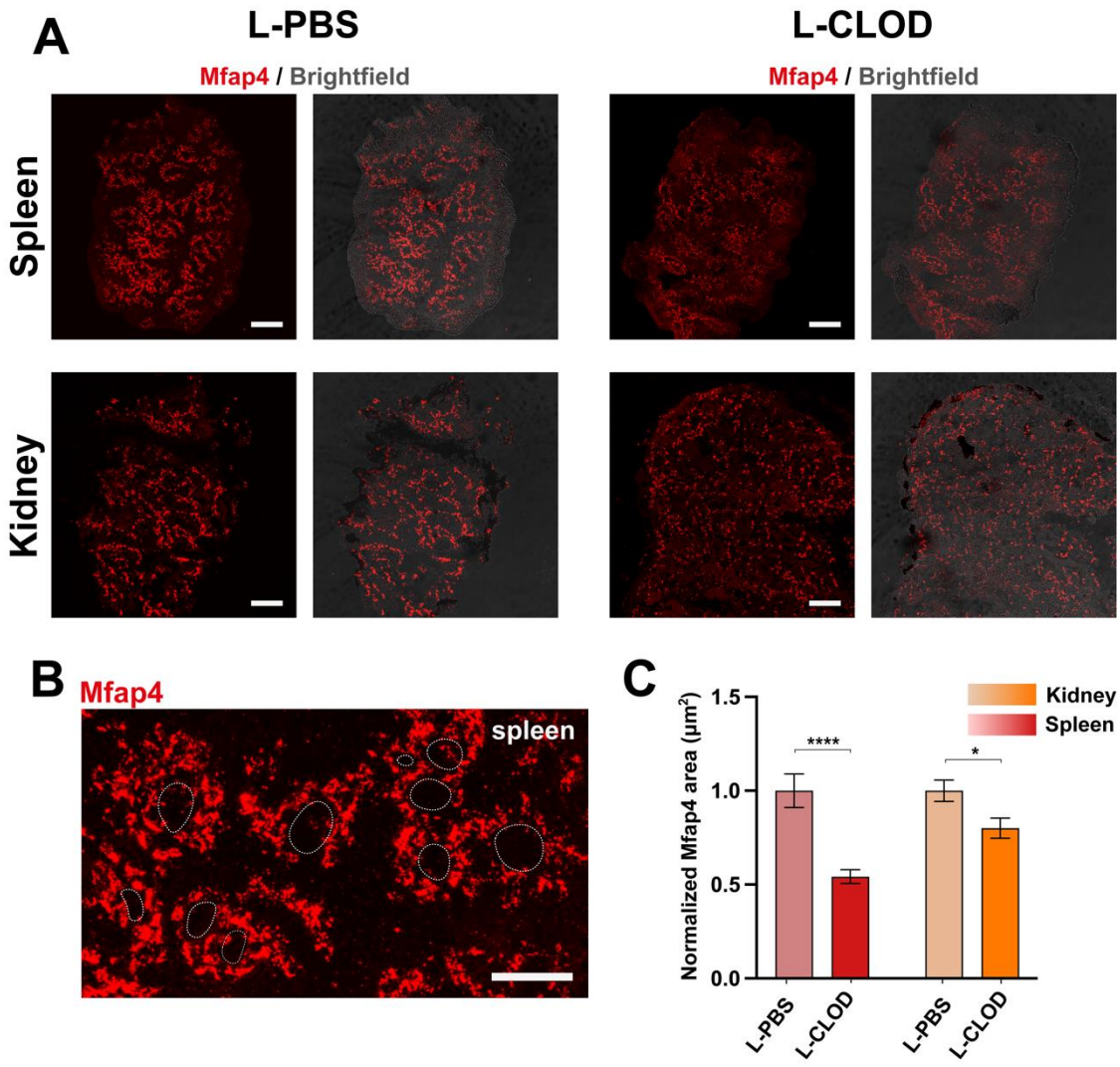

Figure 4.18. Clodronate liposomes partially eliminate macrophages from kidney and spleen. (a) Kidney and spleen sections of L-CLOD (right panel) and L-PBS (left panel) injected fish that were immunostained against Mfap4 (red), with brightfield imagery (grays). (b) High power magnification of a spleen section; Mfap4 (red). (c) Macrophage occupancy in the kidney and spleen. Scale bars: (a) 100 µm, (b) 50 µm

In control animals, Mfap4-positive macrophages occupied 1,0013 μm^2 out of a 100 μm^2 splenic tissue area, while L-CLOD injected fish showed a near 50% reduction with a 0,543 μm^2 occupancy per 100 μm^2 (not shown), which can also be observed from the normalized values displayed in the bar graph (Figure 4.18c; red; $p = 1,6 \times 10^{-5}$; t = 4,75167; df = 52; two tailed unpaired Student's t-test).

Macrophage abundance in the kidney parenchyma was found to be 0,7219 μm^2 on average per 100 μm^2 of kidney tissue in the control animals, while 0,5780 μm^2 space was occupied in the L-CLOD fish (not shown), indicating a near 20% decrease in macrophage numbers (Figure 4.18c; orange). This reduction showed weaker significance in comparison to the spleen dataset (Figure 4.18c; red; $p = 1{,}4 \times 10^{-2}$; t = 2,5; df = 52; two tailed unpaired Student's t-test).

4.5.2. Clodronate Liposomes were Unsuccessful in Depleting Macrophages in the OE

In the previous section, clodronate liposome administration was shown to significantly reduce macrophage numbers in the kidney and spleen. However, it was essential to also investigate whether this method was able to deplete resident macrophages in the OE. Note that the macrophage recruitment was ambiguous after experimental injury, unlike the highly significant influx of neutrophils after TrX exposure. Therefore, the potential effects of resident and recruited macrophages to the OE regeneration and neurogenesis was suspected to be not significant considering no major change in the level of macrophage abundance in the OE. To investigate this hypothesis, it was also necessary to assess the functional behavior of these cells. To do so, clodronate liposome application method needed to be efficacious to partially deplete the macrophage populations in the OE, in addition to the primary hematopoietic organs.

The fish were intraperitoneally injected with L-PBS (n = 3 fish) or L-CLOD (n = 3 fish) using the same procedure as the previous section. The OOs were dissected out 24 hours post injection (hpi), cryosectioned, and immunostained against the macrophage marker Mfap4 and the neuronal marker HuC/D. Representative confocal images of the OEs are displayed in Figure 4.19a. L-CLOD (right panel) and L-PBS (left panel) samples are exhibited in separate columns and anti-Mfap4 staining was provided in isolation on the top row of the figure, while merged 2-channel images are indicated on the bottom row.

Pattern of distribution of the mature OSNs that were recognized by the anti-HuC/D staining (blue), revealed that the intact OEs exhibited a normal, physiological condition and no side effects of the inactive L-PBS was recorded (Figure 4.19a; bottom row; blue).

The Mfap4-positive macrophages were observed to be mostly localized around the peripheral margin of the non-sensory region in both L-PBS and the L-CLOD injected fish indicating that L-CLOD did not affect their localization pattern at 24 hpi in the intact OE (Figure 4.19a; red). There was no visual insight on any level of reduction in the macrophage numbers upon L-CLOD administration (Figure 4.19a; right panels; red).

Visual analysis was supported by further statistical investigation on the macrophage abundance upon clodronate liposome application. In the control animals, 4,1 ± 0,4 cells (mean ± SEM) were recorded in a hemi-OE (Figure 4.19b; pink), and 5,3 ± 0,4 cells were found to be located in a hemi-OE of the L-CLOD injected fish (Figure 4.19b; red). Two-tailed unpaired Student's t-test concluded that the clodronate liposome administration did not result in a significant reduction in macrophage numbers in the OE at 24 hpi (p = 5,0 x 10^{-2}; t = 2,4; df = 58; two-tailed unpaired Student's t-test).

The radial distribution of macrophages were combined in a bar graph representing the number of cells in different sub-regions in Figure 4.19d. ILC of L-PBS and L-CLOD samples did not include any Mfap4 - positive signal (Figure 4.19d; ILC; NA values), and very low levels were detected in the sensory region in both L-PBS (0,2 ± 0,2; cells per hemi-OE; mean ± SEM) and L-CLOD (0,1 ± 0,1; cells per hemi - OE; mean ± SEM) samples. Further examination was made on the spatial distribution of the macrophages upon clodronate exposure (Figure 4.19c). Almost the entire macrophage population was localized at the peripheral region of the non-sensory epithelium in both L-PBS (red line) and L-CLOD (pink line) injected fish (Figure 4.19c).

Consistent with the analysis in the radial distribution graph in Figure 4.19c, the total number of macrophages in the non-sensory region was found to be significantly higher after clodronate liposome administration (Figure 4.19d; p = 1,9 x 10^{-2}; t = 1,99; df = 58; two-tailed unpaired Student's t-test). Although the overall macrophage depletion was found to be inconclusive, potential changes in the number of Mfap4-positive cells were further investigated along the radial axis.

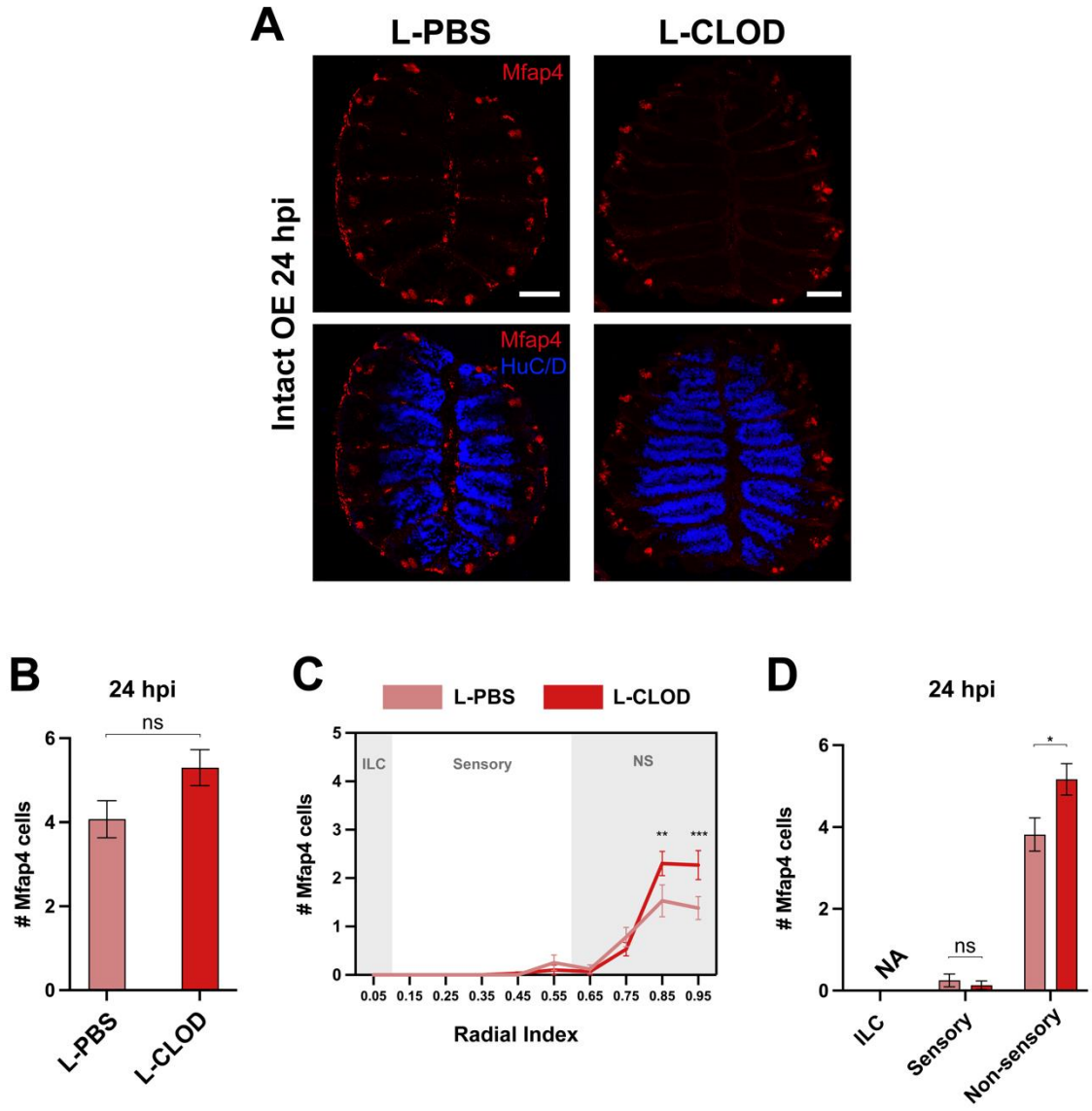

Figure 4.19. Macrophage depletion with clodronate liposomes is substandard in the OE. (a) Confocal images of the OE of L-PBS and L-CLOD injected fish at 24hpi, Mfap4 (red), HuC/D (blue). Scale bars: 100 μm. (b) Number of macrophages in the OE. (c) Radial distribution of macrophages along the OE. (d) Regional distribution of the macrophages in the OE, L-CLOD (red), L-PBS (pink).

Intriguingly, the positional profiling displayed in Figure 4.19c indicated that the number of macrophages increased upon clodronate liposome injection (red line), rather than reduce as would be expected by the depletion procedure, compared to the control animals (pink line) at radial positions 0,85 and 0,95.

In addition, statistical analysis concluded that these changes were significant (0,85 position: p = 2,1 x 10^{-3}; 0,95 position: p = 1,9 x 10^{-4}; two-way ANOVA Šídák's multiple comparisons test). Therefore, clodronate liposome administration did not just fail in depleting macrophages in the OE but caused an increase in the number of Mfap4-positive cells. Further interpretation of these results will be provided in the discussion.

4.5.3. Clodronate Liposomes did not Influence the Neurogenesis Events in the OE

In the previous sections, the efficacy of the clodronate liposome application was found to be reducing systemic macrophage levels but was insufficient in eliminating the resident and recruited macrophages in the OE. In the absence of any significant disturbance in the level of macrophage abundance in the OE with the current application, it would be implausible to dig further into the proliferative response or neurogenesis events. Therefore, clodronate liposome application was switched to a more aggressive dosage protocol that consisted of one 10 µl of IP injection of liposomes per day. To investigate whether there was a notable change in the proliferative activity on the third day after lesion, and to examine whether a significant difference occurred in the OSN neurogenesis after damage, and the OEs were analyzed at 120 hpl. The liposome injections were started 24 h before the nasal irrigation and repeated every 24 h until the penultimate day before dissection. Fish were also injected with EdU containing solutions on the 48th h to track mitotic cell activity and level of neurogenesis. The OEs of L-PBS (n = 3 fish) and L-CLOD (n = 3 fish) treated fish were dissected out, immunostained against the macrophage specific Mfap4 (red), neural marker HuC/D (blue), and EdU-positive cells (green) were marked with the Click-it reaction (Figure 4.20a).

Figure 4.20a displays representative confocal images of the L-PBS (left panel) and L-CLOD (right panel) treated animals at 120 hpl. Intact OEs (top) and TrX lesioned OEs (bottom) are shown in different rows. 2-channel (HuC/D in blue and EdU in green) images are provided on the left side in each panel, while merged images with the addition of Mfap4 (red) are situated on the right side. The pattern of mitotic cell distribution in the intact OEs in both conditions were consistent with a normal maintenance neurogenesis pattern that continuously takes place at the central and peripheral margins of the sensory tissue.

This indicates an expected pattern of GBC activity under physiological conditions (Figure 4.20a; top row; green). Therefore, no significant proliferative activity was found within the core sensory epithelium, where the dormant HBCs are arranged throughout the basal lamina. In addition, OSN distribution and abundance was not disrupted in the intact OEs in both conditions. These observations reveal that inactive L-PBS application did not result in any unexpected consequences in the normal pattern of proliferation, or integrity of the sensory region in the intact OE.

Despite a rather aggressive approach was used regarding the dosage of the clodronate liposome, the resident macrophage population continued to present within the OE and maintained their peripheral position in the non-sensory OE in the intact (top) and TrX lesioned (bottom) OEs in both conditions (Figure 4.20a; red). These observations suggest that although clodronate liposomes were successful in partial elimination of macrophage populations in the primary hematopoietic organs, the efficacy of the drug did not reach the OO. Visual analysis further indicates that the majority of the OSN population was regained at 120 hpl in the lesioned OEs of L-CLOD injected fish, similar to L-PBS injected samples (Figure 4.20a; bottom row; blue).

The EdU-positive cells on the third day post injury was observed to be greater in number and dispersed along the subregions of the OE in a more balanced manner in both L-PBS and L-CLOD injected fish (Figure 4.20a; bottom row; green). No notable difference was found regarding the level and pattern of proliferative activity in the lesioned OEs upon clodronate liposome treatment, in comparison to the internal control that were treated with inactive L-PBS.

To support the visual insight with quantitative analysis, ROIs that represent each hemi-OE were cropped and EdU-positive cells were counted using FIJI software. The results revealed that 68 ± 3 (mean ± SEM) cells in the intact OEs (light green) and 194 ± 9 (mean ± SEM) cells in the lesioned OEs (dark green) of the L-PBS injected animals were found on average in a hemi-OEs, while 82 ± 4,5 cells in the intact OE (pink) and 210 ± 8 cells in the lesioned OEs (red) of the L-CLOD treated fish were recorded to be EdU-positive (Figure 4.20b; top).

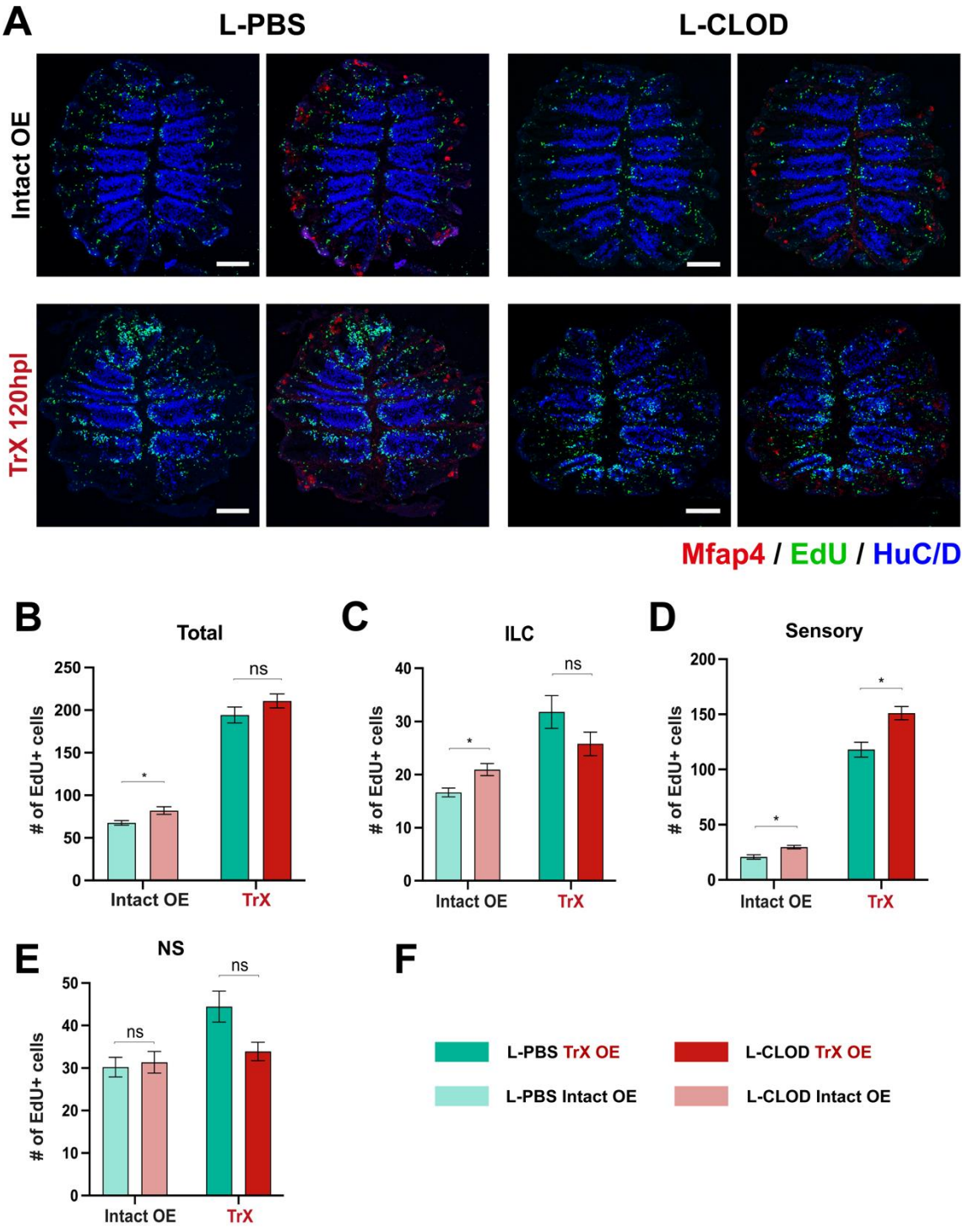

Figure 4.20. Clodronate liposomes did not significantly influence proliferative activity in the OE. (a) Confocal images of the intact (top) and lesioned (bottom) OEs of L-PBS (left panel) and L-CLOD (right panel) injected animals, stained against Mfap4 (red), EdU (green), and HuC/D (blue). Scale bars: 100 μm. (b, c, d, e) Number of EdU-positive cells. (f) Figure legend.

Intriguingly, the statistical analysis revealed that there was a slight significance between the intact OEs, with an increase in the L-CLOD treated samples (Figure 4.20b; light green and pink bars; $p = 8{,}7 \times 10^{-3}$, t = 2,7; df = 58; Unpaired Two-tailed Student's t-test). However, there was no notable change in the proliferative activity between the lesioned OEs (Figure 4.20b; top; dark green and red bars; $p = 0{,}19$, t = 1,3; df = 58; Unpaired Two-tailed Student's t-test).

Mitotic activity at the 3rd dpl was also investigated in the subregion level. Figure 4.20c, d, and e exhibit the number of EdU-positive cells in the ILC, the sensory and the non-sensory region respectively. According to this assessment, there was a nonsignificant decrease of mitotic cells located in the ILC region (Figure 4.20c) of the lesioned OEs of L-CLOD treated animals with 26 ± 2 (mean ± SEM) dividing cells, compared to that of L-PBS injected fish, which had 32 ± 3 cells on average ($p = 0{,}12$, t = 1,6; df = 58; Unpaired Two-tailed Student's t-test). In contrast, there was a slight change between the intact OEs, in which the level of proliferative activity in ILC of the L-PBS treated control animals (17 ± 1 cells; mean ± SEM) were below that of the L-CLOD injected samples (21 ± 1; mean ± SEM; $p = 3{,}4 \times 10^{-3}$, t = 3,1; df = 58; Unpaired Two-tailed Student's t-test).

Intriguingly, datasets in the sensory regions (Figure 4.20d) showed a slight change in both intact OEs (L-PBS: 21 ± 2 cells; L-CLOD: 30 ± 1,6 cells; mean ± SEM) and the lesioned OEs (L-PBS: 118 ± 7 cells; L-CLOD: 151 ± 6 cells; mean ± SEM), which resulted in an statistical significance (Intact OEs: $p = 7{,}5 \times 10^{-4}$, t = 3,6, df = 58; Lesioned OEs: TrX: $p = 5{,}6 \times 10^{-4}$, t = 3,6, df = 58; Unpaired Two-tailed Student's t-test).

Finally, proliferative activity in the non-sensory region (Figure 4.20e) showed a decrease in the lesioned OEs of the L-CLOD treated samples, which exhibited 34 ± 2 cells that were EdU-positive, in comparison to that of L-PBS samples, which had 44 ± 4 cells in a hemi-OE on average ($p = 0{,}016$, t = 2,5; df = 58; Unpaired Two-tailed Student's t-test). On the opposite, a similar level of mitotic activity was recorded in the intact OEs of L-PBS (30 ± 2 cells; mean ± SEM) and L-CLOD (31 ± 2 cells; mean ± SEM) injected animals (Intact: $p = 0{,}74$, t = 0,33; df = 58; Unpaired Two-tailed Student's t-test).

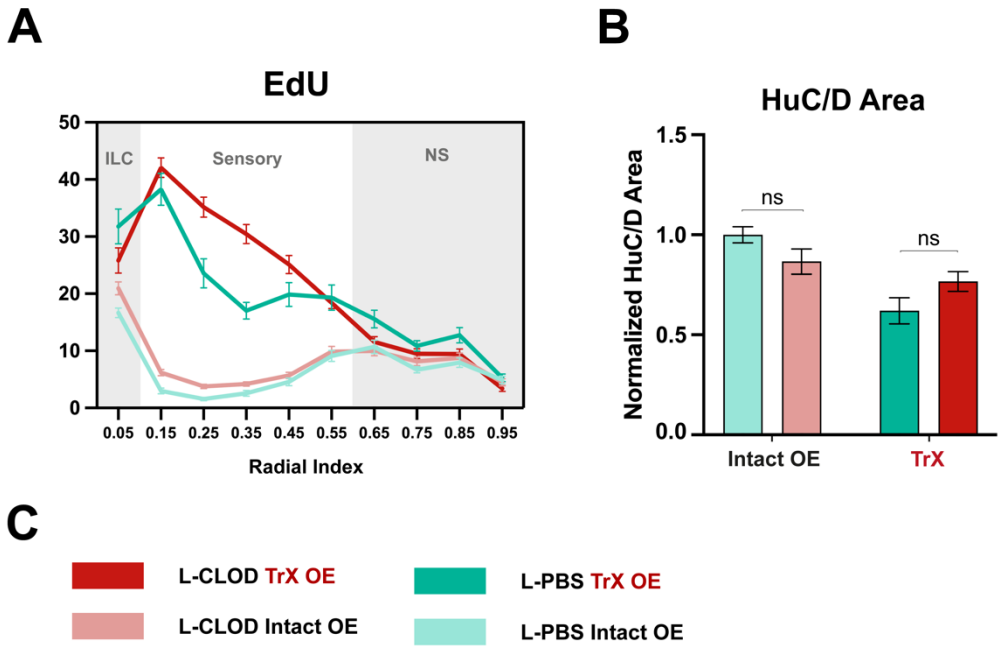

Figure 4.21. Clodronate liposomes did not affect the efficiency of neurogenesis in the OE. (a) Positional profiling of mitotic cells. (b) Area occupied by HuC/D-positive cells. (c) Figure legend.

Figure 4.21a demonstrates a more detailed profile of the radial distribution of the EdU-positive cells along the hemi-OE. Green and red colors represent L-PBS and L-CLOD treated animals respectively, while dark red and dark green lines indicate the TrX-lesioned OEs, and the corresponding light colors denote the intact OEs. Number of EdU-positive cells were indicated in the y-axis, while the radial positions were given in the x-axis. Regional boundaries were indicated with gray shading on the graph.

The radial distribution profiles of the intact OEs of both L-PBS (light green) and L-CLOD (pink) fish were observed to be remarkably consistent, indicating a normal physiological condition of both fish (Figure 4.21a). The linear profile of the TrX-lesioned OEs maintain similar levels especially in the ILC and the non-sensory region. A more extended interval between the dark green (TrX lesioned L-PBS injected) and dark red (TrX lesioned L-CLOD injected) lines can be observed in the sensory region, which was found to be exhibiting a slight significance as mentioned above.

Altogether, the proliferative activity followed a similar level and pattern of distribution in the L-PBS and the L-CLOD treated samples exhibiting an overall unsignificant change with slight regional fluctuations.

To assess the level of restoration of the lost OSNs after injury, the area occupied by the HuC/D-positive cells was analyzed in the L-PBS and L-CLOD treated fish. The data was normalized to the average value that calculated from the intact OEs of the L-PBS treated fish. Figure 4.21b displays the normalized HuC/D area values at 120 hpl. The same color labelling as other subfigures was applied to the graph (Figure 4.21c). In the L-PBS treated fish, the 62 ± 6,5 % of the lost OSNs were regained 120 hours after TrX, while a near 88% of the sensory tissue was restored in the L-CLOD samples. However, neither the Intact OEs (p = 0,50; t = 0,68; df = 28; Unpaired Two-tailed Student's t-test) nor the TrX lesioned tissues (p = 0,12; t = 1,6; df = 28; Unpaired Two-tailed Student's t-test) showed any significant alteration in HuC/D restoration. In conclusion, no significant effect of clodronate liposome administration was recorded in terms of OSN neurogenesis and the overall proliferative activity in the OE.

5. DISCUSSION

Tissue injury is immediately followed by an acute immune response which goes along with the recruitment of immune cells, mainly neutrophils and macrophages to the site of damage (Rock et al., 2010). A self-limiting immune response with a quick resolution has been shown to mediate the restorative events in tissues with high regenerative capacity, while a prolonged inflammatory period usually results in fibrotic scar formation and incapacity to achieve a full functional and structural recovery (Julier et al., 2017). Providing a quick and transient acute inflammatory period is strongly dependent on the functional efficiency of the first responders, that are the innate immune cells. In other words, the quality of tissue regeneration is mostly decided during the pro-inflammatory period (Oishi and Manabe, 2018; Peiseler and Kubes, 2019). Therefore, functional recovery and tissue regeneration is strongly correlated with the dynamic machinery of the immune system, and the innate immune factors constitute one of the key mediators in the events that will eventually result in either a full tissue regeneration or an imperfect functional recovery (Aurora and Olson, 2014). In recent decades, the crucial interplay between the immune system and tissue regeneration has been a subject of interest of many research groups which have focused on a several model organisms with high regenerative capacities as well as different tissue types (Havixbeck and Barreda, 2015; Keightley et al., 2014; Oishi and Manabe, 2018). However, potential contributions of members of the innate immune system to regenerative events in the adult zebrafish olfactory system have not been fully established.

This study aimed to provide a descriptive analysis of the contribution of the innate immune cells to the zebrafish olfactory epithelium neurogenesis and tissue regeneration. The purpose of the experimental procedures presented in this thesis consists of two major objectives: Understanding the neutrophil and macrophage behavior under physiological conditions, as well as upon injury induced inflammatory response; understanding the interplay between the innate immune cells and the proliferative events in the OE, and further elucidate whether neutrophils and/or macrophages dynamically contribute to the efficiency of the injury induced OSN neurogenesis.

To achieve the proposed aims, the innate immune cell occupancy and spatial behavior under physiological conditions, as well as additional neutrophil and/or macrophage recruitment after chemical injury were detected in the OE. The primary hematopoietic organs were also monitored to elucidate neutrophil and macrophage behaviors in the adult zebrafish. The selective functional impact of these cell types to the initiation and outcome of the regenerative events in the OE were then assessed by systemic cell depletion experiments.

5.1. Mpx Expression and Neutrophil Abundance in the OE

Neutrophil extracellular traps (NETs) are one of the most effective methods used by neutrophils to trap and eliminate unwanted pathogens or substances in the inflamed area. They consist of DNA filaments with approximately 15-17 nm in diameter (Li et al., 2020). Histone proteins including H1, H2A, H2B, H3, H4, and antimicrobial granular proteins like Mpx, cathepsin G, and several defensins are also attached to the DNA and contribute to the entrapment and elimination of harmful agents (Lakshmanan et al., 2022; Li et al., 2020). In addition, these bound proteins form globular structures along the filament, that can reach to approximately 50 nm in diameter (Havixbeck and Barreda, 2015). The existence of NETs in the zebrafish and their functional and morphological similarity with mammals have previously been demonstrated (Palić et al., 2007).

Histochemical staining patterns of the OE generally indicated a high level of significance in labelling neutrophilic granulocytes with anti-Mpx antibodies (Figure 4.1). However, the evidence from literature indicates that Mpx is present within the extracellular NET structures that neutrophils release during the early phase of the inflammatory response (Li et al., 2020). Therefore, it is reasonable to suspect a potential false-positive signaling pattern with anti-Mpx application, which would mean that this marker may label the granular domains within the NETs in the extracellular space and therefore ceased to be cell-specific. To ensure the cell-specific labelling of neutrophils, a counterstaining with DAPI would be beneficial.

5.1.2. Defining the Acute and the Resolution Phase of the inflammatory Response

Neutrophils are the primary regulators of the initial acute phase of the inflammatory response (Renshaw and Trede, 2012). They are important regulators of how long this initial transient phase will last, which ultimately decides the quality of the tissue restoration process later (Iribarne, 2021). The evidence from literature supports the observations obtained from this study, which indicates that the neutrophils come for a transient period and quickly lead the process into resolution and is characterized by their own elimination from the inflamed area (section 4.2.1.). Therefore, in the context of the experimental injury model of the zebrafish olfactory system utilized in this study, the initial or acute phase of the inflammatory response can be considered as the period covering the 6 and 24 hpl, where a high level of neutrophil infiltration to the injured tissue was observed (Figure 4.5). On the other hand, the period encapsulating 72 and 120 hpl exhibits consistent profile with the resolution phase, with neutrophil occupancy returning to basal levels, and high proliferative activity in all regions along the OE (Figure 4.5).

5.1.3. Acute Phase of the Inflammatory Response

Neutrophils are equipped with an intensive and diverse array of anti-pathogenic factors that are stored in the cytoplasmic granules (Havixbeck and Barreda, 2015). Their quick response to tissue injury and the fast emigrational activity towards the inflamed area is one of the highly conserved innate immune events across phyla (Havixbeck et al., 2016). Potent lysosomic enzymes provides quick intracellular elimination of the engulfed pathogens and/or necrotic debris, while extracellularly secreted granular substances such as ROS, nitrogen compounds, pro-inflammatory cytokines, growth factors and strong cytotoxic peroxidases, further contribute sterilizing the injured area (Bennett et al., 2001; Havixbeck and Barreda, 2015). The effectivity of this process is crucially important for the regenerative fate of the damaged tissue (Peiseler and Kubes, 2019).

According to the evidence obtained from this study, the neutrophil numbers in the OE peak at 6 hpl. Several tissue injury studies have found common domain in neutrophil numbers peaking within 24 h after exposure to experimental injury.

An experimental laser injury model in larval zebrafish heart, revealed a quick neutrophil recruitment to the injured area from 2 h post injury, which peaked at 6 h post injury and gradually dropped to pre-injury levels 48 h post injury (Kaveh et al., 2020). In another study investigating spinal cord injury in mice, demonstrated that neutrophils infiltrate to the inflamed area quickly after damage and peaked within 6 to 12 h post injury (Stirling et al., 2009). Consistent with the previous findings in other tissue contexts and species, zebrafish OE exhibits a quick and transient recruitment of a large neutrophil population within the first 6 h, which maintains high levels at 24 hpl and shows a gradual reduction towards the later experimental time points.

5.1.4. Resolution of Inflammation

Two mechanisms involving neutrophils contribute to inflammation resolution by reducing the density of neutrophils in the inflammatory site. First, most apoptotic neutrophils in the injury site send “eat-me” signals, mediating their own efferocytosis by macrophages (Chazaud, 2020; Isles et al., 2019). Secondly, they leave the inflammatory site, migrating back to blood circulation via the anti-inflammatory process called *reverse migration* or *retrograde chemotaxis* (Isles et al., 2019; Mathias et al., 2006). Efferocytosis also triggers the macrophages to switch from pro-inflammatory M1 to pro-regenerative M2 phenotype, which further promotes the initiation of tissue renewal and remodeling related events (Keightley et al., 2014).

Resolution of inflammation is proposed to be characterized by the elimination of neutrophils from the OE approximately three days after chemical injury (Figure 4.5), according to the experimental evidence described in section 4.2.1. In the period including 72 to 120 hpl the neutrophils might have left the area via reverse migration or by efferocytosis after completing their duties on eliminating foreign substances and clearing debris from the inflamed area. Inflammatory process is lead towards the resolution phase, which is typically characterized by the release of growth factors, anti-inflammatory cytokines, and other mediatory molecules. Regenerative processes take over and promote cell division to regain tissue integrity and function.

Time related profile of neutrophil recruitment in the OE after chemical injury induced degeneration, is highly consistent with the findings in literature regarding the characteristics of the early (acute) inflammatory period. Shortly after tissue injury, a transient rise of neutrophil numbers is seen in the inflamed region, and they are eliminated from the area to initiate the resolution phase, which is largely regulated by the restorative events (Sommer et al., 2020). According to the experimental evidence from previous studies on adult zebrafish OE, the period between 72 and 120 hpl is characterized by the high proliferative activity and most of the lost OSNs are regained at this stage in the post injury period, which is also consistent with the proposed time-related profile of the inflammatory response in the OE.

5.2. Mfap4 Expression and Macrophage Behavior in the OE

Due to the unavailability of other macrophage-specific markers that have been proved to be reactive in the zebrafish, the study could only feature anti-Mfap4 histochemistry to monitor macrophages. An overall granular signaling pattern was observed in general with the anti-Mfap4 immunostainings in the OE, which could be resulting from the density of dendritic extensions of the ramified macrophages, or the nearby cells located dorsally or ventrally in the OE. However, to confirm the specificity of this marker in the zebrafish OE, investigation of macrophages in the transgenic fish is essential, especially in the lack of any other commercially available macrophage specific antibodies. *In situ* hybridization would be another good approach to verify and monitor macrophage behavior in the OE. However, *in vivo* evidence from transgenic reporter lines would provide a more reliable information.

5.2.1. Macrophages in Acute Phase of the Inflammatory Response

Section 4.2.3. described the macrophage behavior in the OE at regeneration related time points after nasal irrigation with TrX. An intriguing drop in the macrophage occupancy was detected in the lesioned OEs compared to the intact tissues at early time points, but they were regained after 72 hpl and increased significantly at 120 hpl.

Macrophages are traditionally observed to be recruited to the inflammation zone later than neutrophils (Li et al., 2020). Consistent with this notion, the experimental evidence on the zebrafish OE indicates that the macrophages may be avoiding the chaotic microenvironment of the pro-inflammatory period, as observed from the significant drop in their number shortly after TrX exposure. Immediately after tissue damage, the first phase of the inflammatory response is initiated where a substantial amount of pro-inflammatory mediators and DAMPs including toxic reagents and necrotic cell components are released from the inflamed tissue, in addition to the presence of the pathogenic agents or irritant chemicals are still present at the early stages after damage. As the first responders to the area, the neutrophils are observed to be involved in handling the rough work quickly after TrX exposure. The rise in neutrophil numbers in the scale of hundreds shortly after nasal irrigation supports this argument. While neutrophils provide an unspecific response to regain tissue homeostasis quickly after chemical injury, macrophages eliminate themselves from the area and wait for the later phases to fulfill their restorative duties.

5.2.2. Non-Responsive Behavior of Macrophages to Chemical Irritant Treatment

The evidence indicated in section 4.2.3. Figure 4.8 the macrophages had fixed and restricted spatial placement in the OE, and they did not change location of any behavioral property upon a chemical injury is introduced to the tissue. They would be expected to show a change in the morphological properties and/or spatial distribution if they would be directly involved in the injury induced inflammatory response. These observations suggest that most of the macrophages in the OE are resident to the tissue and may be responsible of the surveillance of the tissue under physiological conditions, to contribute to the maintenance neurogenesis by the phagocytosis of the apoptotic OSNs. Macrophages populate the intact OE in higher numbers than neutrophils under physiological conditions. They maintain tissue homeostasis by the continuous surveillance and contribute to tissue turnover by engulfing dying OSNs and debris. In contrast to macrophages, neutrophils are present in scarce numbers in the intact tissue and a grave increase is seen only after a major stress is introduced to the epithelium as explained in section 4.2.1. Neutrophils take over the responsibility of regaining the tissue homeostasis under stress conditions, while macrophages avoid the inflamed area in the early post injury period.

5.2.4. Morphologic Plasticity of Macrophages and Selective Labeling *in vivo*

A previous study on OE of juvenile zebrafish has demonstrated that resident macrophages in the intact tissue adopted ramified profiles, and that they change to a more spherical and ameboid shape following phagocytic activity during sterile injury induced inflammatory responses (Palominos and Whitlock, 2021). In contrast, a separate study revealed that unstimulated (M0) and pro-inflammatory (M1) macrophages acquired a more spherical profile than the late M2 subtype, which exhibited a more dendritic cellular morphology (Italiani and Boraschi, 2014). In addition, it was also reported that macrophages, upon pro-inflammatory stimulation, possessed dendritic cellular shapes (Palominos and Whitlock, 2021). Yet in another recent study, Nguyen-Chi et.al. (2015) suggested a new method to distinguish different subtypes of macrophages and marked them according to their cytokine expression patterns (Nguyen-Chi et al., 2015). Although there is a significant amount of research that concentrate on the morphological behavior of macrophages in injury-induced inflammatory response, literature still holds contrasting evidence regarding this issue.

In addition to the ambiguous evidence in the field regarding macrophage subtypes, this thesis constitutes the first experimental evidence featuring selective depletion assays to establish the functional effect and morphologic behavior of macrophages in the OE of adult zebrafish. The presence of different macrophage subtypes in the OE of zebrafish has not been established to this date. Selective markers that distinguish these subtypes have been proposed by a few research groups (Nguyen-Chi et al., 2015). However, both the literature findings and the evidence recorded in this study (section 4.1.3.) indicate that macrophage morphological plasticity may be much more fluid than anticipated previously. This thesis and a considerable number of recent studies in the field has claimed that macrophages can obtain distinct phenotypes that are on a continuous spectrum rather than existing as a discrete number of subtypes. Nevertheless, the immune system of vertebrates has long been adjusted to evolutionary development which has enabled the innate immune cells to develop distinct chemical and inter-cellular behaviors that may differ among different tissue types. Therefore, there is significant need for additional studies that focus on the innate immune cell morphology and behavior in olfactory system of the zebrafish and mammals, to build a confidence to claim solid hypotheses on the subject.

The outcome of the morphological analysis in the OE in section 4.1.3. indicates that the resident macrophages are not observed to be associated with any of the extreme phenotypes in the opposing points of the phenotypic spectrum. Following tail amputation experiments in the larval zebrafish, Nguyen-Chi et. al. (2015) suggested a method to selectively label macrophages that obtain M1 and M2 sbutypes (Nguyen-Chi et al., 2015), which argued that morphological properties refer to the different functional macrophage subtypes (Nguyen-Chi et al., 2015). This literature outcome coupled with the related evidence from this study may lead to the conclusion that the intact OE is inhabited by a heterogenous population of macrophages that exhibit different intermediatory subtypes. Although promising outcomes have been obtained from the research of Nguyen-Chi et. al. (2015), several concerns rise regarding the existance of a reliable application to the adult zebrafish olfactory system. First and foremost, the initiation and outcome of the inflammatory response may differ according to changing tissue types. Therefore, the dynamic behavior of the members of the innate immune system may be different in the tail fin comparing to the oldactory epithelium. The difference in the injury type (chemical versus physical) is also an important contributor to the potential difference between behavioral and morphological properties of macrophages. Zebrafish hematopoiesis is composed of complicated systemic events that result in a notable difference in the innate immune system in different developmental stages. Therefore, although the studies that feature larval and embryonic fish offer beneficial information, there still needed to be reliable research on adult zebrafish to assess the applicability of the outcomes to the current study of interest. Nevertheless, from the limited evidence obtained from the literature, one could speculate that macrophage populations that are morphologically proximate with M1 and M2 subtypes exist in the intact and the injured OE. Without further evidence on the adult zebrafish olfactory system, this claim would be nothing more than an educated speculation, at least for the time being.

In summary, the M1/M2 phenotypes sit in opposing poles of a morphological spectrum of intermediatory phenotypes. Therefore, it is not realistic to look for absolute M1 or absolute M2 subtypes *in vivo*. Thus, it is consonant with the fact that the macrophages in the intact OE were not observed to be associated with any of the extreme phenotypes in the opposing poles of the proposed spectrum.

In addition, there is very limited evidence in zebrafish, about distinguishing different subtypes within the heterogenous phenotype spectrum that macrophages have potential to obtain. Therefore, discussing on their visual characteristics is not a reliable scientific way to define the exact phenotypes, and more importantly, it is not a confident measure to define which subtype they attain and consequently what function do they express. The definitive markers that distinguish different macrophage subtypes and parameters of their phenotypic properties have not been fully established in adult zebrafish. It is crucial to first unveil the definitive properties/parameters that can distinguish different subtypes of macrophages.

5.3. Neutrophil versus Macrophage Roles in Injury Induced Regeneration

The functional and behavioral evidence established in this study give an insight into the interplay between neutrophils and macrophages in regulating the early and late inflammatory periods in the adult zebrafish OE. The experimental observations suggest that the neutrophils provide more of an unspecific and quick transient response upon chemical irritant exposure, with the aim of eliminating foreign pathogens and chemicals from the inflamed area as quickly as possible. They do not exhibit high degree of morphological and functional plasticity, at least in the early inflammatory period. Therefore, neutrophilic response in the acute inflammatory period can be considered as a non-specific, protrusive, and relatively aggressive reaction to provide restoration of microenvironmental homeostasis as quickly as possible. Macrophages on the other hand, may be avoiding the chronic inflammatory milieu, aiming more on the later phase of the inflammatory response, featuring the resolution and regenerative events. Macrophages adapt to function in a tissue environment according to the individual necessities of the particular tissue type, for regaining tissue function and homeostasis, which may explain their ability to show extensive phenotypic and functional plasticity.

5.5. The Role of Neutrophils in Tissue Repair and Regeneration

As the first line of defense against any type of tissue injury, neutrophils accumulate at the site of damage in large numbers (Wang, 2018). The first and foremost role of neutrophils is to sterilize the inflamed area by phagocytosing necrotic cell debris and any potential foreign invaders. These cells carry highly cytotoxic substances within their granules and by the time they arrive at the damaged area, they undergo “degranulation” to release these toxic reagents to combat foreign pathogens and to provide a quick decontamination of the area (Wang, 2018). These toxic reagents including ROS and various proteolytic enzymes, may also endanger the endogenous cells of healthy tissue around the inflamed region in case of a prolonged chronic inflammatory state (Havixbeck et al., 2016). Therefore, neutrophils have traditionally been considered to be disruptive to the healing process of the damaged tissues if present (Peiseler and Kubes, 2019). However, a considerable amount of research in the recent decade have demonstrated remarkable capacity of these cells to promote and even mediate the regenerative processes in certain tissue contexts such as lungs, central and peripheral nervous system, liver, heart, and skin (Phillipson and Kubes, 2019).

Several diverse mechanisms allow neutrophils to act on the onset of inflammation. For example, neutrophils eliminate foreign pathogens and proinflammatory factors by utilizing their own genomic DNA as NETs, which also contain bound proteases and histone proteins (Li et al., 2020). This remarkable mechanism is coupled by the release of pro-resolution factors including protectins, resolvins, growth factors, angiogenic factors, defensins and anti-inflammatory cytokines that help drive the acute-inflammatory period towards the resolution phase (Phillipson and Kubes, 2019). When neutrophils are accumulated at the site of damage, they also trap pro-inflammatory cytokines and chemoattractant factors to slow down further neutrophil infiltration (Peiseler and Kubes, 2019). Therefore, although neutrophils have been considered to be the infantryman of the innate immune system that is only equipped to kill and release toxic reagents into the microenvironment, they have highly sophisticated mechanisms to terminate the pro-inflammatory period as quickly as possible and promote healing at the same time.

5.5.2. Neutrophil Contributions to the Central and Peripheral Nervous System Regeneration

A study by Stirling et.al. demonstrated impressive contribution of neutrophils to spinal cord injury in mice (Stirling et al., 2009). The time course of neutrophil recruitment after sterile injury was introduced to the spinal cord was convenient with the profile observed in this study on the experimental injury model in the OE of zebrafish. Shortly within several hours after injury, neutrophil accumulation reached a peak and more than 90% of neutrophils were eliminated systemically upon depletion with anti-Ly6G/Gr-1 antibody (Stirling et al., 2009). Antibody based depletion of neutrophils is a well-established conventional method that is unfortunately not applicable in zebrafish. Despite using different methods, both VMO and antibody-based applications successfully depleted neutrophils systemically. Wound healing and axonal and brain tissue conservation were severely impaired in the mice in neutrophil scarcity. These results give a promising insight into the role of neutrophils in neuro-regeneration in mice, which is supportive evidence to the outcome of the neutrophil depletion experiments in the current study, which has indicated a positive contribution of neutrophils to the OSN neurogenesis in zebrafish.

Different tissue types require distinct combination of mediatory factors to achieve a successful regeneration after sterile injury. These factors are usually released from the endogenous cells, or the cells recruited in response to damage. As described above, neutrophils have a diverse collection of cytotoxic and pro-regenerative granular contents and release them according to the stimulus they receive from the injured tissue upon arrival. Neuronal tissue regeneration after injury is normally not possible in many circumstances, especially in higher vertebrates. However, a study from the last decade, demonstrated that neutrophils secrete an essential growth factor that enables optic nerve regeneration after injury in mice (Kurimoto et al., 2013). Depletion experiments further confirmed that neurogenesis in the optic nerve was impaired in the absence of neutrophils. In addition, consistent to the observations in this thesis (section 4.4.), the study indicated that macrophages came late in the inflammatory period and did not provide any sufficient contribution to neurogenesis.

In another study on peripheral nerve regeneration in mice, Lindborg et.al. revealed that neutrophils are crucially important in myelin clearance, which is a perquisite stage for axonal regeneration (Lindborg et al., 2017). Systemic neutrophil depletion with anti-Ly6G antibodies successfully eliminated 90% of the cells in the animals which had peripheral nerve axotomy. The axon regeneration was severely halted in these mice compared to controls.

Neutrophils have traditionally not been on the spotlight in terms of their potential contribution to central and peripheral nervous system regeneration. Current research indicates that there is promising evidence on the regulatory function of neutrophils in regeneration of brain and peripheral nerves. Nevertheless, the studies that have focused on this subject are still very few and mostly centered around the rodent models. Zebrafish is a remarkable model to study the interplay between immune system and neuro-regeneration. However, the contribution of neutrophils to the neuronal regeneration have not been fully explored in zebrafish. More studies on neutrophil mediated neuronal regeneration are needed to be established in the future, to elevate the current evidence.

5.6. The Success of RO Delivery of VMOs to Deplete Neutrophils in Adult Zebrafish

RO injection protocol has been developed for the zebrafish, in the recent decade as an effective approach to deliver drugs or experimental substances to the circulatory system. Alternative IV delivery methods used in zebrafish including intracardiac injection or injection to the common cardinal vein exhibit high risk factors that can lead to high mortality rate. Ineffective delivery of the drugs due to the small diameter of the fish veins is one of the most common problems. In addition, if not applied delicately, injector may disrupt the spinal cord which is located close to the common cardinal vein. Excessive bleeding is another high-risk outcome that may be encountered especially in intracardiac applications. RO route provides a relatively safe protocol in contrast to other alternative methods. Retro orbital venous sinus offers a much easier entry route and accessibility with injectors.

Several downfalls of this application involve sudden death or brain damage caused by a puncture wound to the OB, telencephalon, or excessive bleeding due to the rupture of a big blood vessel. Nevertheless, RO injection offers the most applicable route for the delivery of experimental drugs to the circulatory system of adult zebrafish.

VMO against *csf3r* is affective on the neutrophil precursors that are dedicated to undergo granulopoiesis and express high levels of this cell surface receptor. Neutrophil differentiation from myeloid lineage takes place in the kidney marrow as described earlier. Therefore, VMO injection solution would need to effectively reach the kidney, to provide knockdown. The most practical and efficacious approach to deliver VMO solution to the kidney, was the RO injection protocol. This method also required minimal amounts of injection solution (2 µl VMO + 2 µl FITC-Dextrane) compared to IP injection, which would require at least 10 - 15 µl of solution for delivery. Considering the commercially expensive properties of the VMOs that are custom made to the customer's requested sequence, it is both economically and functionally more efficient to deliver via RO injection. Delivery directly to the circulation may also provide a faster arrival of the VMOs to the kidney in comparison to the other routes. In addition, there is reliable evidence from previous studies on zebrafish that RO injection of VMOs significantly and successfully reduced neutrophil numbers systemically (Liongue et al., 2009; Pazhakh et al., 2017).

MO knockdown of neutrophils enables to significantly reduce neutrophil numbers systemically without a complete elimination, which would significantly reduce the lifetime of the morphant and compromise the experimental process. In contrast to a complete immunodeficient fish, basal levels of neutrophil presence may serve to sustain innate immune activity which is necessary to sustain the vitals of the fish until the end of the experimental period. Despite a small number of neutrophils were still circulating after VMO-knockdown, a rather high mortality rate was observed among the VMO-csf3r injected fish. Several other factors including the lower temperatures of the stereomicroscope room, where the RO injection was applied to be able to monitor the fluorescence signal immediately may have contributed to the decreased lifetime. Anesthetic MS222 might also be a negative effector in this aspect, even though the dosage was decreased, and fish were given 60-70% dilution during imaging.

Finally, complications may have occurred after the RO injection procedure that were invisible to the researcher and contributed to the reduced lifetime of the fish. However, such a high level of mortality was not observed in the VMO-ctr injected fish. Another aspect to consider is that every injection is a different process by its nature since it is not operated by automatic machinery but manually applied by operating people. Therefore, the injection procedures should also not be considered as uniform applications either.

5.7. Neutrophils Selectively Modulate Injury Induced Repair Neurogenesis in the OE

VMOs against *csf3r* transcript were administered via RO injection to adult zebrafish and were successful in eliminating a significant portion of neutrophil populations in the primary hematopoietic organs and in the OE. The peak of the neutrophil occupancy which was observed at the early inflammatory periods (6 and 24 hpl), was not detected in the KD animals. Neutrophil abundance in the KD animals reduced to pre-injury levels (Figure 4.13a; bottom right; green).

Temporal systemic neutrophil depletion resulted in a remarkable decrease in proliferative activity in the OE, which suggests that neutrophils have significant functional role in promoting and/or mediating proliferation after chemical irritant exposure. OE switches to injury-induced repair neurogenesis mechanism when there is a big scale traumatic injury causing significant disruption to the structural integrity and tissue loss (Bayramli et al., 2017; Demirler et al., 2020). In repair neurogenesis, normally dormant HBCs are activated to give rise to all types of neuronal and non-neuronal cell types of the epithelium to repopulate the tissue and achieve full functional recovery (Calvo-Ochoa et al., 2021). Highly significant disruption in the number and pattern of proliferating cells was detected in the lesioned OEs in the KD animals. Intriguingly, there was no notable alteration in level and pattern of mitotic activity in the intact OEs of KD animals. this evidence suggest that neutrophils are functionally influence the neurogenic activity only after a traumatic injury is introduced, but not under physiological conditions.

The interplay between HBCs and neutrophils in the pro-inflammatory milieu is therefore necessary to investigate, which may give important insight into molecular patterns and signaling mechanisms governing the neutrophil-stem cell crosstalk.

In summary, according to the evidence established in this study, it is essential to provide further experimental evidence that will contribute to understand and support the hypothesis that indicates: “Tissue damage activates the neutrophils but not macrophages to mediate the repair neurogenesis in the OE. On the other hand, neutrophilic activity does not significantly regulate the maintenance neurogenesis and tissue turnover of the OE under physiological conditions.”

5.8. Efficacy of Clodronate Liposomes in the OE

Clodronate (Dichloroethylene - Bisphosphonate) has been widely utilized since 1960s to prevent resorption in bone related diseases like osteoporosis and Paget’s disease, as well as in treatment of cancer to inhibit tumor growth in multiple myeloma (Opperman et al., 2019) and breast cancer (Fleisch, 2001; Pavlakis et al., 2005). Injection of the substance provides a temporal elimination of macrophage populations and offers an advantage over transgenic models in the sense that the husbandry of immune-deficient transgenic zebrafish may be challenging.

Clodronate is a synthetic analogue of inorganic pyrophosphate (Fleisch, 2001). When cells use clodronate instead of endogenous pyrophosphate, a non-hydrolysable form of ATP is produced, blocking the respiratory pathway (Moriyama and Nomura, 2018). Encapsulating clodronate into liposomes provides an efficacious *in vivo* delivery approach (Rosowski, 2020). When introduced into animals via IV or IP injection, clodronate liposomes are effectively and specifically engulfed by macrophages but not by other phagocytes due to their relatively large size (van Rooijen and Hendrikx, 2010). Because of its highly hydrophilic nature, clodronate cannot pass the liposomal membranes as well as the phospholipid bilayer of the cell membrane after release into the cytoplasm.

When a certain intracellular concentration of clodronate is reached, macrophages undergo apoptosis (Moreno, 2018). Clodronate does not pose a toxicity in the blood-stream when released from dead macrophages since its lifespan in circulation is quite short and is immediately eliminated from the body by the renal system. (Moreno, 2018)

The experimental evidence described in section 4.4.3. suggest that although clodronate liposomes were successful in partial elimination of macrophage populations in the primary hematopoietic organs, the efficacy of the drug did not reach the OO. In other words, clodronate liposomes were found to be non-accessible to the resident and/or recruited macrophages in the OE. It has been indicated that the efficacy and potency of this method is largely decided by the accessibility of the liposomes to the macrophages in the tissue of interest (van Rooijen and Hendrikx, 2010). Although IP route of delivery successfully depleted a significant portion of cells in the primary hematopoietic organs, it is evident that the macrophages in the OE were not possible to reach. It is intriguing that the application was efficacious enough to deplete at least a significant portion of splenic macrophages and those in the kidney but fail to do so for a not more than a handful of cells within the OE. One of the possible reasons of this result is the fact that the multilayered liposomal vesicles cannot penetrate the vascular barrier. In addition, the olfactory system may be anatomically protected by a dense connective tissue in the head that includes multiple vital organs in a limited amount of space, which could be hard to diffuse into.

One might claim that it was a time related issue that resulted in inefficient depletion of macrophages in the OE and 24 hours may not be sufficient for clodronate liposomes to diffuse all the way to the OO. However, as it was confirmed in the 5-day experiment described in section 4.4.3., similar level of macrophage occupancy was present in both intact and lesioned OEs after liposomes injection was performed every 24 h for 5 consecutive days.

To investigate the accessibility of the macrophages in the OE, testing different delivery methods would be beneficial for the future research. Delivery to the circulation may ease the way for clodronate liposomes to access the OE within the already streaming blood in the vessels. This would also eliminate the potential concern of selective impermeability of the capillary walls to the liposomes.

Effectivity of the RO injection has been demonstrated in previous studies and further confirmed with the experimental evidence in this thesis. Therefore, RO injection may be the best candidate to effectively deliver the clodronate liposomes to the circulation. The proximity of the injection location to the OO further contributes to this suggestion. Another delivery route for clodronate liposomes to easily reach the OO, is nasal delivery of the suspension, similar to the nasal irrigation with TrX in the experiments described in the study. A direct contact may be possible with this application. However, it would not provide a systemic elimination of macrophages. Therefore, to achieve a temporal systemic depletion of macrophages to assess the functional effects of these cells, it would be more effective to a perform nasal delivery and IP injection together.

Altogether, IV route would be a better administration approach to access resident macrophages in OE and the ones circulating in the blood stream. However, in the absence of a convincing dynamic change in macrophage behavior in response to chemical injury, the hypothesis claiming that the macrophages may regulating or contributing the regenerative events in the OE becomes compromised. One other evidence that contradicts this hypothesis is that even an aggressive dosage of clodronate liposomes did not result in any considerable change in the proliferative activity or OSN neurogenesis in the injured OE. Altogether, the unsatisfactory evidence from functional studies on macrophage behavior in the OE suggests that macrophages do not have any significant mediatory role in the injury induced neurogenesis and tissue regeneration in the OE of adult zebrafish. Further investigation is crucial to confirm such hypothesis with significant evidence on all the aspects that may have been omitted in this study because of economic and time related circumstances.

5.9. Interplay Between the Immune System and the Neural Stem Cells

Higher vertebrates like mammals have very limited regenerative and restorative capacity especially in the nervous system, mostly due to the sparsity of the neurogenic stem cell niches and highly sophisticated cellular and molecular organization that creates difficulty in generating new cells of the tissue.

The NSCs in the adult mammalian central nervous system are found only in the subventricular zone of the lateral ventricles and sub granular zone of the dentate gyrus in the hippocampus (Bond et al., 2015), while in lower vertebrates, these neurogenic sites are more frequently distributed throughout the brain tissue (Kizil et al., 2015). Zebrafish, on the other hand, undergoes a lifelong constitutive regeneration of the nervous system due to the abundance of the neurogenic niches (sixteen located in the CNS; Kizil et al., 2012). In addition, it can repair brain tissue after damage, and remarkably regain full function without neuronal scar deposition (Kyritsis et al., 2012) .

Intriguingly, the peripheral olfactory system has the ability to undergo lifelong turnover of the OSNs due to two distinct stem cell populations found in the basal lamina of the epithelium GBCs and HBCs (Lakshmanan et al., 2022). The OSNs are directly exposed to the outside environment, which delivers harmful pathogens and chemicals continuously. This remarkable ability of the OE has been the focus of substantial number of studies with the aim to unveil the underlying mechanisms behind this unique ability. In recent 2-3 years, neurogenesis in the OE and the inflammation induced OSN loss has been the focus of attention due to the characteristic side effects of the global pandemic COVID-19, which caused severe smell and taste loss (Finlay et al., 2022). Therefore, OSN loss in injury-induced inflammation is considered as a “hot topic” now more than ever. To find new and more effective therapeutic approaches to OSN loss and to injury and age-related neuronal loss in general, functional studies on organisms with high regenerative capacity, like zebrafish, is essential.

Inflammation in the neuronal tissues in mammals shows a striking difference with the regenerating organisms. The first wave of leukocyte infiltration is the common denominator between two, but the length of the overall inflammatory process differs significantly (Kizil et al., 2015). In mammals chronic phase of the inflammatory response is often followed by a prolonged resolution phase, which results in an imperfect functional and structural recovery of the tissue, while the extended inflammatory period is not observed in regenerating organisms like zebrafish (Kizil et al., 2015). In addition, mammals fail to undergo a full regeneration of the neuronal tissue in inflammatory microenvironment unlike zebrafish, which is able to accomplish neuronal regeneration under inflammatory conditions (Kizil et al., 2015).

One of the prospective aims of this study is to give insight into the undisclosed aspects of neurodegenerative diseases, which are usually linked with chronic neuro-inflammation, including but not limited to Alzheimer's disease (Knopman et al., 2021), Parkinson's disease (Poewe et al., 2017), and multiple sclerosis (Filippi et al., 2018), to establish novel therapeutic strategies. Therefore, investigating key differences in the neuronal regeneration in the context of inflammatory response between higher vertebrates and regenerating organisms should be the aim of the future regenerative studies.

Although both harmful and beneficial effects of inflammation on neurogenesis, more and more studies show that a mutual interplay exists between the immune system and the NSCs. In a traumatic brain injury model in zebrafish, inflammatory milieu was found to be necessary for NSC activation (Kyritsis et al., 2012). The fish were adjusted to immunosuppressive drug dexamethasone (Dex) and the efficiency of neurogenesis was analyzed. the results indicated that neuronal regeneration in the injured brain tissue of the immunosuppressed fish was significantly impaired (Kyritsis et al., 2012). Adult mammalian organisms cannot accomplish a full regeneration of their neuronal tissue and there is evidence from literature that indicates inflammation negatively affects NSC activity in higher vertebrates (Karin and Clevers, 2016). However, revealing key aspects of inflammation in promoting and regulating neuronal regeneration in regenerating organisms like zebrafish is important for future research, which may focus on finding applicable approaches to stimulate efficient NSC activity in mammals.

In a recent study on the OE neurogenesis, Chen et.al. (2017) showed that certain molecular factors that are specifically enriched in the acute-inflammatory period directly regulates the crosstalk between the innate immune response and the OSN neurogenesis by activating HBCs in the basal lamina of the OE (Chen et al., 2017). This study revealed insight into underlying molecular mechanisms of the remarkable regenerative capability of the OE, which is characterized by a transient innate immune activity which is quickly resolved. The HBC induced neurogenesis was demonstrated to be dependent on the TNF- α signaling and the NF-κB cascade in the OE of mice (Chen et al., 2017). In addition, impairing the innate inflammatory response by anti-inflammatory drug tests or genetic assays resulted in a compromised and hindered repair neurogenesis lead by the HBCs (Chen et al., 2017).

These results constitute important evidence indicating that transient innate immune response, which is characterized by leukocyte (mostly neutrophils in large numbers) recruitment and release of diverse molecular factors, directly involves, and even regulates the efficiency and outcome of the repair neurogenesis in the OE. These observations also support the outcomes of this thesis described in sections 4.2.1. and 4.3., which indicated that during the early stages of the inflammatory period neutrophils are recruited in large numbers and quickly resolve after the acute period ends. In addition, systemic neutrophil depletion severely impairs the repair neurogenesis mediated by HBC activity in the OE of zebrafish. Altogether, the important insight from rodent models should encourage future researchers to investigate the molecular mechanisms of the interplay between neutrophils and HBC activity in the acute inflammatory response in OE of the zebrafish.

In summary, this thesis revealed that neutrophil depletion severely impedes the injury induced OSN neurogenesis in the OE, which is characterized by the HBC activity. Specific molecular mediators of this interplay should be investigated to unveil the underlying machinery behind the regulatory role of neutrophils in injury induced regeneration in the OE. This would serve as an encouraging reference point on the road to discover efficient therapeutic applications for neurodegenerative disorders that feature chronic inflammatory conditions such as Alzheimer's disease (Knopman et al., 2021), Parkinson's disease (Poewe et al., 2017), multiple sclerosis (Filippi et al., 2018), and psychiatric disorders, which result in irreversible NSC degeneration and functional disability.

5.10. Future Aspects

The immunostaining assays in this thesis were established following a detailed literature filtration and significant experimentation of the efficiency and accuracy of the antibodies. Unfortunately, zebrafish reactive antibodies that selectively label immune cells and their subtypes are in very limited commercial availability, and in some cases nonexistent. In addition, innate immune cells undergo frequent secretion of the molecular factors they carry within as of their nature.

The signaling pattern of the cryosectioned thin tissue sections may not express sufficient specificity in labelling neutrophils and macrophages at certain situations. For example, Mpx is the most abundant cytotoxic reagent secreted by neutrophils (Le Guyader et al., 2008), which is also the recognition target for the antibody used in many studies including this one. However, analysis solely depend on the immunohistochemical approaches may not express a satisfactory specificity in certain cases like kidney and spleen staining. Therefore, further applications that can provide visual or quantitative confirmation on the presence and behavior of the innate immune cells in zebrafish is essential for the future research. Using transgenic fish offers a highly specific and efficient way to monitor innate immune cells *in vivo*. One of the advantages of *in vivo* studies is that one can observe the innate immune cells in their natural environment, in the sense that dissection and prefixation-like approaches may hinder and alter the ongoing molecular and cellular environment post sacrifice. In addition, the innate immune system requires an even more delicate approach, because unintentional injury introduced by the researcher during the experimental procedures, may cause further inflammatory response.

Molecular key molecular regulators possibly released by neutrophils to specifically activate OSNs should be investigated. To do so, candidate molecules must be detected with the reference to the existing evidence from the literature. Recent studies on the neutrophil contributions on inflammation induced regeneration in the central and peripheral nervous system in regenerating organisms like teleost fish should also be investigated in detail. Proteomic analyses may be helpful in establishing the library of diverse granular contents carried by neutrophils. Functional analyses on certain molecular candidates on their selective activation in different tissue types should also be considered. Single-cell RNA sequencing and RT q-PCR approaches are also potential applications to further reveal the neutrophilic contents in detail in tissue and organ base. Neutrophilic activity posed promising evidence on its regulatory role in OSN neurogenesis. Further confirmation on neutrophil behavior and function may be monitored by assessing the amount of cellular debris and DAMPs around the inflamed area in the injured OE in the presence and also deficiency of neutrophils.

REFERENCES

Atkinson, M. A., G. S. Eisenbarth, and A. W. Michels, 2014, "Type 1 Diabetes", *The Lancet*, Vol. 383, No. 9911, pp. 69–82.

Aurora, A. B., and E. N. Olson, 2014, "Immune Modulation of Stem Cells and Regeneration", *Cell Stem Cell*, Vol. 15, No. 1, pp. 14–25.

Bader, A., J. Gao, T. Rivière, B. Schmid, B. Walzog, and D. Maier-Begandt, 2021, "Molecular Insights Into Neutrophil Biology from the Zebrafish Perspective: Lessons From CD18 Deficiency", *Frontiers in Immunology*, Vol. 12, No. 8, pp. 1–11.

Bayramli, X., Y. Kocagöz, U. Sakizli, and S. H. Fuss, 2017, "Patterned Arrangements of Olfactory Receptor Gene Expression in Zebrafish are Established by Radial Movement of Specified Olfactory Sensory Neurons", *Scientific Reports*, Vol. 7, No. 1, pp. 1–16.

Bennett, C. M., J. P. Kanki, J. Rhodes, T. X. Liu, B. H. Paw, M. W. Kieran, D. M. Langenau, A. Delahaye-Brown, L. I. Zon, M. D. Fleming, and A. Thomas Look, 2001, "Myelopoiesis in the Zebrafish, Danio Rerio", *Blood*, Vol. 98, No. 3, pp. 643–651.

Bernut, A., C. A. Loynes, R. A. Floto, and S. A. Renshaw, 2020, "Deletion of cftr Leads to an Excessive Neutrophilic Response and Defective Tissue Repair in a Zebrafish Model of Sterile Inflammation", *Frontiers in Immunology*, Vol. 11, No. 7, pp. 1–13.

Bertrand, J. Y., A. D. Kim, E. P. Violette, D. L. Stachura, J. L. Cisson, and D. Traver, 2007, "Definitive Hematopoiesis Initiates through a Committed Erythromyeloid Progenitor in the Zebrafish Embryo", *Development*, Vol. 134, No. 23, pp. 4147–4156.

Bevan, L., Z. W. Lim, B. Venkatesh, P. R. Riley, P. Martin, and R. J. Richardson, 2020, "Specific Macrophage Populations Promote Both Cardiac Scar Deposition and Subsequent Resolution in Adult Zebrafish", *Cardiovascular Research*, Vol. 116, No. 7, pp. 1357–1371.

Bollaerts, I., J. Van Houcke, A. Beckers, K. Lemmens, S. Vanhunsel, L. De Groef, and L. Moons, 2019, "Prior Exposure to Immunosuppressors Sensitizes Retinal Microglia and Accelerates Optic Nerve Regeneration in Zebrafish", *Mediators of Inflammation*, Vol. 2019, No. 6, pp. 1–16.

Bond, A. M., G. L. Ming, and H. Song, 2015, "Adult Mammalian Neural Stem Cells and Neurogenesis: Five Decades Later", *Cell Stem Cell*, Vol. 17, No. 4, pp. 385–395.

Borders, A. S., M. A. Hersh, M. L. Getchell, N. Van Rooijen, D. A. Cohen, A. J. Stromberg, and T. V. Getchell, 2007, "Macrophage-Mediated Neuroprotection and Neurogenesis in the Olfactory Epithelium", *Physiological Genomics*, Vol. 31, No. 3, pp. 531–543.

Braubach, O. R., A. Fine, and R. P. Croll, 2012, "Distribution and Functional Organization of Glomeruli in the Olfactory Bulbs of Zebrafish (Danio rerio)", *Journal of Comparative Neurology*, Vol. 520, No. 11, pp. 2317–2339.

Byrd, C. A., and P. C. Brunjes, 1995, "Organization of the Olfactory System in the Adult Zebrafish: Histological, Immunohistochemical, and Quantitative Analysis", *Journal of Comparative Neurology*, Vol. 358, No. 2, pp. 247–259.

Caldwell, L. J., N. O. Davies, L. Cavone, K. S. Mysiak, S. A. Semenova, P. Panula, J. D. Armstrong, C. G. Becker, and T. Becker, 2019, "Regeneration of Dopaminergic Neurons in Adult Zebrafish Depends on Immune System Activation and Differs for Distinct Populations", *Journal of Neuroscience*, Vol. 39, No. 24, pp. 4694–4713.

Calvo-Ochoa, E., and C. A. Byrd-Jacobs, 2019, "The Olfactory System of Zebrafish as a Model for the Study of Neurotoxicity and Injury: Implications for Neuroplasticity and Disease", *International Journal of Molecular Sciences*, Vol. 20, No. 7, pp. 1–20.

Calvo-Ochoa, E., C. A. Byrd-Jacobs, and S. H. Fuss, 2021, "Diving into the Streams and Waves of Constitutive and Regenerative Olfactory Neurogenesis: Insights from Zebrafish", *Cell and Tissue Research*, Vol. 383, No. 1, pp. 227–253.

Chazaud, B., 2014, "Macrophages: Supportive Cells for Tissue Repair and Regeneration", *Immunobiology*, Vol. 219, No. 3, pp. 172–178.

Chazaud, B., 2020, "Inflammation and Skeletal Muscle Regeneration: Leave It to the Macrophages!", *Trends in Immunology*, Vol. 41, No. 6, pp. 481–492.

Chen, G. Y., and G. Nuñez, 2010, "Sterile inflammation: Sensing and Reacting to Damage", *Nature Reviews Immunology*, Vol. 10, No. 12, pp. 826–837.

Chen, M., R. R. Reed, and A. P. Lane, 2017, "Acute Inflammation Regulates Neuroregeneration through the NF-Kb Pathway in Olfactory Epithelium", *Proceedings of the National Academy of Sciences of the United States of America*, Vol. 114, No. 30, pp. 8089–8094.

Coates, D. R., J. M. Chin, and S. T. L. Chung, 2011, "Oncogenic CSF3R Mutations in Chronic Neutrophilic Leukemia and Atypical CML", *Bone*, Vol. 23, No. 1, pp. 1–7.

Das, A., M. Sinha, S. Datta, M. Abas, S. Chaffee, C. K. Sen, and S. Roy, 2015, "Monocyte and Macrophage Plasticity in Tissue Repair and Regeneration", *American Journal of Pathology*, Vol. 185, No. 10, pp. 2596–2606.

Davidson, A. J., and L. I. Zon, 2004, "The “Definitive” (and ’Primitive’) Guide to Zebrafish Hematopoiesis", *Oncogene*, Vol. 23, No. 43, pp. 7233–7246.

Demetri, G., and J. Griffin, 1991, "Granulocyte colony-Stimulating Factor and its Receptor", *Blood*, Vol. 78, No. 11, pp. 2791–2808.

Demirler, M. C., U. Sakizli, B. Bali, Y. Kocagöz, S. E. Eski, A. Ergönen, A. S. Alkiraz, X. Bayramli, T. Hassenklöver, I. Manzini, and S. H. Fuss, 2020, "Purinergic Signalling Selectively Modulates Maintenance but not Repair Neurogenesis in the Zebrafish Olfactory Epithelium", *FEBS Journal*, Vol. 287, No. 13, pp. 2699–2722.

Ellett, F., and G. J. Lieschke, 2010, "Zebrafish as a Model for Vertebrate Hematopoiesis", *Current Opinion in Pharmacology*, Vol. 10, No. 5, pp. 563–570.

Farache Trajano, L., and N. Smart, 2021, "Immunomodulation for optimal Cardiac Regeneration: Insights from Comparative Analyses", *Npj Regenerative Medicine*, Vol. 6, No. 1, pp. 1–11.

Filippi, M., A. Bar-Or, F. Piehl, P. Preziosa, A. Solari, S. Vukusic, and M. A. Rocca, 2018, "Multiple Sclerosis", *Nature Reviews Disease Primers*, Vol. 4, No. 1, pp. 1–27.

Finlay, J. B., D. H. Brann, R. Abi-Hachem, D. W. Jang, A. D. Oliva, T. Ko, R. Gupta, S. A. Wellford, E. A. Moseman, S. S. Jang, C. H. Yan, H. Matusnami, T. Tsukahara, S. R. Datta, and B. J. Goldstein, 2022, "Persistent Post-COVID-19 Smell Loss is Associated with Inflammatory Infiltration and Altered Olfactory Epithelial Gene Expression", *Science Translational Medicine*, Vol. 14, No. 676, pp. 1–13.

Fleisch, H., 2001, "The Role of Bisphosphonates in Breast Cancer: Development of Bisphosphonates", *Breast Cancer Research*, Vol. 4, No. 1, pp. 1–5.

Freire, M. O., and T. E. Van Dyke, 2013, "Natural Resolution of Inflammation", *Periodontology 2000*, Vol. 63, No. 1, pp. 149–164.

Friedrich, E. E., L. T. Sun, S. Natesan, D. O. Zamora, R. J. Christy, and N. R. Washburn, 2014, "Effects of Hyaluronic Acid Conjugation on Anti-TNF-α Inhibition of Inflammation in Burns", *Journal of Biomedical Materials Research - Part A*, Vol. 102, No. 5, pp. 1527–1536.

Ghosh, S., and S. P. Hui, 2018, "Axonal Regeneration in Zebrafish Spinal Cord", *Regeneration*, Vol. 5, No. 1, pp. 43–60.

Goodman, S. B., J. Pajarinen, Z. Yao, and T. Lin, 2019, "Inflammation and Bone Repair: From Particle Disease to Tissue Regeneration", *Frontiers in Bioengineering and Biotechnology*, Vol. 7, No. 9, pp. 1–11.

Gorlin, R. J., B. Gelb, G. A. Diaz, K. G. Lofsness, M. R. Pittelkow, and J. R. Fenyk, 2000, "WHIM Syndrome, an Autosomal Dominant Disorder: Clinical, Hematological, and Molecular Studies", *American Journal of Medical Genetics*, Vol. 91, No. 5, pp. 368–376.

Gray, C., C. A. Loynes, M. K. B. Whyte, D. C. Crossman, S. A. Renshaw, and T. J. A. Chico, 2011, "Simultaneous Intravital Imaging of Macrophage and Neutrophil Behaviour During Inflammation Using a Novel Transgenic Zebrafish", *Thrombosis and Haemostasis*, Vol. 105, No. 5, pp. 811–819.

Gusev, E. Y., Y. A. Zhuravleva, and N. V. Zotova, 2019, "Correlation of the Evolution of Immunity and Inflammation in Vertebrates", *Biology Bulletin Reviews*, Vol. 9, No. 4, pp. 358–372.

Hansen, A., and E. Zeiske, 1998, "The Peripheral Olfactory Organ of the Zebrafish, Danio Rerio: An Ultrastructural Study", *Chemical Senses*, Vol. 23, No. 1, pp. 39–48.

Harvie, E. A., and A. Huttenlocher, 2015, "Neutrophils in Host Defense: New Insights from Zebrafish", *Journal of Leukocyte Biology*, Vol. 98, No. 4, pp. 523–537.

Hasegawa, T., C. J. Hall, P. S. Crosier, G. Abe, K. Kawakami, A. Kudo, and A. Kawakami, 2017, "Transient Inflammatory Response Mediated by Interleukin-1β is Required for Proper Regeneration in Zebrafish Fin Fold", *ELife*, Vol. 6, No. 2, pp. 1–22.

Havixbeck, J. J., and D. R. Barreda, 2015, "Neutrophil Development, Migration, and Function in Teleost Fish", *Biology*, Vol. 4, No. 4, pp. 715–734.

Havixbeck, J. J., A. M. Rieger, M. E. Wong, J. W. Hodgkinson, and D. R. Barreda, 2016, "Neutrophil Contributions to the Induction and Regulation of the Zcute Inflammatory Response in Teleost Fish", *Journal of Leukocyte Biology*, Vol. 99, No. 2, pp. 241–252.

Iqbal, T., and C. Byrd-Jacobs, 2010, "Rapid Degeneration and Regeneration of the Zebrafish Olfactory Epithelium after Triton x-100 Application", *Chemical Senses*, Vol. 35, No. 5, pp. 351–361.

Iribarne, M., 2021, "Inflammation Induces Zebrafish Regeneration", *Neural Regeneration Research*, Vol. 16, No. 9, pp. 1693–1701.

Isles, H. M., K. D. Herman, A. L. Robertson, C. A. Loynes, L. R. Prince, P. M. Elks, and S. A. Renshaw, 2019, "The CXCL12/CXCR4 Signaling Axis Retains Neutrophils at Inflammatory Sites in Zebrafish", *Frontiers in Immunology*, Vol. 10, No. 1784, pp. 1–12.

Italiani, P., and D. Boraschi, 2014, "From Monocytes to M1/M2 Macrophages: Phenotypical vs. Functional Differentiation", *Frontiers in Immunology*, Vol. 5, No. 514, pp. 1–22.

Iwasaki, H., and K. Akashi, 2007, "Myeloid Lineage Commitment from the Hematopoietic Stem Cell", *Immunity*, Vol. 26, No. 6, pp. 726–740.

Julier, Z., A. J. Park, P. S. Briquez, and M. M. Martino, 2017, "Promoting Tissue Regeneration by Modulating the Immune System", *Acta Biomaterialia*, Vol. 53, No. 4, pp. 13–28.

Kameka, A. M., S. Haddadi, F. J. Jamaldeen, P. Moinul, X. T. He, F. H. P. Nawazdeen, S. Bonfield, S. Sharif, N. van Rooijen, and M. F. Abdul-Careem, 2014, "Clodronate treatment Significantly Depletes Macrophages in Chickens", *Canadian Journal of Veterinary Research*, Vol. 78, No. 4, pp. 274–282.

Karin, M., and H. Clevers, 2016, "Reparative Inflammation Takes Charge of Tissue Regeneration", *Nature*, Vol. 529, No. 7586, pp. 307–315.

Kaveh, A., F. A. Bruton, C. Buckley, M. E. M. Oremek, C. S. Tucker, J. J. Mullins, J. M. Taylor, A. G. Rossi, and M. A. Denvir, 2020, "Live Imaging of Heart Injury in Larval Zebrafish Reveals a Multi-Stage Model of Neutrophil and Macrophage Migration", *Frontiers in Cell and Developmental Biology*, Vol. 8, No. 10, pp. 1–22.

Keightley, M. C., C. H. Wang, V. Pazhakh, and G. J. Lieschke, 2014, "Delineatinæg the Roles of Neutrophils and Macrophages in Zebrafish Regeneration Models", *International Journal of Biochemistry and Cell Biology*, Vol. 56, No. 11, pp. 92–106.

Kell, M. J., R. E. Riccio, E. A. Baumgartner, Z. J. Compton, P. J. Pecorin, T. A. Mitchell, J. Topczewski, and E. E. LeClair, 2018, "Targeted Deletion of the Zebrafish Actin-Bundling Protein L-Plastin (lcp1)", *PLoS ONE*, Vol. 13, No. 1, pp. 1–23.

Khandekar, G., N. Iyer, and P. Jagadeeswaran, 2020, "Prostasin and Hepatocyte Growth Factor B in Factor VIIa Generation: Serine Protease Knockdowns in Zebrafish", *Research and Practice in Thrombosis and Haemostasis*, Vol. 4, No. 7, pp. 1150–1157.

Kim, J., K. Clark, C. Barton, R. Tanguay, and H. Moulton, "*Exon Skipping and Inclusion Therapies*", Humana Press, New York, 2018.

Kim, S., U. P. Radhakrishnan, S. K. Rajpurohit, V. Kulkarni, and P. Jagadeeswaran, 2010, "Vivo-Morpholino Knockdown of αIIb: A Novel Approach to Inhibit Thrombocyte Function in Adult Zebrafish", *Blood Cells, Molecules, and Diseases*, Vol. 44, No. 3, pp. 169–174.

Kitaguchi, T., K. Kawakami, and A. Kawahara, 2009, "Transcriptional Regulation of a Myeloid-Lineage Specific Gene Lysozyme C During Zebrafish Myelopoiesis", *Mechanisms of Development*, Vol. 126, No. 5–6, pp. 314–323.

Kizil, C., A. Iltzsche, J. Kaslin, and M. Brand, 2013, "Micromanipulation of Gene Expression in the Adult Zebrafish Brain Using Cerebroventricular Microinjection of Morpholino Oligonucleotides.", *Journal of Visualized Experiments : JoVE*, Vol. 1, No. 75, pp. 1–6.

Kizil, C., J. Kaslin, V. Kroehne, and M. Brand, 2012, "Adult Neurogenesis and Brain Regeneration in Zebrafish", *Developmental Neurobiology*, Vol. 72, No. 3, pp. 429–461.

Kizil, C., N. Kyritsis, and M. Brand, 2015, "Effects of Inflammation on Stem Cells: Together They Strive?", *EMBO Reports*, Vol. 16, No. 4, pp. 416–426.

Knopman, D. S., H. Amieva, R. C. Petersen, G. Chételat, D. M. Holtzman, B. T. Hyman, R. A. Nixon, and D. T. Jones, 2021, "Alzheimer Disease", *Nature Reviews Disease Primers*, Vol. 7, No. 1, pp. 1–21.

Kocagöz, Y., M. Can, D. Sema, E. Eski, K. Güler, and Z. Dokuzluoglu, 2022, "Disparate Progenitor Cell Populations Contribute to Maintenance and Repair Neurogenesis in the Zebrafish Olfactory Epithelium", *Cell and Tissue Research*, Vol. 388, No. 2, pp. 331–358.

Kokaia, Z., G. Martino, M. Schwartz, and O. Lindvall, 2012, "Cross-Talk Between Neural Stem Cells and Immune Cells: The Key to Better Brain Repair?", *Nature Neuroscience*, Vol. 15, No. 8, pp. 1078–1087.

Kurimoto, T., Y. Yin, G. Habboub, H. Y. Gilbert, Y. Li, S. Nakao, A. Hafezi-Moghadam, and L. I. Benowitz, 2013, "Neutrophils Express Oncomodulin and Promote Optic Nerve Regeneration", *Journal of Neuroscience*, Vol. 33, No. 37, pp. 14816–14824.

Kyritsis, N., C. Kizil, S. Zocher, V. Kroehne, J. Kaslin, D. Freudenreich, A. Iltzsche, and M. Brand, 2012, "Acute Inflammation Initiates the Regenerative Response in the Adult Zebrafish Brain", *Science*, Vol. 338, No. 6112, pp. 1353–1356.

Lakshmanan, H. G., E. Miller, A. E. White-Canale, and L. P. McCluskey, 2022, "Immune Responses in the Injured Olfactory and Gustatory Systems: a Role in Olfactory Receptor Neuron and Taste Bud Regeneration?", *Chemical Senses*, Vol. 47, No. 8, pp. 1–19.

Le Guyader, D., M. J. Redd, E. Colucci-Guyon, E. Murayama, K. Kissa, V. Briolat, E. Mordelet, A. Zapata, H. Shinomiya, and P. Herbomel, 2008, "Origins and Unconventional Behavior of Neutrophils in Developing Zebrafish", *Blood*, Vol. 111, No. 1, pp. 132–141.

Li, L., H. Jin, J. Xu, Y. Shi, and Z. Wen, 2011, "Irf8 Regulates Macrophage Versus Neutrophil Fate During Zebrafish Primitive Myelopoiesis", *Blood*, Vol. 117, No. 4, pp. 1359–1369.

Li, Q., and B. A. Barres, 2018, "Microglia and Macrophages in Brain Homeostasis and Disease", *Nature Reviews Immunology*, Vol. 18, No. 4, pp. 225–242.

Li, T., Z. Zhang, X. Li, G. Dong, M. Zhang, Z. Xu, and J. Yang, 2020, "Neutrophil Extracellular Traps: Signaling Properties and Disease Relevance", *Mediators of Inflammation*, Vol. 2020, No. 7, pp. 1–14.

Lieschke, G. J., A. C. Oates, M. O. Crowhurst, A. C. Ward, and J. E. Layton, 2001, "Morphologic and Functional Characterization of Granulocytes and Macrophages in Embryonic and Adult Zebrafish", *Blood*, Vol. 98, No. 10, pp. 3087–3096.

Lindborg, J. A., M. Mack, and R. E. Zigmond, 2017, "Neutrophils are Critical for Myelin Removal in a Peripheral Nerve Injury Model of Wallerian Degeneration", *Journal of Neuroscience*, Vol. 37, No. 43, pp. 10258–10277.

Liongue, C., C. J. Hall, B. A. O'Connell, P. Crosier, and A. C. Ward, 2009, "Zebrafish Granulocyte Colony-Stimulating Factor Receptor Signaling Promotes Myelopoiesis and Myeloid Cell Migration", *Blood*, Vol. 113, No. 11, pp. 2535–2546.

Mackay-Sim, A., and P. W. Kittel, 1991, "On the Life Span of Olfactory Receptor Neurons", *European Journal of Neuroscience*, Vol. 3, No. 3, pp. 209–215.

Martins, R. R., P. S. Ellis, R. B. MacDonald, R. J. Richardson, and C. M. Henriques, 2019, "Resident Immunity in Tissue Repair and Maintenance: The Zebrafish Model Coming of Age", *Frontiers in Cell and Developmental Biology*, Vol. 7, No. 12, pp. 1–11.

Mathias, J. R., B. J. Perrin, T.-X. Liu, J. Kanki, A. T. Look, and A. Huttenlocher, 2006, "Resolution of Inflammation by Retrograde Chemotaxis of Neutrophils in Transgenic Zebrafish", *Journal of Leukocyte Biology*, Vol. 80, No. 6, pp. 1281–1288.

Medzhitov, R., 2008, "Origin and Physiological Roles of Inflammation", *Nature*, Vol. 454, No. 7203, pp. 428–435.

Menke, A. L., J. M. Spitsbergen, A. P. M. Wolterbeek, and R. A. Woutersen, 2011, "Normal Anatomy and Histology of the Adult Zebrafish", *Toxicologic Pathology*, Vol. 39, No. 5, pp. 759–775.

Mescher, A. L., 2017, "Macrophages and Fibroblasts During Inflammation and Tissue Repair in Models of Organ Regeneration", *Regeneration*, Vol. 4, No. 2, pp. 39–53.

Morcos, P. A., Y. Li, and S. Jiang, 2008, "Vivo-Morpholinos: A Non-Peptide Transporter Delivers Morpholinos into a Wide Array of Mouse Tissues", *BioTechniques*, Vol. 45, No. 6, pp. 613–623.

Moreno, S. G., *Macrophages*, Humana Press, New York, 2018.

Moriyama, Y., and M. Nomura, 2018, "Clodronate: A Vesicular ATP Release Blocker", *Trends in Pharmacological Sciences*, Vol. 39, No. 1, pp. 13–23.

Morley, S. C., 2012, "The Actin-Bundling Protein L-Plastin: A Critical Regulator of Immune Cell Function", *International Journal of Cell Biology*, Vol. 2012, No. 1, pp. 1–10.

Nguyen-Chi, M., B. Laplace-Builhé, J. Travnickova, P. Luz-Crawford, G. Tejedor, G. Lutfalla, K. Kissa, C. Jorgensen, and F. Djouad, 2017, "TNF Signaling and Macrophages Govern Fin Regeneration in Zebrafish Larvae", *Cell Death & Disease*, Vol. 8, No. 8, pp. 1–12.

Nguyen-Chi, M., B. Laplace-Builhe, J. Travnickova, P. Luz-Crawford, G. Tejedor, Q. T. Phan, I. Duroux-Richard, J. P. Levraud, K. Kissa, G. Lutfalla, C. Jorgensen, and F. Djouad, 2015, "Identification of Polarized Macrophage Subsets in Zebrafish", *ELife*, Vol. 4, No. 7, pp. 1–14.

Ochs, H. D., and A. J. Thrasher, 2006, "The Wiskott-Aldrich Syndrome", *Journal of Allergy and Clinical Immunology*, Vol. 117, No. 4, pp. 725–738.

Oishi, Y., and I. Manabe, 2018, "Macrophages in Inflammation, Repair and Regeneration", *International Immunology*, Vol. 30, No. 11, pp. 511–528.

Opperman, K. S., K. Vandyke, K. C. Clark, E. A. Coulter, D. R. Hewett, K. M. Mrozik, N. Schwarz, A. Evdokiou, P. I. Croucher, P. J. Psaltis, J. E. Noll, and A. C. Zannettino, 2019, "Clodronate-Liposome Mediated Macrophage Depletion Abrogates Multiple Myeloma Tumor Establishment In Vivo", *Neoplasia (United States)*, Vol. 21, No. 8, pp. 777–787.

Orecchioni, M., H. Matsunami, and K. Ley, 2022, "Olfactory Receptors in Macrophages and Inflammation", *Frontiers in Immunology*, Vol. 13, No. 1, pp. 1–9.

Palić, D., C. B. Andreasen, J. Ostojić, R. M. Tell, and J. A. Roth, 2007, "Zebrafish (Danio Rerio) Whole Kidney Assays to Measure Neutrophil Extracellular Trap Release and Degranulation of Primary Granules", *Journal of Immunological Methods*, Vol. 319, No. 1–2, pp. 87–97.

Palominos, M. F., C. Calfún, G. Nardocci, D. Candia, J. Torres-Paz, and K. E. Whitlock, 2022, "The Olfactory Organ is a Unique Site for Neutrophils in the Brain", *Frontiers in Immunology*, Vol. 13, No. 5, pp. 1–15.

Palominos, M. F., and K. E. Whitlock, 2021, "The Olfactory Organ Is Populated by Neutrophils and Macrophages During Early Development", *Frontiers in Cell and Developmental Biology*, Vol. 8, No. 1, pp. 1–15.

Pavlakis, N., R. L. Schmidt, and M. R. Stockler, 2005, "Bisphosphonates for Breast Cancer", *Cochrane Database of Systematic Reviews*, Vol. 3, No. 7, p. 1.

Pazhakh, V., S. Clark, M. C. Keightley, and G. J. Lieschke, 2017, "A GCSFR/CSF3R Zebrafish Mutant Models the Persistent Basal Neutrophil Deficiency of Severe Congenital Neutropenia", *Scientific Reports*, Vol. 7, No. 11, pp. 1–11.

Peiseler, M., and P. Kubes, 2019, "More friend than foe: The Emerging Role of Neutrophils in Tissue Repair", *Journal of Clinical Investigation*, Vol. 129, No. 7, pp. 2629–2639.

Petrie, T. A., N. S. Strand, C.-T. Yang, J. S. Rabinowitz, and R. T. Moon, 2015, "Macrophages Modulate Adult Zebrafish Tail Fin Regeneration", *Development*, Vol. 142, No. 2, pp. 406–406.

Phillipson, M., and P. Kubes, 2019, "The Healing Power of Neutrophils", *Trends in Immunology*, Vol. 40, No. 7, pp. 635–647.

Poewe, W., K. Seppi, C. M. Tanner, G. M. Halliday, P. Brundin, J. Volkmann, A. E. Schrag, and A. E. Lang, 2017, "Parkinson Disease", *Nature Reviews Disease Primers*, Vol. 3, No. 1, pp. 1–21.

Poncelet, G., and S. M. Shimeld, 2020, "The Evolutionary Origins of the Vertebrate Olfactory System: Evolution of the Olfactory System", *Open Biology*, Vol. 10, No. 12, pp. 1–17.

Powell, D., S. Tauzin, L. E. Hind, Q. Deng, D. J. Beebe, and A. Huttenlocher, 2017, "Chemokine Signaling and the Regulation of Bidirectional Leukocyte Migration in Interstitial Tissues", *Cell Reports*, Vol. 19, No. 8, pp. 1572–1585.

Pugach, E. K., P. Li, R. White, and L. Zon, 2009, "Retro-Orbital Injection in Adult Zebrafish", *Journal of Visualized Experiments*, Vol. 34, No. 12, pp. 4–6.

Raman, R., M. Ryon, and P. Jagadeeswaran, 2020, "RNaseH-Mediated Simultaneous Piggyback Knockdown of Multiple Genes in Adult Zebrafish", *Scientific Reports*, Vol. 10, No. 1, pp. 1–11.

Renshaw, S. A., C. A. Loynes, D. M. I. Trushell, S. Elworthy, P. W. Ingham, and M. K. B. Whyte, 2006, "Atransgenic Zebrafish Model of Neutrophilic Inflammation", *Blood*, Vol. 108, No. 13, pp. 3976–3978.

Renshaw, S. A., and N. S. Trede, 2012, "A Model 450 Million Years in the Making: Zebrafish and Vertebrate Immunity", *DMM Disease Models and Mechanisms*, Vol. 5, No. 1, pp. 38–47.

Richards, M. K., F. Liu, H. Iwasaki, K. Akashi, and D. C. Link, 2003, "Pivotal Role of Granulocyte Colony-Stimulating Factor in the Development of Progenitors in the Common Myeloid Pathway", *Blood*, Vol. 102, No. 10, pp. 3562–3568.

Robertson, A. L., S. Avagyan, J. M. Gansner, and L. I. Zon, 2016, "Understanding the Regulation of Vertebrate Hematopoiesis and Blood Disorders: Big Lessons from a Small Fish", *Physiology & Behavior*, Vol. 176, No. 1, pp. 139–148.

Rock, K. L., E. Latz, F. Ontiveros, and H. Kono, 2010, "The Sterile Inflammatory Response", *Annual Review of Immunology*, Vol. 28, No. 3, pp. 321–342.

Rosowski, E. E., 2020, "Determining Macrophage Versus Neutrophil Contributions to Innate Immunity Using Larval Zebrafish", *DMM Disease Models and Mechanisms*, Vol. 13, No. 1, pp. 1–14.

Rubartelli, A., M. T. Lotze, E. Latz, and A. Manfredi, 2013, "Mechanisms of Sterile Inflammation", *Frontiers in Immunology*, Vol. 4, No. 398, pp. 2012–2013.

Sabin, K., and K. Echeverri, 2020, "The Role of the Immune System During Regeneration of the Central Nervous System", *Journal of Immunology and Regenerative Medicine*, Vol. 7, No. 3, pp. 1–10.

Salic, A., and T. J. Mitchison, 2008, "A Chemical Method for Fast and Sensitive Detection of DNA Synthesis In Vivo", *Proceedings of the National Academy of Sciences of the United States of America*, Vol. 105, No. 7, pp. 2415–2420.

Sanders, J. L., and M. L. Kent, 2014, "The Zebrafish as a Model for Microsporidiosis", *Microsporidia: Pathogens of Opportunity: First Edition*, Vol. 29, No. 11, pp. 357–370.

Schindelin, J., I. Arganda-Carreras, E. Frise, V. Kaynig, M. Longair, T. Pietzsch, S. Preibisch, C. Rueden, S. Saalfeld, B. Schmid, J. Y. Tinevez, D. J. White, V. Hartenstein, K. Eliceiri, P. Tomancak, and A. Cardona, 2012, "Fiji: An Open-Source Platform for Biological-Image Analysis", *Nature Methods*, Vol. 9, No. 7, pp. 676–682.

Schwob, J. E., W. Jang, E. H. Holbrook, B. Lin, D. B. Herrick, J. N. Peterson, and J. Hewitt Coleman, 2017, "Stem and Progenitor Cells of the Mammalian Olfactory Epithelium: Taking Poietic License", *Journal of Comparative Neurology*, Vol. 525, No. 4, pp. 1034–1054.

See, H. W., and J. M. Lord, 2004, "Factors Underlying Chronic Inflammation in Rheumatoid Arthritis", *Archivum Immunologiae et Therapiae Experimentalis*, Vol. 52, No. 6, pp. 379–388.

Shanley, L. C., O. R. Mahon, D. J. Kelly, and A. Dunne, 2021, "Harnessing the Innate and Adaptive Immune System for Tissue Repair and Regeneration: Considering More Than Macrophages", *Acta Biomaterialia*, Vol. 133, No. 10, pp. 208–221.

Shiau, C. E., Z. Kaufman, A. M. Meireles, and W. S. Talbot, 2015, "Differential Requirement for irf8 in Formation of Embryonic and Adult Macrophages in Zebrafish", *PLoS ONE*, Vol. 10, No. 1, pp. 1–15.

Sipka, T., R. Peroceschi, R. Hassan-Abdi, M. Groß, F. Ellett, C. Begon-Pescia, C. Gonzalez, G. Lutfalla, and M. Nguyen-Chi, 2021, "Damage-Induced Calcium Signaling and Reactive Oxygen Species Mediate Macrophage Activation in Zebrafish", *Frontiers in Immunology*, Vol. 12, No. 1, pp. 1–19.

Sommer, F., V. Torraca, and A. H. Meijer, 2020, "Chemokine Receptors and Phagocyte Biology in Zebrafish", *Frontiers in Immunology*, Vol. 11, No. 2, pp. 1–14.

Stachura, D. L., and D. Traver, *Methods in Cell Biology*, Elsevier, London, 2011.

Stirling, D. P., S. Liu, P. Kubes, and V. W. Yong, 2009, "Depletion of Ly6G/Gr-1 Leukocytes after Spinal Cord Injury in Mice Alters Wound Healing and Worsens Neurological Outcome", *Journal of Neuroscience*, Vol. 29, No. 3, pp. 753–764.

Su, C. Y., K. Menuz, and J. R. Carlson, 2009, "Olfactory Perception: Receptors, Cells, and Circuits", *Cell*, Vol. 139, No. 1, pp. 45–59.

Subasinghe, D., N. M. M. Nawarathna, and D. N. Samarasekera, 2011, "Disease Characteristics of Inflammatory Bowel Disease (IBD)", *Journal of Gastrointestinal Surgery*, Vol. 15, No. 9, pp. 1562–1567.

Sugimoto, M. A., J. P. Vago, M. Perretti, and M. M. Teixeira, 2019, "Mediators of the Resolution of the Inflammatory Response", *Trends in Immunology*, Vol. 40, No. 3, pp. 212–227.

Sullivan, C., and C. H. Kim, 2008, "Zebrafish as a Model for Infectious Disease and Immune Function", *Fish and Shellfish Immunology*, Vol. 25, No. 4, pp. 341–350.

Sullivan, C., and C. H. Kim, *Innate Immunity of Plants, Animals and Humans*, Springer Berlin, Heidelberg, 2008.

Summan, M., G. L. Warren, R. R. Mercer, R. Chapman, T. Hulderman, N. Van Rooijen, and P. P. Simeonova, 2006, "Macrophages and skeletal muscle regeneration: A Clodronate-Containing Liposome Depletion Study", *American Journal of Physiology - Regulatory Integrative and Comparative Physiology*, Vol. 290, No. 6, pp. 1488–1495.

Summerton, J., 1999, "Morpholino Antisense Oligomers: the Case for an RNase H-Independent Structural Type", *Biochimica et Biophysica Acta*, Vol. 1489, No. 1, pp. 141–158.

Tauber, A. I., 2003, "Metchnikoff and the Phagocytosis Theory", *Nature Reviews Molecular Cell Biology*, Vol. 4, No. 11, pp. 897–901.

Tedgui, A., 2011, "Focus on Inflammation", *Arteriosclerosis, Thrombosis, and Vascular Biology*, Vol. 31, No. 5, pp. 958–959.

Teixeira, C. F. P., S. R. Zamunér, J. P. Zuliani, C. M. Fernandes, M. A. Cruz-Hofling, I. Fernandes, F. Chaves, and J. M. Gutiérrez, 2003, "Neutrophils do not Contribute to Local Tissue Damage , But Play a Key Role in Skeletal Muscle Regeneration, in Mice", *Muscle & Nerve*, Vol. 28, No. 10, pp. 449–459.

Timme-Laragy, A. R., S. I. Karchner, and M. E. Hahn, 2012, "Gene Knockdown by Morpholino-Modified Oligonucleotides in the Zebrafish (Danio Rerio) Model: Applications for Developmental Toxicology", *Methods in Molecular Biology*, Vol. 889, No. 11, pp. 51–71.

Travnickova, J., S. Nhim, N. Abdellaoui, F. Djouad, M. Nguyen-Chi, A. Parmeggiani, and K. Kissa, 2021, "Macrophage Morphological Plasticity and Migration is Rac Signalling and MMP9 Dependant", *Scientific Reports*, Vol. 11, No. 1, pp. 1–10.

Tulotta, C., C. Stefanescu, Q. Chen, V. Torraca, A. H. Meijer, and B. E. Snaar-Jagalska, 2019, "CXCR4 Signaling Regulates Metastatic Onset by Controlling Neutrophil Motility and Response to Malignant Cells", *Scientific Reports*, Vol. 9, No. 1, pp. 1–16.

Uemoto, T., G. Abe, and K. Tamura, 2020, "Regrowth of Zebrafish Caudal Fin Regeneration is Determined by the Amputated Length", *Scientific Reports*, Vol. 10, No. 1, pp. 1–11.

van Rooijen, N., and E. Hendrikx, *Liposomes*, Humana Press, London, 2010.

Var, S. R., and C. A. Byrd-Jacobs, 2020, "Role of Macrophages and Microglia in Zebrafish Regeneration", *International Journal of Molecular Sciences*, Vol. 21, No. 13, pp. 1–17.

Walton, E. M., M. R. Cronan, R. W. Beerman, and D. M. Tobin, 2015, "The Macrophage-Specific Promoter Mfap4 Allows Live, Long-Term Analysis of Macrophage Behavior During Mycobacterial Infection in Zebrafish", *PLoS ONE*, Vol. 10, No. 10, pp. 1–17.

Wang, J., 2018, "Neutrophils in Tissue Injury and Repair", *Cell and Tissue Research*, Vol. 371, No. 3, pp. 531–539.

Wang, X., S. Fu, Y. Wang, P. Yu, J. Hu, W. Gu, X. M. Xu, and P. Lu, 2007, "Interleukin-1β Mediates Proliferation and Differentiation of Multipotent Neural Precursor Cells through the Activation of SAPK/JNK Pathway", *Molecular and Cellular Neuroscience*, Vol. 36, No. 3, pp. 343–354.

Wentzel, A. S., J. Petit, W. G. van Veen, I. R. Fink, M. H. Scheer, M. C. Piazzon, M. Forlenza, H. P. Spaink, and G. F. Wiegertjes, 2020, "Transcriptome Sequencing Supports a Conservation of Macrophage Polarization in Fish", *Scientific Reports*, Vol. 10, No. 1, pp. 1–15.

Widera, D., I. Mikenberg, M. Elvers, C. Kaltschmidt, and B. Kaltschmidt, 2006, "Tumor Necrosis Factor α Triggers Proliferation of Adult Neural Stem Cells via IKK/NF-κB Signaling", *BMC Neuroscience*, Vol. 7, No. 64, pp. 1–18.

Wiegertjes, G. F., A. S. Wentzel, H. P. Spaink, P. M. Elks, and I. R. Fink, 2016, "Polarization of Immune Responses in Fish: The 'Macrophages First' Point of View", *Molecular Immunology*, Vol. 69, No. 1, pp. 146–156.

Willett, C. E., A. Cortes, A. Zuasti, and A. G. Zapata, 1999, "Early Hematopoiesis and Developing Lymphoid Organs in the Zebrafish", *Developmental Dynamics*, Vol. 214, No. 4, pp. 323–336.

Xu, J., L. Du, and Z. Wen, 2012, "Myelopoiesis During Zebrafish Early Development", *Journal of Genetics and Genomics*, Vol. 39, No. 9, pp. 435–442.

Xu, S., S. E. Webb, T. C. K. Lau, and S. H. Cheng, 2018, "Matrix Metalloproteinases (MMPs) Mediate Leukocyte Recruitment During the Inflammatory Phase of Zebrafish Heart Regeneration", *Scientific Reports*, Vol. 8, No. 1, pp. 1–14.

Yang, W., and P. Hu, 2018, "Skeletal Muscle Regeneration is Modulated by Inflammation", *Journal of Orthopaedic Translation*, Vol. 13, No. 1, pp. 25–32.

Yoo, S. K., and A. Huttenlocher, 2011, "Spatiotemporal Photolabeling of Neutrophil Trafficking During Inflammation in Live Zebrafish", *Journal of Leukocyte Biology*, Vol. 89, No. 5, pp. 661–667.

Zhang, J., Y. Yang, Z. Yang, T. Li, and F. Chen, 2018, "Snapshot: Targeting Macrophages as a Candidate for Tissue Regeneration", *Current Issues in Molecular Biology*, Vol. 29, No. 1, pp. 37–48.

Zhu, Z., J. Ding, Z. Ma, T. Iwashina, and E. E. Tredget, 2016, "Systemic Depletion of Macrophages in the Subacute Phase of Wound Healing Reduces Hypertrophic Scar Formation", *Wound Repair and Regeneration*, Vol. 24, No. 4, pp. 644–656.

Zizioli, D., M. Mione, M. Varinelli, M. Malagola, S. Bernardi, E. Alghisi, G. Borsani, D. Finazzi, E. Monti, M. Presta, and D. Russo, 2019, "Zebrafish Disease Models in Hematology: Highlights on Biological and Translational Impact", *Biochimica et Biophysica Acta - Molecular Basis of Disease*, Vol. 1865, No. 3, pp. 620–633.

APPENDIX A: Chemicals and Reagents

Table A.1. List of chemicals and reagents.

Name	Manufacturer
Normal Goat Serum, P30-1001	PAN Biotech, Germany
Bromodeoxyuridine (BrdU)	Alfa Caesar, Germany
Hidrochloric Acid	Sigma-Aldrich, USA
Phenol Red	AppliChem, USA
Triton X-100	AppliChem, USA
Tween 20	Roche, Germany
Tricaine Methanesulfonate	Sigma-Aldrich, USA
Paraformaldehyde (PFA)	Sigma-Aldrich, USA
Sodium Chloride	Sigma-Alrdich, USA
Potassium Chloride	Sigma-Alrdich, USA
Sodium Phosphate Dibasic	Sigma-Alrdich, USA
Potassium Phosphate Monobasic	Sigma-Alrdich, USA
Clodronate Liposomes	Liposoma, The Netherlands
Control Liposomes (PBS)	Liposoma, The Netherlands
Csf3r Vivo Morpholino	Gene Tools, USA
Vivo Standard Control	Gene Tools, USA
FITC-Dextrane (70 kDa)	Kindly offered by Prof. Amitav Sanyal
Sodium Hidroxide	Sigma-Alrdich, USA
OCT	Sakura Finetek, USA
Calcium Sulfate	Alfa Caesar, Germany

Table A.1. List of chemicals and reagents (cont.).

Name	**Manufacturer**
Sodium Bicarbonate	Sigma-Alrdich, USA
Click-iT EdU Alexa Fluor488	Life Technologies
DPBS (10X)	Kindly offered by Assoc. Prof. Batu Erman

APPENDIX B: Disposable and Non-disposable Equipment

Table B.1. List of disposable and non-disposable equipment.

Name	Manufacturer
-20 ^{o}C Freezer	Uğur, Turkey
-80 ^{o}C Freezer	ThermoForma, USA
Laboratory Glassware	Isolab, Germany
Coplin Staining Jars	VWR International, LLC, USA
Confocal Microscope TCS SP5	Leica Microsystems, USA
Confocal Microscope TCS SP8	Leica Microsystems, USA
Leica CM3050 S Cryostat	Leica Microsystems, USA
+4 ^{o}C Refregirator	Arçelik, Turkey
Glass Slides - Superfrost® Plus	Thermo Scientific, USA
Drying Oven	Nüve, Turkey
Paraflim	Parafilm, USA
Microvawe Oven	Vestel Turkey
Water Bath	Memmert, Germany
Micropipettes (2,5 – 1000 μl)	Eppendorf, Germany
Micropipette Tips (10 – 1000 μl)	CAPP, Germany
Magnetic Stirrer	IKA Works Inc.,USA
Microinjector	Eppendorf, USA
Magnetic Stirrer without Heating	IKA Works Inc., USA
Forceps	Dumont, Switzerland
Microinjection Capilarry Tubes	Warner Instruments, USA
Flaming/Brown Micropipette Puller	Shutter Instrument Co., USA
Borosilicate Glass Capillary Tubes	Shutter Instrument Co., USA

Table B.1. List of disposable and non-disposable equipment (cont.).

Name	**Manufacturer**
Petri Dishes	Fıratmed, Turkey
Microinjector Femtojet	Eppendorf, Germany
Micromanipulator IM-6 09033	Narishige, Japan
Dissection Microscope	Zeiss, Germany
Steinless Steel Surgical Blades	Swann Morton LTD., UK
U-100 Insulin Syringe (30G)	Beckon Dickinson, USA
Hamilton Microliter Syringe	Hamilton, Switzerland
0,5, 1,5, 2.0 ml Centrifuge Tubes	
Heat Block	Eppendorf, Germany
Vortex Genie 2	Scientific Industries Inc., USA
Spin Down	Fisher Scientific, USA
pH Meter	WTW, Germany
Nanodrop Spectrophotometer, 2000	Thermo Scientific, USA
Dissection Micro Scissors	
Dissection pins	Austerlitz Insect Pins, Czech Republic
PAP Pen	Liquid Blocker, Japan
Incubation Chamber	Nüve, Turkey
Heidolph Rotamax 120 Orbital Shaker	Heidolph, Germany
15, 50 ml Centrifuge Tubes	Corning, USA
Pasteur Pipettes	ISOLAB, Germany

APPENDIX C: Figures and Images

The figures and images that emerged within the scope of the work in this thesis and whose copyrights were transferred to the publishing house were utilized in the thesis booklet in accordance with the "publishing policy valid for the reuse of the text and graphics produced by the author" on the publishing house's own page.